IN VITRO PROPERTIES OF HUMAN MESENCHYMAL STEM CELLS AND THEIR ABILITY TO MODULATE INFLAMMATION IN VIVO

A Dissertation

by

NIKOLAY BAZHANOV

Submitted to the Office of Graduate and Professional Studies of
Texas A&M University
in partial fulfillment of the requirements for the degree of

DOCTOR OF PHILOSOPHY

Chair of Committee,	Darwin J. Prockop
Committee Members,	Deborah E. Sullivan
	Carl A. Gregory
	Anatoliy A. Gashev
Head of Department,	Van G. Wilson

May 2015

Major Subject: Medical Sciences

ABSTRACT

Mesenchymal stem cells (MSCs), are plastic adherent cells that are readily isolated from various sources, possess stem-cell-like properties and show unique beneficial features in in vivo models of diseases.

In present dissertation we investigated the aspects of MSCs biology related to both in vitro properties and in vivo abilities to benefit in diseases.

The in vitro part of the dissertation addresses the question of heterogeneity in single-cell derived cultures of human MSCs. Laser capture microdissection was used to isolate distinct inside and outside regions of the colony for RNA isolation. When assayed by microarray the cells from inside and outside regions of the colony showed distinct patterns of gene expression profile. In functional studies, however, we did not find any differences – the cells perform similarly in cloning and in vitro growth assays.

In the in vivo part of the dissertation we investigated the effects of human MSCs and their secreted protein tumor-necrosis factor stimulated gene/protein 6 (TSG-6) in two models of lung injury - hydrocloric-acid (HCl)-induced lung injury and bleomycin-induced lung injury in mice. We showed that intraperitoneal administration (IP) of human MSCs improved lung function and inhibited inflammation in the lungs after HCl lung injury. Human recombinant TSG-6 inhibited inflammation in both, HCl-induced lung injury and bleomycin-induced lung injury, however it improved lung function only in mice injured with bleomycin.

Finally we investigated the effects of MSCs administered inside the peritoneal

cavity to explain the beneficial effects in HCl-induced lung injury. We showed that MSCs aggregated rapidly after the injection IP and preconditioned immune system by recruiting immune cells to peritoneal cavity and by triggering the production of various classes of cytokines. We utilized real-time polymerase chain reaction (PCR) and in vivo imaging to estimate the amount MSCs present in various organs of peritoneal cavity. Most of MSCs were found in omentum and mesenteric tissues, only negligible amount of cells was recovered from lymph nodes and spleen.

In conclusion, the dissertation is expanding the existing knowledge about MSCs, increases our knowledge both in understanding the basic biology of the cells and their interaction with the host organism.

ACKNOWLEDGMENTS

For me, writing the dissertation was similar to traveling down the memory lane. I could not have imagined that purely academic exercise of putting together the data, words and images of the work that took almost 7 years to complete would bring up the kaleidoscope of people, places and experiences. This certainly created a distraction but also put things into a perspective.

First I would like to thank my mentor Dr. Darwin J. Prockop. For his mentoring, his patience, support and encouragement. For creating an absolutely unique research environment where everybody is heard and no idea is off the table – even if it is about milky spots and omentums! Especially I want to thank Dr. Prockop for replying to my email from Russia in 2005 and accepting me as an equal member of the team at Center for Gene Therapy at Tulane University, even though it was a tough time because of hurricane Katrina. For supporting me in my decision in starting my PhD and being very patient about me actually getting it. I will keep the book of Strunk and White handy at all the time and try to do things “one step at a time”.

I would like to thank all my committee members for their extreme patience with me and for being so cordial, accessible and supportive. A big portion of this work was related to studying the lungs. I want to specifically thank Deborah Sullivan for her expertise and for the discussions that we had during PPG meetings, committee meetings and for the articles that I enjoyed reading. I thank Carl Gregory for his help and his

encyclopedic knowledge in MSCs and biochemistry and molecular biology and just for being a great person. Whenever I needed help in science or personally I knew I could always count on Carl for help. I thank Anatoliy Gashev for basically jump-starting IP project looking at the effects of MSCs in peritoneal cavity. Your advice to "just inject GFP MSCs and look around the guts" produced my most favorite figures of the dissertation (of course, everything was approved by Texas A&M IACUC).

I would like to especially thank people that I was privileged to be a coworker and a friend of: Joni Ylostalo – for being a great friend and collaborator on many projects. Andrea Foskett – for sharing a load of lung projects. Roxanne Reger – for her tremendous help with writing, submitting and everything else for IACUC. April Tiblow for her amazing help with in vivo experiments. TJ Bartosh for great discussions and sharing the vision. My classmate in gradschool Mohammadipoor Arezoo, for her friendship. Our discussions and occasional help with experiments. My dear friend Greg Block for lengthy discussions about science and not only.

All current and former members of Institute for Regenerative Medicine in Temple, Texas and Center for Gene Therapy At Tulane University.

I would like to thank my family all around the world - my grandmother Delphine in Cote d'Ivoire, Africa, my sister in law Corinne, my US family Luis and Linda Fry in Dripping Springs, Carol in Cleveland, my mother in Russia, my sister and her husband Andre in Germany.

Last, but not the least I would like to thank my beautiful wife Sonia for her love,

support and for our two beautiful kids Abby and Matthew. They bring joy to every day of my life. I thank Sonia for her strength and stepping up in taking care of our kids so I can finish the work on my dissertation.

I thank God for giving me strength in carrying out the work and finishing it.

New Orleans, LA – Temple, TX – Galveston, TX, 2015

The work was supported in part by grants from the NIH: VCP01HL075161, P01RR 17447, P40OD011050 and Louisiana Gene Therapy Research Consortium.

NOMENCLATURE

ALI	Acute Lung Injury
ARDS	Acute Respiratory Distress Syndrome
BALB/c	Bagg Albino (inbred research mouse strain)
BMP	Bone Morphogenetic Protein
CCM	Complete Culture Medium
CCR	CC chemokine receptor
CD	Cluster Of Differentiation
cDNA	Complementary Deoxyribonucleic Acid
CFU-F	Colony Forming Unit - Fibroblast
COX2	cyclooxygenase 2
CXCL	CXC chemokine ligand
CXCR	CXC chemokine receptor
DAPI	4',6-diamidino-2-phenylindole
DKK	Dickkopf homolog
DNA	Deoxyribonucleic Acid
ECM	Extracellular Matrix
EDTA	Ethylenediaminetetraacetic Acid
EGF	Epidermal Growth Factor
ELISA	Enzyme-Linked Immuno Assay
Fgf	Fibroblast Growth Factor

GAPDH	Glyceraldehyde 3-Phosphate Dehydrogenase
GFP	Green Fluorescent Protein
GVHD	Graft-Versus-Host Disease
HCl	Hydrochloric Acid
HLA	Human Leukocyte Antigen
HSC	Hematopoietic Stem Cell
IDO	Indoleamine-2,3-dioxygenase
IGF	Insulin-Like Growth Factor
IN	Inner Region Of A Colony
iNOS	Nitric Oxide Synthase
IFN	Interferon
ISCT	International Society For Cell Therapy
ITGA	Integrin α
IP	Intraperitoneal
IV	Intravenous
IT	Intratracheal
JLN	Jejunal Lymph Nodes
kDa	Kilodalton
LPS	Lypopolysaccharide
MCP1	Monocyte Chemoattractant Protein-1
MHC	Major Histocompatibility Complex
MLR	Mixed Lymphocyte Reaction

MSCs	Mesenchymal Stem Cells
mRNA	Messenger Ribonucleic Acid
MT	Mesentery
NaCl	Sodium chloride
NCBI	National Center for Biotechnology Information
NIH	National Institutes of Health
NO	Nitric Oxide
OI	Osteogenesis Imperfecta
OM	Omentum
OUT	Outer Region of a Colony
PCR	Polymerase Chain Reaction
PFA	Paraformaldehyde
pH	Potency of Hydrogen
PGE_2	Prostaglandin E_2
PLP	Peritoneal Lavage Pellet
PODXL	Podocalyxin-Like
RFU	Relative Fluorescence Units
RLU	Relative Luminescence Units
ROS	Reactive Oxygen Species
RS	Rapidly Self-Renewing
RT	Reverse Transcriptase
SD	Standard Deviation

SDF	Stromal Cell-Derived Factor
SEM	Standard Error of Mean
SOX	Sex Determining Region Y-Box
SP	Spleen
SR	Slowly Replicating
STC-1	Stanniocalcin-1
SYNPO	Synaptopodin
TNF-α	Tumor Necrosis Factor alpha
TGF	Transforming Growth Factor
THBS	Thrombospondin
Treg	T-Regulatory Cell
Th1/Th2	T-helper Cell Type 1 or 2
UV	Ultra-Violet
VEGF	Vascular Endothelial Growth Factor
VCAM	Vascular Cell Adhesion Molecule

TABLE OF CONTENTS

Page

LIST OF FIGURES

FIGURE Page

FIGURE Page

LIST OF TABLES

CHAPTER I

INTRODUCTION

I.1 Mesenchymal Stem Cells – Introduction

Human mesenchymal stem cells, or MSCs, have been occupying the minds of many brilliant scientists for more than half a century. These cells, commonly isolated from bone marrow, fat and other tissues, were originally discovered by Soviet biologist Aleksandr Friedenstein [1] in preparations of bone marrow from rabbits, allegedly, while trying to find a remedy to cure the effects of nuclear weapon attack. Thus Friedenstein and his colleagues discovered that plastic-adherent fraction of bone marrow is capable of forming bone once placed in peritoneal cavities [1].

Since then the research on MSCs has exploded in geometric progression. The metrics behind it are impressive: MSCs are being studied by numerous teams across the globe, that produce on average 100 publications each week [2]. In 2014-2015 the US National Institutes of Health spent more than $170,000,000 funding projects directly or indirectly involving MSCs [3]. Clinicaltrials.gov reports 439 trials with MSCs being carried out virtually on every continent, with China (147), European Union (104) and United States (71) in the lead [4].

The popularity of MSCs is based on several properties of these cells. First, the stem- and progenitor-cells-like properties. MSCs have been repeatedly shown to differentiate into various types of cells including bone [5]–[8], fat [5], [6], [8], [9],

cartilage [10]–[13] neurons and glial cells [14], [15] and others, including alveolar epithelium cells, retinal and skin epithelial cells [16]–[24]. The ability of MSCs cells to differentiate warranted the research in regenerative medicine, especially in diseases that affect bone and cartilage. Secondly, MSCs showed promising results in various models of diseases by modulating inflammation and immunity [25]. Lastly, the practicality of work with MSCs. The cells are relatively easy to obtain and maintain in culture and basic protocols for cells isolation, expansion and differentiation are freely available. Moreover, to facilitate the research of these cells Texas A&M Health Science Center is hosting NIH-funded MSCs distribution center that provides characterized MSCs to researchers worldwide [26]

The following sections of introduction will discuss these properties in more detail and will provide rationale for the studies described in the main body of dissertation.

I.2 MSCs: characteristics and heterogeneity

As mentioned in previous section, MSCs were originally discovered as plastic-adherent cells in bone marrow of rabbits by Friedenstein and colleagues in 1960s-1970s [1], [27]. Surprisingly, the transplantation of these cells inside peritoneal cavity did not result in generation of hematopoetic cells. Instead formation of heterotopic bone tissue was observed [1]. The discovered plastic adherent cells resembled fibroblasts in appearance, grew rapidly in culture and were able to form single-cell-derived colonies and were named colony-forming unit-fibroblast [28]. The term “mesenchymal stem cells” was first used in 1990's to underline the multipotentiality of MSCs and their

similarity with embryonic stem cells [29]. In current literature MSCs appear under various names – multipotent adult stromal cells, bone marrow stromal cells, mesenchymal stem/progenitor cells and others. In 2005 the International Society for Cellular Therapy (ISCT) published a position paper defining minimal criteria for MSCs [30]. It covers three areas – in vitro culture requirements (plastic adherence), differentiation requirements (bone, cartilage and fat) and epitope marker requirements (negative for hematopoetic markers CD45, CD34, CD14 or CD11b, CD79alpha, CD19 and HLA-DR) and positive for CD105, CD73, CD90. The ISCT definition is being actively used by researchers and was being cited more than 3400 times [2].

Clonogenicity of MSCs is an important quality of MSCs showing their potential for self renewal [31]. Although the cells in colonies arise from a single progenitor, their homogeneity is questionable. When MSCs clones were subjected to differentiating conditions some of them produced only cells of one lineage – either bone, fat or cartilage, while others were able to produce cells of two or more origins [5], [31], [32]. It has been suggested that the MSCs colony represents a quasi in vitro niche [33] where different regions of colony vary in the composition of produced factors that play important roles in maintenance of the undifferentiated state or, in contrast, promoting of differentiation processes.

The heterogeneity of MSCs has been shown on other levels as well. Thus it was shown that the culture of MSCs undergo changes in their gene expression profile [34] and antigen presentation [35]. Earlier passages of MSCs contain larger amount of cells

that have high clonogenic ability [10] and preferentially engraft in vivo [36].

Another level of heterogeneity exists between MSCs donors and was described in terms of their capacity for differentiation and growth in vitro [37] as well as in vivo performance [38]. The differences were attributed to the variations in isolation procedure [37] and recently it was shown that the in vivo performance of MSCs positively correlates with the expression levels of TSG-6 gene [38].

One of striking examples of interspecies differences is the one between mouse and human MSCs [39]. When similar conditions are used, mouse MSCs contain larger population of hematopoetic contamination and exhibit prolonged lag phase [40].

It has been shown that MSCs can be isolated from various tissues including adipose tissue, dental pulp, placenta, amniotic fluid and many others in addition to bone marrow [41].

The omnipresence of MSCs and their heterogeneity raises a question about their origin. Currently two main theories are recognized.

First theory suggests that MSCs are perivascular cells or pericytes [42], [43]. It is supported by the fact that MSCs can be isolated from virtually any tissue and the presence of common markers, such as CD146 [44]. Second theory suggests that MSCs take origin from neuroectoderm via epithelial-to-mesenchymal transition [45]. It was shown that mouse bone marrow contains MSCs-like cells that share a common marker with neuroepithelial cells – Nestin [46]. These cells were shown to support hematopoesis and have the ability to differentiate into bone fat and cartilage similar to MSCs. In

support of epithelial-to-mesenchymal transition theory it has also been shown that introduction of TWIST gene drives epithelial cells toward mesenchymal differentiation [47].

I.3 MSCs in in vivo models of diseases

One of the major driving forces behind the interest in MSCs is their potential benefits in clinical applications. As mentioned in earlier parts of the introduction 439 clinical trials are being conducted with MSCs. The majority are phase 2 and 3 trials (258 and 278 respectively). Phase 0, 3 and 4 have 7, 33 and 1 trials respectively.

The impressive spread of conditions that MSCs are being used for in the clinic represents the evolution of paradigms for repair of tissues by MSCs [48]. Thus, early paradigms were based on the multipotentiality of MSCs and their ability to support the hematopoetic niche. It was proposed that MSCs would replenish or substitute the deficient cells in the host by means of engraftment. In one of the initial studies beneficial effects of MSCs administration and their subsequent engraftment was shown in children with osteogenesis imperfecta – a congenital condition, characterized by brittle bones and frequent fractures [49], [50]. Furthermore, systemic administration of MSCs had a positive effect in models of kidney injury, myocardial infarction, stroke and others [51]–[53]. However, it has been extensively shown that beneficial effects of MSCs occur with minimal or temporary engraftment [54], [55].

The notion that MSCs support and organize hematopoetic niche formed the basis for co-administration of MSCs during hematopoetic stem cell transplantation [56], [57].

The later paradigms emerged from observations that MSCs exhibit beneficial effects with limited engraftment. Among the modes of action that fall under this category are cell-to-cell contact and fusion of MSCs with host cells and production of secreted factors.

Spees et al. showed that human MSCs rescue small airway epithelial cells that are devoid of mitochondria by means of fusion and transfer of mitochondria [58]. The latter was also shown in vivo in a model of LPS-induced lung injury [59].

Direct cell-to-cell contact has been shown important in glial differentiation of neural stem cells in a co-culture system with MSCs [60]. Contact of MSCs with macrophages was necessary for reprogramming them into non-inflammatory phenotype [61].

Secreted factors, produced by MSCs can be classified by their mode of action: anti-apoptotic, pro-regenerative and anti-inflammatory/immunomodulatory [62].

The anti-apoptotic effect of MSCs was recently attributed to the production of a secreted protein called stanniocalcin-1 (STC-1) [63]. This protein exhibits its action through inhibition of oxidative stress via uncoupling oxidative phophorylation [64]. It has been shown that MSCs produce the protein both in vitro upon co-culture with lung epithelial cells and in vivo in aggregates formed in peritoneal cavity [65].

Several factors secreted by MSCs could be classified as pro-regenerative as they promote local vasculo- and angiogenesis (EGF and VEGF) or recruit local tissue progenitors (SDF-1, IGF-1). The production of these factors by MSCs was shown

beneficial in models of myocardial infarction [66]–[68], acute kidney injury [51], [69] and brain injury [70]–[73].

One of the qualities of MSCs is their ability to modulate the inflammation. The research in this area was pioneered in early 2000's by Katarina Le Blanc and her colleagues [74] who showed that MSCs inhibit stimulation of mixed lymphocyte reaction (MLR) in vitro and independently from her by Bartholomew et al. [75] who demonstrated the inhibition of MLR but also inhibition of skin graft rejection due to MSCs administration in vivo.

Since these two pioneering studies, a plethora of anti-inflammatory factors produced by MSCs were discovered. Few molecules attracted more attention from researchers than the others and will be reviewed here.

Indoleamine 2,3-Dioxygenase (IDO) was shown to be produced by MSCs after their exposure to IFN-γ in vitro [76]. IDO is known to inhibit T-cell proliferation by local depletion of tryptophan and production of its toxic derivative kynurenine [77]. In support, human MSCs have been shown to inhibit T-cell activation and proliferation both in in vitro [76] and in vivo models of heart and kidney transplantation [78], [79]. However, only human MSCs are known to utilize this mechanism. MSCs isolated from rodents were shown to utilize immunosuppressive mechanism via production of NO by iNOS [80]. Interestingly, as with the IDO in human MSCs, IFN- γ stimulation is required for NO production.

Prostaglandin E_2 was shown to be produced by human and mouse MSCs [61],

[81]. The production of PGE_2 by MSCs is dependent on their stimulation with TNF-α, LPS, IL6 [82] or by MSCs aggregation in vitro [81] and in vivo [65]. PGE_2-related inhibition of inflammation occurs via several ways, including conversion of M1 macrophages to the M2 phenotype [61], suppression of T-cells proliferation [83],and induction of T-reg differentiation [84].

As it was mentioned in previous sections, the systemic administration of MSCs in immunocompromized mice results in the embolization of lung vasculature [54] and stimulation of MSCs to produce anti-inflammatory protein TSG-6. This 35 kDA protein, originally discovered in fibroblasts, was previously shown to inhibit inflammation in models of arthritis, air pouch and others reviewed in [85]. TSG-6 produced by human MSCs was shown to be beneficial in models of myocardial infarction [54], LPS-induced lung injury [86], corneal inflammation [87] and zymosan-induced peritonitis [88]. Although its mechanism of action is not completely understood, it was proposed that TSG-6 could stabilize the pro-inflammatory fragments of hyaluronan or inhibit translocation of NFκB via direct or indirect interaction with CD44 [88], inhibit neutrophil infiltration [89] and others (reviewed in [85]).

I.4 Systemic routes of delivery and MSCs biodistribution

Various routes of MSCs administration are being used in preclinical studies. They can be categorized as systemic, local and specialized methods of delivery such as by association with scaffold [90].

The majority of studies utilize the systemic route of delivery via intravenous

injection. Immediately after the injection MSCs distribute to lungs and few other organs [54], [55]. Although the exact fate of MSCs in those organs is not described, it is believed that the cells respond to local cues, such as pro-inflammatory cytokines [54]. In turn, MSCs upregulate the expression of genes, such as TSG-6 [54], [86] and COX2 [61]. The intravenous route of injection proved to be beneficial in myocardial infarction model [54], [55], corneal injury model [91], LPS-induced lung injury [86], [92], [93], bleomycin lung injury [18], [94] and many others.

Intraperitoneal (IP) administration could be placed in both categories – local and systemic based on the studied disease model. Thus, it was shown that in model of colitis, IP-injected MSCs migrate toward inflamed colon and don't leave peritoneal cavity [95], however other studies showed the presence of MSCs in virtually all organs after their administration inside peritoneal cavity [96], [97]. In addition, it was shown that IP administration of MSCs results in formation of MSCs spheroids [65] similar to the spheroids formed in vitro [98]. Formation of spheroids was associated with the upregulation of the expression of TSG-6, STC-1 and COX2 genes [65]. The production of these and other factors by MSCs in peritoneal cavity could be linked to distant effects of MSCs in models of inflammation [86], [91], [99].

CHAPTER II

REVERSIBLE COMMITMENT TO DIFFERENTIATION BY HUMAN MULTIPOTENT STROMAL CELLS IN SINGLE-CELL–DERIVED COLONIES*

II.1 Overview

II.1.1 Objective

Human multipotent stromal cells readily form single-cell–derived colonies when plated at clonal densities. However, the colonies are heterogeneous because cells from a colony form new colonies that vary in size and differentiation potential when replated at clonal densities. The experiments here tested the hypothesis that cells in the inner regions of colonies are partially differentiated, but the differentiation is reversible.

II.1.2 Materials and Methods

Cells were separately isolated from the dense inner (IN) regions and less-dense outer regions (OUT) of single-cell–derived colonies. Cells were then compared by assays of their transcriptomes and proteins, and for clonogenicity and differentiation.

II.1.3 Results

IN cells expressed fewer cell-cycle genes and higher levels of genes for extracellular matrix than the OUT cells. When transferred to differentiation medium, differentiation of the colonies occurred primarily in the IN regions. However, the IN

---

cells were indistinguishable from OUT cells when replated at clonal densities and assayed for rates of propagation and clonogenicity. Also, colonies formed by IN cells were similar to colonies formed by OUT cells because they had distinct IN and OUT regions. Cultures of IN and OUT cells remained indistinguishable through multiple passages (30 to 75 population doublings), and both cells formed colonies that were looser and less dense as they were expanded.

II.1.4 Conclusions

The results demonstrated that cells in the IN region of single-cell–derived colonies are partially differentiated, but the differentiation can be reversed by replating the cells at clonal densities.

II.2 Introduction

There is currently interest in both the biology and potential therapeutic uses of the adult stem/progenitor cells from bone marrow, referred to in initial reports as fibroblastic colony-forming units (CFU-F), then in the hematological literature as marrow stromal cells, subsequently as mesenchymal stem cells, and most recently as multipotent mesenchymal stromal cells or MSCs [30]. Although there is general agreement that the cells can be isolated as the plastic adherent cells from human marrow, there is no consensus as to how the cells should be expanded in culture. In particular, there has been no consensus as to whether cells in culture are homogeneous [5], [10], [100]. Human MSCs (hMSCs) that are expanded as confluent cultures appear homogeneous [5], [101] and several antibodies have been developed to surface epitopes on confluent

cultures of MSCs [102]–[111]. In contrast to studies on confluent cultures of hMSCs, a number of reports emphasized the heterogeneity of earlier stage cultures. Early investigators observed that the first cells that appear in low-density cultures are spindle-shaped, and they are replaced by much larger and flatter cells as the cultures mature [112]. Evidence for heterogeneity of MSCs was subsequently emphasized by expansion of the cells at low density. When adherent cells initially isolated by plating mononuclear cells from bone marrow were replated at low densities of about 1 to 100 cells/cm^2, the cells underwent dramatic changes in morphology, rates of proliferation, and patterns of gene expression as they expand in culture [33]. MSCs from low-density cultures were readily cloned as single cell–derived colonies [6], [10], [100], [101], [113], [114], and up to 90% of the MSCs generated colonies when tested by a single-cell CFU-F assay [115]. Some of the single-cell–derived colonies differentiated into osteoblasts, adipocytes, or chondrocytes in culture, but some of the colonies were less multipotential. Low-density cultures contained both small, rapidly self-renewing cells (RS-MSCs) and larger, more slowly replicating cells. Cultures enriched for RS-MSCs had a greater potential to differentiate than cultures of the large, mature cells. Also, RS-MSCs engrafted more efficiently in immunodeficient mice [36]. The confluent cultures of the large, mature cells continued to secrete a number of growth factors, an observation consistent with their ability to serve as feeder layers for hematopoietic stem/progenitor cells. Remarkably, if the cultures were harvested before they reached confluency and replated at low density, the sequence of events repeated itself in that the cells initially were RS-

MSCs and these gradually were replaced by slowly replicating cells. The sequence repeated itself through several passages until the cells approached senescence. Here we report that single-cell–derived colonies are heterogeneous because cells in the inner regions (IN) differed from cells in the outer regions (OUT) in terms of morphology and their commitment to differentiation. However, the differences disappear if the cells are replated at clonal densities.

II.3 Materials and methods

II.3.1 Human MSCs isolation and expansion

Human MSCs were obtained from the Tulane Center for the Preparation and Distribution of Adult Stem Cells (http://www.som.tulane.edu/gene_therapy/distribute). Human MSCs were isolated and expanded as described previously [34]. Preparations were standardized because they demonstrated trilineage differentiation in culture, were negative for hematopoietic markers (<1% for CD34, -36, -45, and -117), and positive for several general markers for MSCs (>95% for CD29, -44, -49c, -59 -90, -105, -147, and -166). For experiments here, a frozen vial of MSCs (donor 5064, 7012 or 240) was thawed and cells were plated in a 145-cm^2 culture dish (Nunc) in complete culture medium (CCM): a-minimal essential medium (αMEM; GIBCO/BRL, Carlsbad, CA, USA), 17% fetal bovine serum (FBS) lot selected for rapid growth of MSCs (Atlanta Biologicals, Norcross, GA, USA), 100 U/mL penicillin, 100 mg/mL streptomycin, and 2 mM L-glutamine (GIBCO/BRL). After 24-hour incubation at 37ºC and 5% CO_2, the medium was removed, cells were washed with phosphate-buffered saline (PBS), and

adherent viable cells were harvested with 0.25% trypsin and 1 mM ethylenediamine tetraacetic acid (EDTA) for 5 minutes at 37ºC as recovered passage 1 cells.

II.3.2 Time-lapse microscopy

Recovered passage 1 MSCs (donor 5064) were plated onto 57-cm^2 dishes (Nunc) at 0.5 cells/cm^2 and incubated at 37ºC and 5% CO_2 without medium change. After 2 hours, adherent single cells on a plate were marked with a scratch on the bottom of the plate under light microscopy. Pictures of partially overlapping fields of view around initial cell location were taken every 24 hours for 11 days by phase contrast (Nikon digital camera DXM 1200F; Kawasaki, Japan, attached to Nikon Eclipse microscope TE200; Japan). Multiple images were combined into one image using Adobe Photoshop 6.0.1. (Adobe Systems Inc., San Jose, CA, USA).

II.3.3 Laser capture microdissection of IN and OUT regions of colonies

Recovered passage 1 MSCs (donor 5064) were plated at 2 cells/cm^2 on laser capture microdissection and pressure catapulting (LMPC) slides (PALM MembraneSlides NF, P.A.L.M. Microlaser Technologies GmbH; Bernried, Germany) that were placed into 57cm^2 plastic dishes (Nunc). Cells were cultured for 10 to 12 days in CCM at 37ºC and 5% CO_2 without medium change until dense colonies that were at least 4 mm in diameter were observed. Slides were washed with PBS, fixed with ice-cold 100% ethanol, and dried. Colonies with distinct OUT and IN regions were outlined and laser microdissected (P.A.L.M. MicroBeam System with UV laser, P.A.L.M. RoboMover, driven by Palmwin software 2.2 and Zeiss Axiovert S-100 microscope; Carl

Zeiss MicroImaging GmbH, Oberkochen, Germany). Dissected OUT or IN cells from two colonies were catapulted separately into one cap, filled with 20 μL extraction buffer (PicoPure RNA Isolation Kit; Molecular Devices, Sunnyvale, CA, USA). Cells were spun down at 800g for 2 minutes, mixed by pipetting, and incubated at 42ºC for 30 minutes before cooling to 4ºC and extracting total RNA.

II.3.4 Isolation of live cells from OUT or IN regions of colonies

Recovered passage 1 MSCs (donors 5064, 7012, and 240) were plated onto 57-cm^2 plastic dishes (Nunc) at 2 cells/cm^2 and incubated at 37ºC and 5% CO_2 without medium change for 10 to 12 days. Colonies that were selected for the isolation were similar in size (at least 4 mm in diameter), round morphologies, distinct dense IN and less-dense OUT regions with readily distinguishable cell phenotypes in each region. The cell phenotypes of the OUT regions were thin, spindle-shaped cells rarely contacting with each other; while the major population of the IN region composed of bigger cells, that were in contact with each other but not overlapping and that formed linear streams of cells, oriented toward OUT region. Before isolation, 5 to 12 OUT regions or IN regions were outlined with marker. To isolate the OUT region of the colony, the central region was destroyed with pipette tip. The cells from the IN region of the colony were isolated after scraping the OUT region with a cell scraper (Corning, Lowell, MA, USA). Dishes were washed with PBS, and cloning cylinders (Bel-Art Products, Pequannock, NJ, USA) with grease (Dow Corning 7 Release Compound; Dow Corning, MI, USA) were placed over the outlined region (either IN or OUT of the colony). Cells in the

inside of the cloning cylinder were harvested with trypsin/EDTA. From 8 to 12 colonies from one or more plates were pooled for OUT region sample, while 5 to 8 were pooled for IN region sample. Samples were centrifuged at 1000g for 6 minutes and washed with PBS, followed by centrifugation. Cells were either used for RNA isolation or used for growth curve, CFU-F, or subcloning assays.

II.3.5 RNA isolation and quality

IN and OUT cells were isolated from colonies of MSCs from donor 5064 by LMPC and from donors 7012 and 240 by live cell isolation method. Total RNA was extracted (PicoPure RNA Isolation Kit) with DNase treatment (RNase-Free DNase Set, Qiagen, Germantown, MD, USA). Amount and quality of isolated total RNA was measured either by spectrophotometric assay (SmartSpec 3000; Bio-Rad, Hercules, CA, USA) or capillary electrophoresis (Agilent 2100 Bioanalyzer; Agilent Technologies, Waldbronn, Germany) using RNA 6000 Pico kit (Agilent) and RNA 6000 Ladder (Ambion, Austin, TX, USA). The 18S and 28S ribosomal RNA peaks were identified on the electrophorogram, and RNA Integrity Numbers (RINs) were calculated using the Bioanalyzer software. Six samples, three from the IN region (1 IN, 2 IN, and 5 IN) of colonies and three from the OUT region (2 OUT, 4 OUT, and 5 OUT) of colonies (donor 5064), with at least 20 ng total RNA and RIN of at least 8.5, were chosen for microarrays.

II.3.5 Microarray assays

Ten nanograms total RNA from each sample (three IN and three OUT samples)

were used in the amplification and labeling steps according to manufacturer's instructions (Ovation Biotin RNA Amplification and Labeling System, NuGEN Technologies, San Carlos, CA, USA). The amount of biotin-labeled cDNA was assayed by spectrophotometer (SmartSpec 3000). Biotin-labeled cDNA (1.6 to 2.2 μg) from the six separate samples were hybridized on the microarrays (HG-U133 Plus 2.0; Affymetrix, Santa Clara, CA, USA) and processed as described previously [34]. Scanned images were transferred to the dChip program [116]–[118]. Arrays were normalized using the invariant set normalization method and model-based expression values were calculated using the signal from perfect match and mismatch probes. Negative values were assigned a value of one. Genes were considered significantly different in expression between IN and OUT samples if they had at least a twofold difference (with 90% confidence), were present in all the samples where the gene was upregulated, and had a t-test p-value of 0.05 or lower between groups (IN vs OUT). The 199 transcripts (155 nonredundant genes based on Gene ID) that were significantly different were used in hierarchical clustering of the samples and genes [119], [120]. The resulting two patterns of expression from the IN and OUT regions were examined for Gene Ontology (GO) term enrichment [121]. Next, p-values were calculated for each GO term based on the exact hypergeometric distribution, to compare the frequencies of GO terms within each pattern to their frequencies across the entire microarray ($p<0.01$ were considered significant). Microarray data will be available at the Gene Expression Omnibus database (http://www.ncbi.nlm.nih.gov/geo/).

II.3.6 Real-time RT-PCR

Total RNA (40 ng) samples from IN and OUT regions of colonies from the three donors were converted into cDNA (High-Capacity cDNA Reverse Transcription Kit; Applied Biosystems, Foster City, CA). A custom-designed card (TaqMan Low Density Array; Applied Biosystems) was used to perform real-time reverse transcriptase polymerase chain reaction (RT-PCR) [34]. Sample preparation and analysis was performed as described previously [34].

II.3.7 Immunocytochemistry

Recovered passage 1 MSCs (donor 5064) were plated onto 57-cm^2 plastic dishes or 6-well plates (Nunc) at 2 cells/cm^2 and incubated at 37ºC and 5% CO_2 without medium change. On day 12, cultures were washed with PBS, fixed in ice-cold 4% paraformaldehyde (Electron Microscopy Sciences, Hatfield, PA, USA) for 15 minutes, and washed again.

For labeling with MKI67 (antigen identified by monoclonal antibody Ki-67), cells were permeabilized with 0.5% Triton X-100 (Sigma, St Louis, MO, USA) in PBS for 15 minutes at room temperature. The remaining samples were not permeabilized. Cells were washed and blocked with 3% bovine serum albumin (Albumin bovine fraction V; Sigma) in PBS for 1 hour at room temperature. After blocking step, areas of interest were outlined, sealed with aqua-hold barrier pen (Scientific Device Laboratory, Des Plaines, IL, USA), and incubated with 400 μL primary antibody in PBS and 1% bovine serum albumin for 20 hours at 4ºC in a humidified chamber. The buffer for anti-

MKI67 also contained 0.025% Triton X-100. The primary antibodies were: 10 µg/mL mouse monoclonal anti-human-KI67 (IgG_1 clone Ki-S5; Chemicon International, Inc., Temecula, CA, USA); 2 µg/mL mouse monoclonal anti-human-VCAM1 [IgG_1 clone BBIG-V1(4B2); R&D Systems, Minneapolis, MN, USA]; and 4 µg/mL goat polyclonal antihuman – PODXL (podocalyxin-like) (IgG_1; R&D Systems). Mouse monoclonal IgG_1 (clone 11711; R&D Systems) in the same concentrations as the primary antibodies was used as the isotype control. After incubation with the primary antibody, slides were cut out of plastic dishes using heated blade. Slides were washed in PBS and incubated with 400 µL containing 2 µg/mL secondary fluorescence-conjugated antibody (Alexa fluor-488 goat anti-mouse IgG (H + L), or Alexa fluor 594 donkey anti goat IgG (H + L); Molecular Probes, Eugene, OR, USA) in PBS with 1% bovine serum albumin for 1 hour at room temperature. For permeabilized samples, the buffer contained 0.025% of Triton X-100. After washing with PBS, slides were mounted with VECTASHIELD Mounting Medium with DAPI (Vector Laboratories, Burlingame, CA, USA), covered with coverslips and sealed. Analysis was performed using Nikon Eclipse E800 microscope with attached SPOT color 2.2.0 digital camera (Diagnostic Instruments, Sterling Heights, MI, USA) using SPOT version 3.1 software. The same settings were used to acquire control-labeled images and all pictures on the slide. Subsequent image manipulations were made in Adobe Photoshop 6.0.1.

II.3.7 Differentiation within colonies

Recovered passage 1 MSCs (donor 7012) were plated onto 57-cm^2 plastic dishes (Nunc) at 2 cells/cm^2 and incubated at 37ºC and 5% CO2 in CCM for 9 days without medium change. On day 9, cultures were washed with PBS and the medium on different plates was replaced with either CCM (control), adipogenic medium, or osteogenic medium. Adipogenic medium consisted of CCM supplemented with 0.5 µM dexamethasone (Sigma), 0.5 µM 3-isobutyl-1-methylxanthine (Sigma), and 50 µM indomethacin (Sigma). Osteogenesis medium consisted of CCM supplemented with 1 nM dexamethasone, 20 mM b-glycerolphosphate, 50 µg/ml L-ascorbic acid-2-phosphate. CCM and differentiation media were changed every 3 days for 21 days. After 21 days, cultures were washed with PBS and fixed in formalin at room temperature for 1 hour. To stain lipid droplets within the cells, adipogenic cultures were washed with PBS, incubated with 0.3% Oil-Red-O (Sigma) solution for 20 minutes at room temperature, and washed again. To stain the sites of mineralization, osteogenic cultures were washed with water, incubated with 1% Alizarin Red S solution (Sigma) for 20 minutes at room temperature, and washed again.

II.3.8 Growth curve assay

To study the growth kinetics, MSCs isolated from the whole colony and different colony regions (donor 5064) were plated in CCM at 100 cells/cm^2 onto 6-well dishes (Nunc) in triplicate. Cells were incubated for 1 to 12 days with medium change every 3 days. For counting, cells on individual wells were washed with PBS, lifted with

trypsin/EDTA, washed with CCM by centrifugation, and resuspended in 0.4% Trypan Blue (GIBCO/BRL) before counting in a hemacytometer.

II.3.9 Subcloning and CFU-F assays

To study clonogenicity, cells (donors 5064, 240, and 7012) initially isolated either from the OUT region or the IN region were plated at 2 cells/cm^2 onto 57-cm^2 dishes (Nunc) in CCM. After 10 to 12 days without medium change, IN regions were isolated from colonies generated from IN regions and replated. The same procedure was performed with colonies generated from OUT regions. Subcloning was continued until colonies were no longer compact with distinct IN and OUT regions for up to five cycles of isolation and replating. CFU-F assays from the same cell preparations in each cycle were done in parallel and in triplicate. On day 14, plates were washed with PBS and stained with 3% crystal violet (SigmaAldrich, Inc.) in 100% methanol for 5 minutes, washed with water, and air-dried. Stained colonies that were at least 2 mm in diameter were counted. Percentage of colonies per plate was obtained using total number of colonies and initial amount of the cells plated. For densitometry, pictures of partially overlapping fields of colonies (donor 7012) at 40 magnification were taken with ORCA digital camera (ORCA, ER, Hamamatsu, Japan) attached to an inverted microscope (Nikon Eclise, TE200 Nikon). Final image was obtained by combining multiple images into one using ImageJ 1.38x software. After conversion into 8-bit grayscale format and background subtraction, gray intensity values were obtained for each pixel through the diameter of the colony. The pixels were then plotted against their correspondent gray

intensity values in Excel (Microsoft Corporation, Redmond, WA, USA). Sliding window of 50 pixels was used for smoothing. Images of differentiated colonies were created by combining pictures of partially overlapping fields of view taken by phase contrast. Multiple images were combined into one using Adobe Photoshop 6.0.1. Linear image adjustments were performed by varying brightness and contrast in order to improve image visibility without changing original image structure.

II.4. Results

II.4.1 Expansion of a single-cell–derived colony

To follow expansion of single cells into colonies, vials of frozen passage 1 MSCs (donor 5064) were thawed, plated overnight to recover viable adherent cells, replated at 0.5 cells/cm^2 on 57-cm^2 plastic dishes, and time-lapse photomicrographs taken by phase microscopy. Single adherent cells that were spindle-shaped were detected within 2 hours (Fig. 1). To follow expansion, the areas containing single cells were marked by scratches on the bottom of the plate. Expansion of a single cell into a typical colony is presented in Figure 1. Two cells were seen in the same area on day 1, and the number increased until day 12. Round, refractile cells in mitosis were visible in the photomicrographs as white spots mostly in the periphery of the colony. On days 4 to 6, the cells remained spindle-shaped with a minimum of cell-to-cell contacts. By day 12, the cells at the center of the colony were confluent, but nonconfluent spindle-shaped cells were present around the periphery of the colony.

Figure 1. Expansion of a single-cell–derived colony. Recovered passage 1 human multipotent stromal cells (MSCs) (donor 5064) were plated at 0.5 cells/cm^2 and incubated for 12 days without medium change. Phase photomicrographs were taken approximately every 24 hours for 12 days. Location of single cell after 2-hour incubation was marked by right angle cuts on bottom of dish. Scale bar: 500 μm. Arrows: single cells after 2 hour and 1 day incubation.

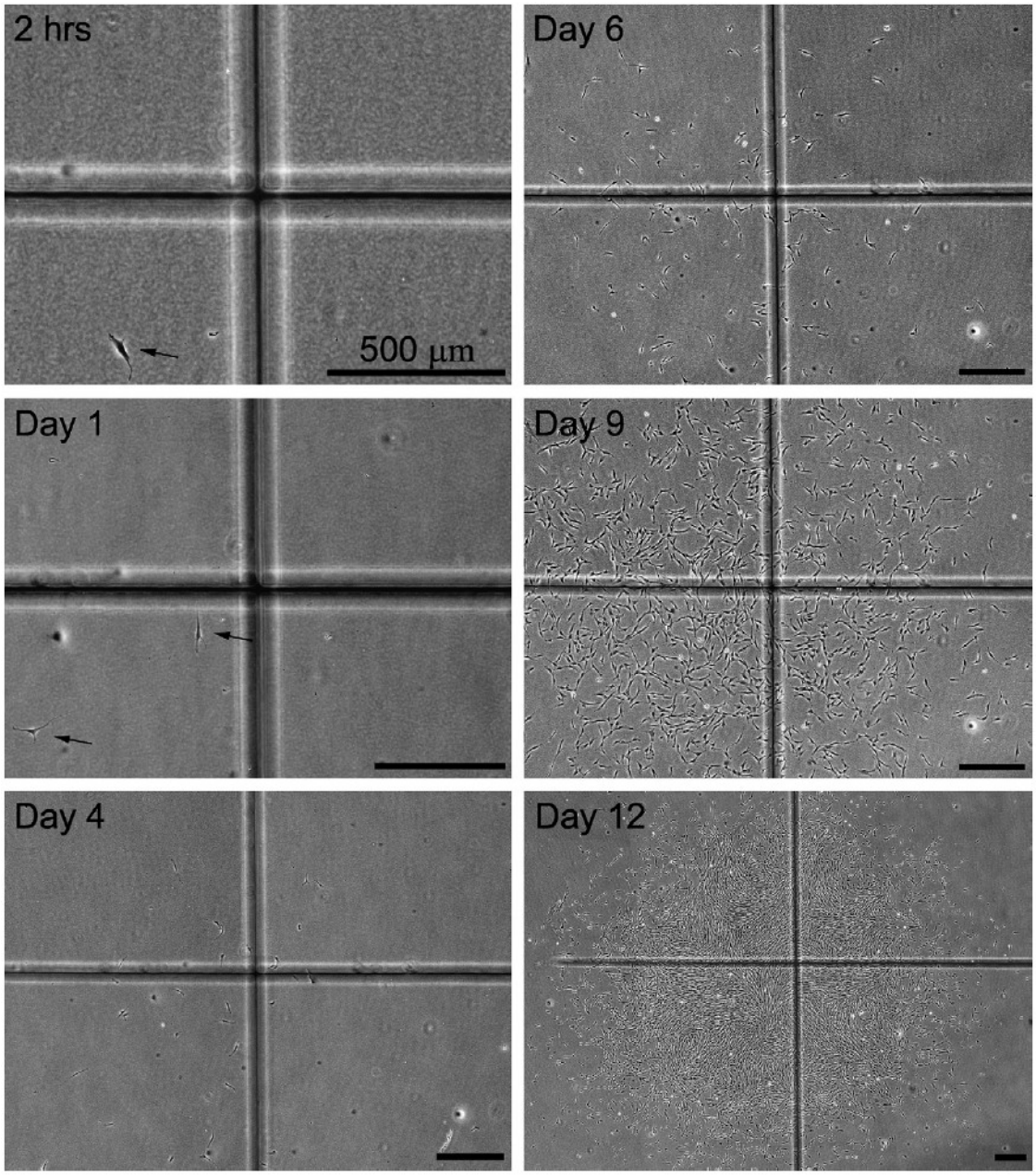

II.4.2 Differences in mRNA expressed by cells in the center and periphery of colonies

Separate samples of cells in the center (IN, 3 samples) and periphery (OUT, 3 samples) of colonies (donor 5064) were isolated by LMPC (Fig. 2A, B, C), RNA was extracted, amplified, and the expressed mRNAs assayed with microarrays. A capillary electrophoretic assay demonstrated that the extracted RNA was intact showing distinct 28S and 18S peaks without background (Fig. A-1). Total of 199 differentially expressed transcripts (155 non-redundant genes) were identified and used in hierarchical clustering of the samples and genes (Fig. 2D, Tables A-1, A-2). The data clearly distinguished the OUT samples from the IN samples from a series of separately analyzed colonies. Cells derived from the IN cells of the colony expressed higher levels of genes for extracellular matrix and inorganic anion transport ($p<0.001$) (Fig. 2D).

Figure 2. Isolation and microarray assays of inner (IN) and outer (OUT) samples. Multipotent stromal cells (MSCs) (donor 5064) were incubated on laser microdissection slides at 2 cells/cm^2 for 12 days without medium change. Cells from IN and OUT were isolated with laser capture microdissection and pressure catapulting (LMPC). The colonies in the figure were stained with crystal violet for illustrative purposes only. (A) Intact colony. (B) Colony after IN was captured. (C) Colony after IN and OUT were captured. (D) Heat map of microarray data from IN and OUT samples using 199 differentially expressed genes. Enriched GeneOntology terms with $p<0.001$ are shown for both clusters. On the heat map, red indicates upregulation and blue downregulation based on gene-wise standardized values. Three OUT samples (2OUT, 4OUT, 5OUT) and three IN samples (1IN, 2IN, 5IN) were used in the microarray assays. Scale bar in (A), (B), and (C): 500 µm. AURKB – aurora kinase B; CDC – cell division cycle; COL21A1 – collagen type 21 a1; ESPL – extra spindle pole bodies homolog; FGF – fibroblast growth factor; GPC – glypican; GTSE – G2 and S-phase expressed; H2AFX – H2A histone family member X; IN – inner region of a colony; LAMA – laminin-a; LUM – lumican; MKI67 – antigen identified by monoclonal antibody Ki-67; MYB – v-myb myeloblastosis viral oncogene homolog; OUT – outer region of a colony; POLE – polymerase epsilon; SGOL – shugoshin-like; SPAG – sperm-associated antigen; TACC – transforming acidic coiled coil-containing protein; THBS – thrombospondin

Figure 2 (continued)

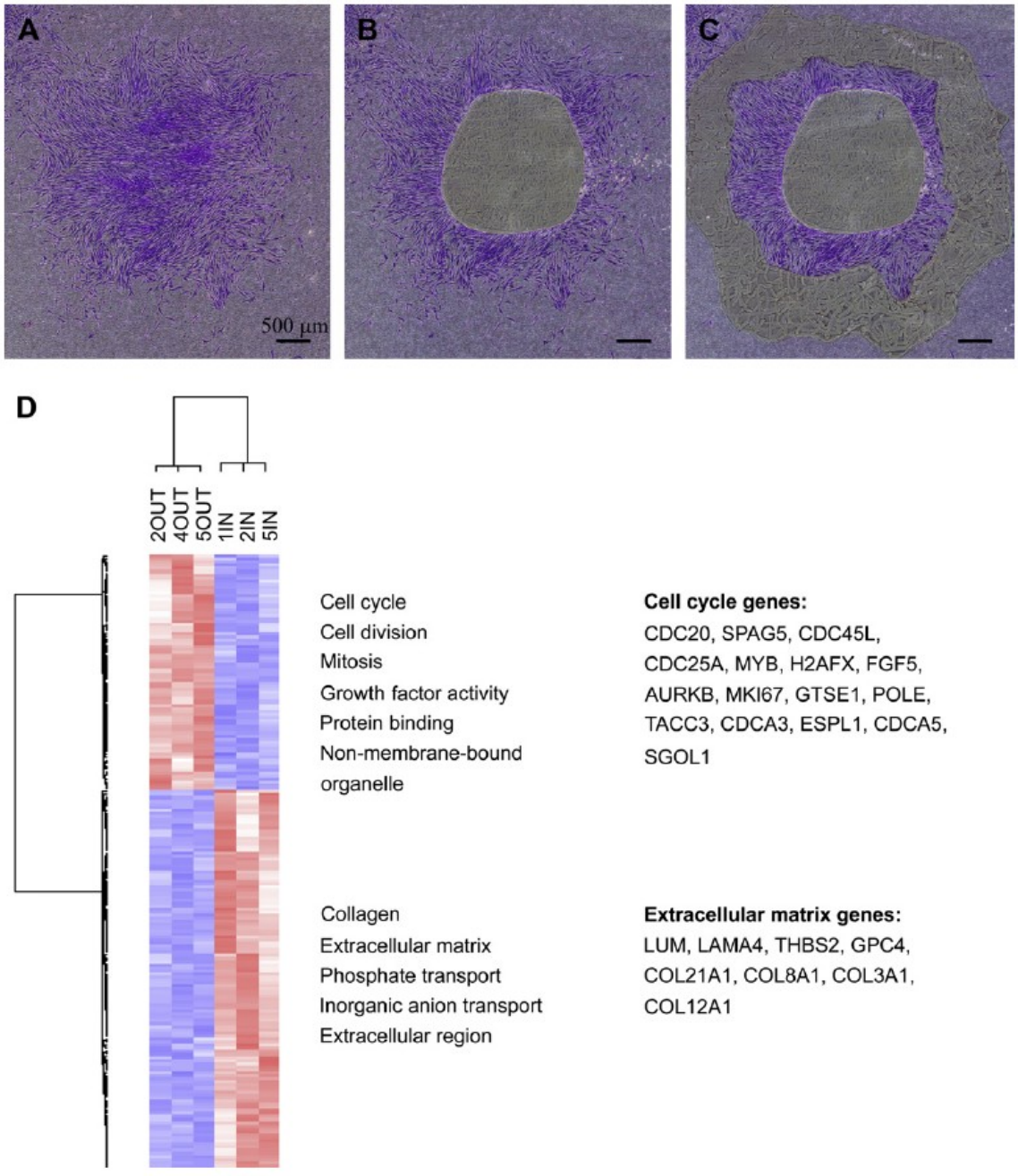

The OUT cells from the periphery expressed higher levels of genes for cell cycle and division, mitosis, growth factor activity, protein binding, and non-membrane–bound organelle ($p<0.001$) (Fig. 2D). In the IN cells, the extracellular matrix molecules upregulated included thrombospondin 2 (THBS2), laminin a4 (LAMA4), lumican (LUM), glypican 4 (GPC4), and a1 chain of collagen III (COL3A1), VIII (COL8A1, XII (COL12A1), and XXI (COL21A1) (Table A-1). In the OUT cells, the cell-division genes upregulated included cell-division cycle homologs 20 (CDC20) and 25 (CDC25), cell-division cycle–associated 3 (CDCA3) and 5 (CDCA5), aurora kinase B (AURKB), sperm-associated antigen 5 (SPAG5), extra spindle pole bodies homolog 1 (ESPL1), centromere protein J (CENPJ), and shugoshin-like 1 (SGOL1) (Table A-1).

To confirm the microarray data, the same samples of RNA were assayed by real-time RT-PCR. Data identified 28 genes upregulated in IN sample relative to the OUT sample and 15 genes showed significant upregulation in the OUT sample compared to the IN sample (Fig. 3A and B). Comparison of data from the real-time RT-PCR assays with data from the microarray data indicated similar differences in the genes expressed by IN and OUT cells (Fig. 3A and B). However, real-time RT-PCR assay was more sensitive to differences in that 16/28 IN genes and 4/15 OUT genes in the microarray assay did not reach the threshold level of a twofold difference. Based on the real-time RT-PCR assays the largest changes in the IN sample were vascular cell-adhesion molecule-1 (VCAM-1) (10.6-fold upregulation), THBS2 (9.9-fold upregulation), LUM (9.0-fold upregulation), growth arrest-specific 1 (GAS1) (8.1-fold upregulation), and

galactosidase b1 (GLB1) (6.7-fold upregulation). The largest changes in the OUT sample were the antigen identified by monoclonal antibody Ki-67 (MKI67 or Ki67) (32.5-fold upregulation), hyaluronan-mediated motility receptor (HMMR or CD168) (30.0-fold upregulation), AURKB (14.8-fold upregulation), podocalyxin-like (PODXL) (7.2-fold upregulation), and leukemia inhibitory factor (LIF) (7.2-fold upregulation).

To confirm the results, real-time RT-PCR assays were performed on colonies generated by MSCs from two additional donors (7012 and 240 in Fig. 3C and D). As expected from previous reports [34], variations were observed with samples from different donors (Fig. 3C and D), but the results were similar for 60% (9 of 15) of the upregulated OUT genes and 32% (9 of 28) of the upregulated IN genes (Fig. 3C and D). Also, IN cells from all the donors expressed much higher levels of two genes for extracellular matrix proteins (THBS2 and LUM) and the GAS1.

Figure 3. **Assays of mRNA from inner (IN) and outer (OUT) regions by microarrays and real-time reverse transcriptase polymerase chain reaction (RT-PCR).** Total RNA was isolated from IN and OUT cells obtained with laser capture microdissection and pressure catapulting (LMPC) (donor 5064) or live cell isolation method (donors 7012 and 240). Genes shown have significant changes in their expression based on real-time RT-PCR. (A) Genes upregulated in the OUT sample (donor 5064). (B) Genes upregulated in the IN sample (donor 5064). (C) Genes upregulated in the OUT region of all three donors (5064, 7012, and 240). (D) Genes upregulated in the IN region of all three donors. Values are fold changes. *Not significant in the microarray assays (less than twofold). Error bars: 95% confidence intervals; n = 3. AGC = aggrecan; ANGPT = angiopoietin; AURKB = aurora kinase B; CCND = cyclin D; CTNNB = catenin-b; CXCL12 = CXC chemokine ligand 12; DCN = decorin; DKK = dickkopf homolog; E2F7 = E2F transcription factor 7; FGF = fibroblast growth factor; FZD = frizzled homolog; GAPDH = glyceraldehyde-3-phosphate dehydrogenase; GAS = growth arrest-specific; GDF = growth differentiation factor; GLB = galactosidase-b; GPC = glypican; GSN = gelsolin; HMMR = hyaluronan-mediated motility receptor; IL = interleukin; IN = inner region of a colony; ITGA = integrin-a; LIF = leukemia inhibitory factor; LPXN = leupaxin; LUM = lumican; MCM = minichromosome maintenance deficient; MKI67 = antigen identified by monoclonal antibody Ki-67; MMP = matrix metalloproteinase; NOTCH = notch homolog; OUT = outer region of a colony; PODXL = podocalyxin-like; RARB = retinoic acid receptor beta; RUNX = runt-related transcription factor; SOCS = suppressor of cytokine signaling; SOX = sex-determining region Y-box; STAT = signal transducer and activator of transcription; SYNPO = synaptopodin; SYTL = synaptotagmin-like; THBS = thrombospondin; VCAM = vascular cell-adhesion molecule; VIL = villin; WNT = wingless-type MMTV integration site; WWTR = ww domain containing transcription regulator.

Figure 3 (continued)

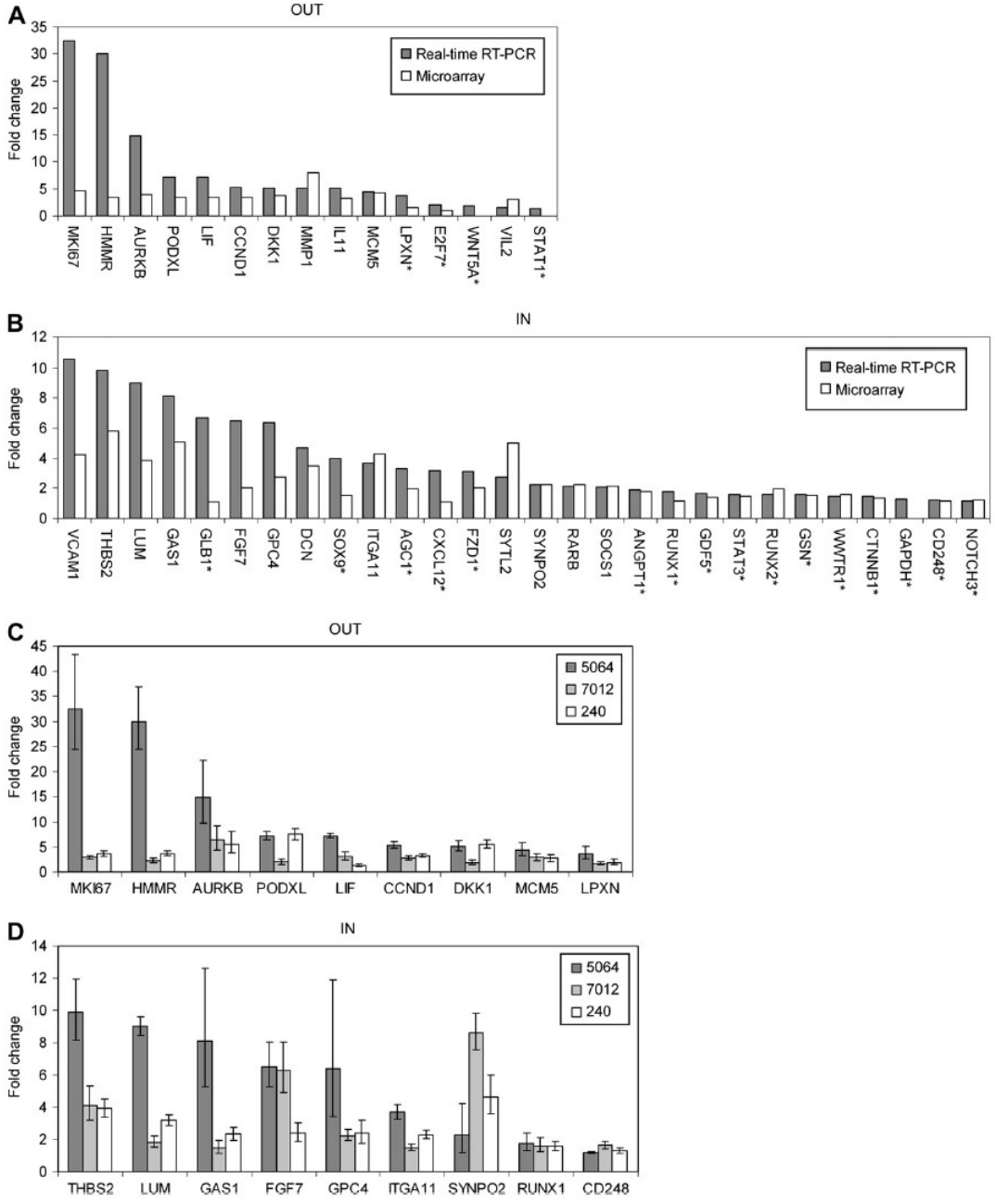

II.4.3 Differences demonstrated by immunocytochemistry

Immunocytochemistry of the colonies confirmed that OUT cells expressed higher levels of MKI67, a marker for proliferating cells, and PODXL, a marker for motile cells (Fig. 4). Immunostaining also confirmed that the IN cells expressed higher levels of cell-adhesion molecule VCAM-1 (Fig. 4). These results suggest that within colonies the OUT cells are proliferating more rapidly than the IN cells.

Figure 4. Immunocytochemistry of MKI67, PODXL, and VCAM-1 in colonies. Three regions of multipotent stromal cell (MSCs) colonies from donor 5064 are shown. Nuclear counterstain: DAPI. Insets: enlarged regions of the same slides. Magnification: x40, x100 (insets). MKI67 = antigen identified by monoclonal antibody Ki-67; PODXL = podocalyxin-like; VCAM-15 = vascular cell-adhesion molecule-1.

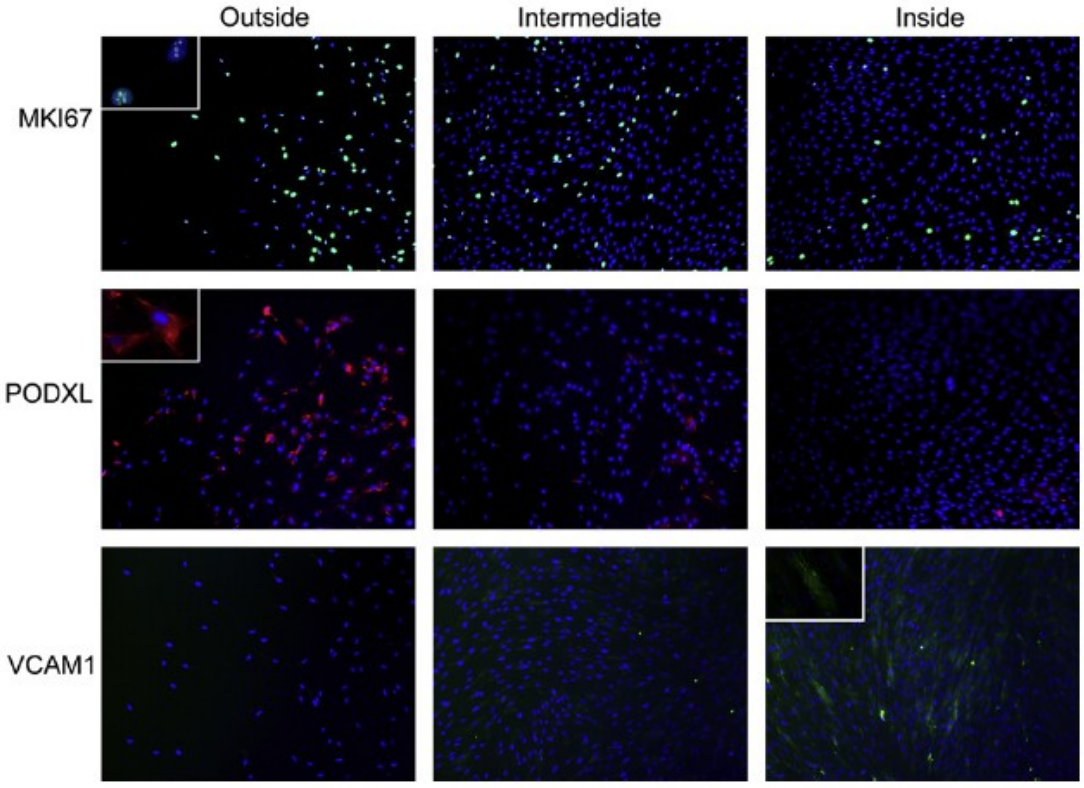

II.4.4 Differentiation of colonies

To study the differentiation capability of IN and OUT cells within a colony, MSCs colonies were cultured under adipogenic and osteogenic conditions for 21 days. Colonies grown under adipogenic conditions and stained with OilRed-O showed lipid droplets preferably in the IN cells (Fig. 5). Similarly, colonies grown under osteogenic conditions and stained with Alizarin Red S showed sites of mineralization mainly in the IN region (Fig. 5). The results further confirmed the observations that the IN cells were more committed to differentiation than OUT cells. The cells in the OUT region have the morphology of fibroblasts that is characteristic of MSCs plated at a low density [112].

Figure 5. Differentiation of colonies. Representative colonies (donor 7012) after adipogenic or osteogenic differentiation. Colonies were fixed with formalin and stained with either Oil-Red-O (adipogenesis) or Alizarin Red S (osteogenesis). Under both conditions, differentiation initiated in the inner (IN) regions of the colonies. Scale bar: 1 mm.

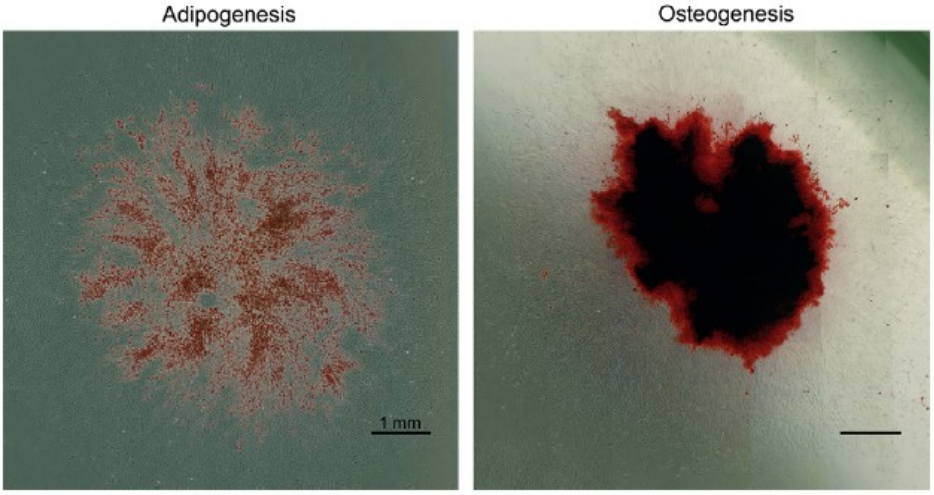

II.4.4 Similar rates of proliferation on IN and OUT cells on replating

To compare the proliferation potential of IN and OUT cells, MSCs were plated on plastic dishes and the two fractions separated by scraping away either the IN or OUT cells of colonies and lifting the remaining cells with a cloning cylinder. The cells were replated at 100 cells/cm^2 and incubated for up to 12 days. The IN and OUT cells proliferated at essentially the same rate (Fig. 6A). Also the doubling times as a function of days in culture were essentially the same with the peak of proliferation around day 3 (Fig. 6A).

II.4.5 Clonogenicity of IN and OUT cells

To compare their clonogenicity, cells from all three donors were grown as previously, and the IN and OUT cells were isolated from passage 2 colonies and replated at low density. The IN and OUT cells from passage 3 were isolated and replated at low density. The sequence was repeated until the cells did not generate colonies with distinct IN and OUT regions (Fig. A-2). Results were analyzed by both the number of colonies generated (CFUs) and the morphology of the colonies.

There were no significant differences in CFU values obtained for IN and OUT cells from passage 3 with MSCs from the three donors (Fig. 6B). As expected [6], however, there was decrease in CFUs with further passages with a distinct decrease with some preparations of MSCs. Colonies with distinct IN and OUT regions were obtained until passage 7 with MSCs from donor 5064, and passage 6 with MSCs from donor 240, but only until passage 4 with MSCs donor 7012.

Figure 6. Expansion and clonogenicity of isolated inner (IN) and outer (OUT) cells. Multipotent stromal cell (MSCs) (donors 5064, 7012, and 240) were plated at 2 cells/cm^2 and incubated for 10 to 12 days. Cells (passage 2) were isolated either from the OUT or the IN and replated at 100 cells/cm^2 for growth curve assay and at 2 cells/cm^2 for fibroblastic colony-forming units (CFU-F) assay. (A) Growth curve assay for donor 5064. Inset: Fold changes per day. (B) CFU-F assays of cells from IN and OUT of all three donors. Subcloning was continued for up to five cycles of isolation and replating (passage 7). Error bars: standard deviations; n = 3. P = passage.

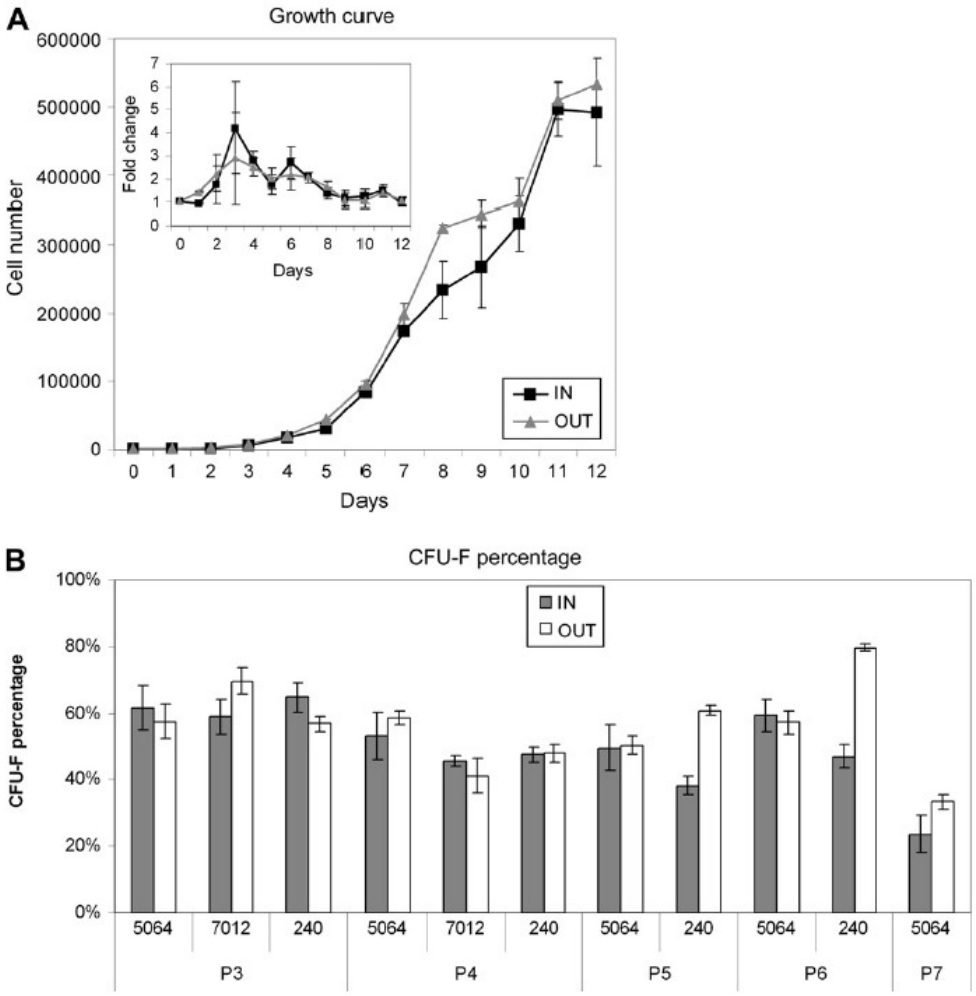

To assess the morphology of the colonies generated, we classified colonies with diameters of 4 mm or more with distinct IN and OUT regions as type I and smaller colonies or loose large colonies as type II (Fig. 7A). The distinctions between the two types of colonies that were apparent by phase microscopy were readily confirmed by densitometry of dye-stained colonies (Fig. A-3). With MSCs from all three donors, the fraction of type I colonies decreased upon subcloning while the fraction of type II increased (Fig. 7B, C, and D). There were no apparent differences between the IN and OUT samples. Interestingly, type II colonies became majority at passage 6 for donor 5064 (Fig. 7B), at passage 5 for donor 240 (Fig. 7C), and at passage 4 for donor 7012 (Fig. 7D). Similarly, the size distribution of colonies in all three donors shifted toward smaller diameter colonies upon passaging (Fig. 8A, B, and C).

Figure 7. Changes in colony morphology upon subcloning. Multipotent stromal cell (MSCs) colonies were stained with crystal violet, measured, and classified either as type I or type II. Type I colonies were at least 4 mm in size with a dense inner (IN) region. Type II colonies were either <4 mm in size with dense IN region or larger but loose. (A) Representative large and small type I colonies (upper panel) and type II colonies (lower panel) from one culture dish of donor 240 MSCs (passage 3). See Fig. A-3 for densitometry of stained type I and type II colonies. Distribution of type I and II colonies during subcloning for donor: (B) 5064, (C) 240, and (D) 7012. Error bars: standard deviations; n = 3. Scale bar: 1 mm. CFU-F=colony-forming unit fibroblast; IN = inner region of a colony; OUT = outer region of a colony; P = passage.

Figure 7 (continued)

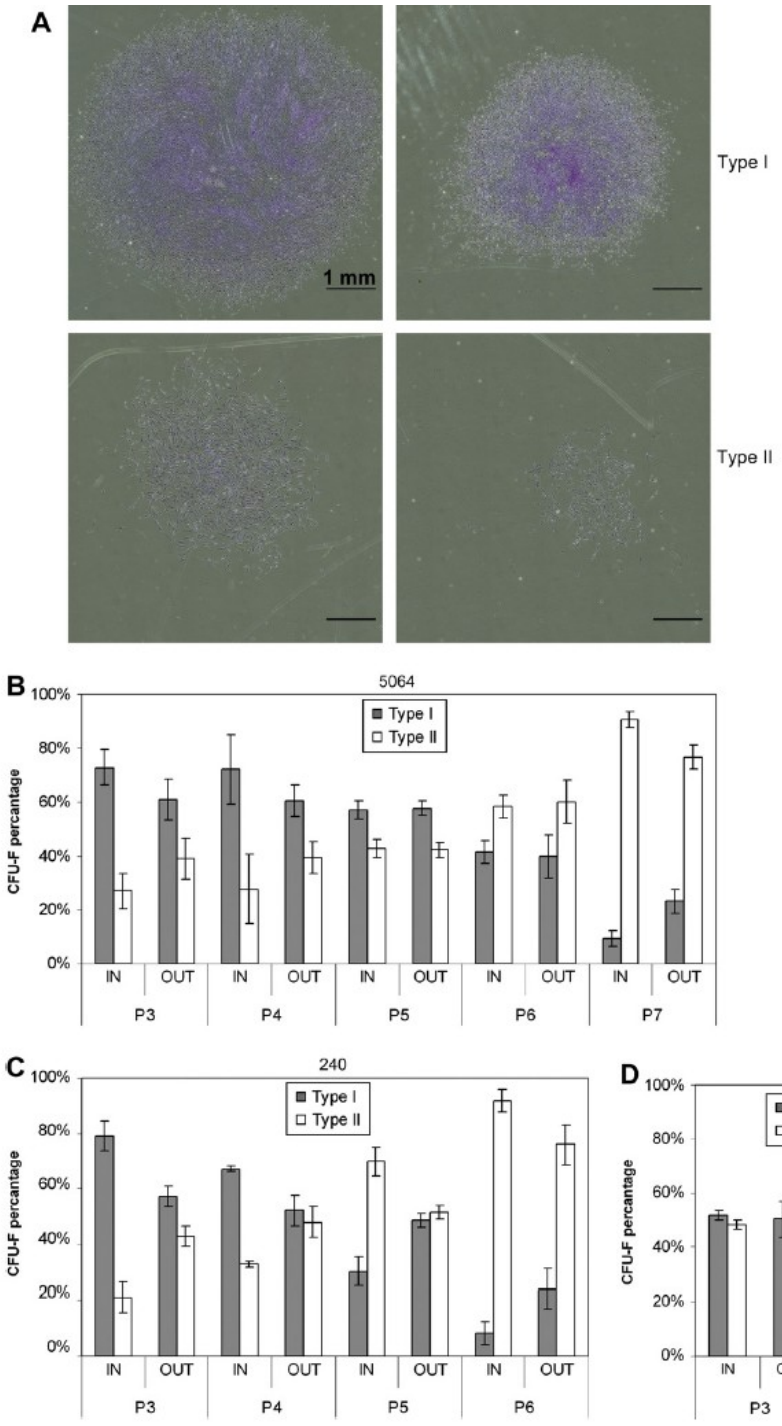

Figure 8. Colony size distribution upon subcloning. Multipotent stromal cell (MSCs) colonies were divided into four groups based on their size (2.0 –3.5 mm, 4.0 – 5.5 mm, 6.0 – 7.5 mm, and 8.0 – 9.5 mm). Size distribution of colonies derived from donor: (A) 5064, (B) 240, and (C) 7012. Error bars: standard deviations; n = 3. IN = inner region of a colony; OUT = outer region of a colony; P = passage.

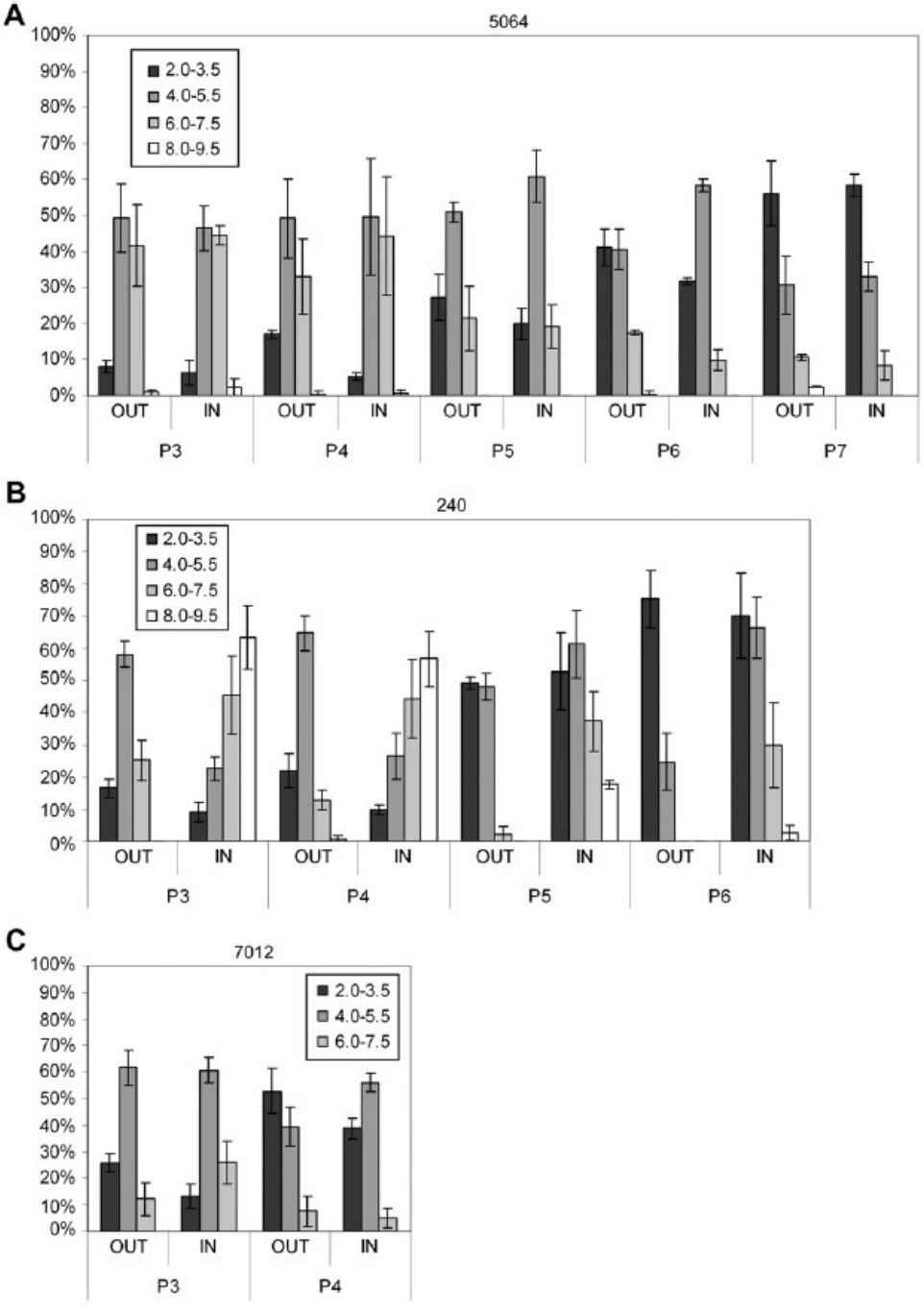

II.5 Discussion

As originally noted by Friedenstein et al. [27], one of the characteristic features of MSCs cultures is their clonal growth, i.e., their ability to form distinct single-cell–derived colonies after plating at very low densities [5], [27], [101]. Previous reports demonstrated that the single-cell–derived colonies of MSCs vary in morphology, growth rates, and differentiation capacity [6], [100], [122]. In addition, MicroSAGE analysis of single-cell–derived colonies showed that MSCs expressed mRNAs common to different mesenchymal cell lineages, suggesting heterogeneity within a colony [123]. In the present study, we focused on the observation that most early culture single-cell–derived colonies had very high–density IN regions, and less-dense OUT regions. Cells in the OUT region have the morphology of fibroblasts that is characteristic of MSCs plated at a low density. Microarray assays demonstrated that cells in the IN region expressed many genes for extracellular matrix, and cells in the OUT region expressed genes involved in cell cycle and division. Validation of microarray data with real-time RT-PCR assays indicated a good correlation between these two methods. However, real-time RT-PCR assays were more sensitive because they detected changes that were not significant in the microarray assays. Also, the changes in several genes detected by real-time RT-PCR were much larger than microarray data suggested. The differences may be explained, in part, by the fact that the real-time RT-PCR assay did not require amplification of the RNA. We demonstrated differences in protein expression by immunocytochemistry of colonies confirming the mRNA data in that the IN cells expressed higher levels of the

cell-adhesion protein (VCAM-1), while the OUT cells expressed higher levels of the cell-cycle protein (MKI67), suggesting that within colonies the OUT cells are proliferating more rapidly than the IN cells. OUT cells also expressed higher levels of an antiadhesion protein (PODXL), which is a member of the CD34 family of sialomucins and has been identified in undifferentiated human embryonic and hematopoietic stem cells [124]–[127]. In addition, PODXL has been shown to increase the aggressive phenotype of malignant cells and thus could be important in MSCs migration and survival in vivo [128]. Recently, we identified higher expression of PODXL in early cultures of MSCs compared to late cultures, suggesting PODXL as a marker of highly proliferative early culture MSCs [34]. Interestingly, the OUT cells resemble the early culture MSCs in their gene expression patterns, while the IN cells are more similar to the late culture MSCs [34]. Therefore, results suggested that the IN cells were more committed to mesenchymal differentiation than the OUT cells. The suggestion was confirmed by transferring the colonies to differentiating in conditions in which, in agreement with previous observations [100], differentiation into both adipocytes and osteoblasts initially occurred in the IN regions of colonies. However, when IN cells were replated at clonal densities, the IN cells were indistinguishable from OUT cells in their rates of propagation, clonogenicity, and formation of colonies with distinct IN and OUT regions. Therefore, results indicated that partial differentiation of the IN cells was reversible. Proliferation of MSCs is limited by density in culture and, therefore, probably in vivo under physiological and pathological conditions. The heterogeneity and plasticity

observed in the cultures suggest that the protocols used to expand human MSCs in culture may have a major influence on how efficiently the cells engraft and repair tissues in animal models and in patients [36].

CHAPTER III

ADULT HUMAN MESENCHYMAL STEM CELLS FROM BONE MARROW PREVENT FUNCTIONAL DECLINE AND DECREASE INFLAMMATION IN MOUSE MODEL OF HCl-INDUCED LUNG INJURY

III.1 Overview

III.1.2 Rationale

Gastric aspiration is the fourth leading cause of acute respiratory distress syndrome characterized by uncontrolled inflammation resulting in high mortality rates among patients. In current study we used the hydrochloric acid (HCl)-induced lung injury model to mimic the conditions of gastric aspiration. Here we tested whether human mesenchymal stem cells from bone marrow (MSCs), known for their anti-inflammatory and immune-modulatory properties, could prevent the decline in lung function by reducing inflammation in the lungs of injured mice.

III.1.3 Methods

HCl was administered via tracheal intubation in 0.3% NaCl into BALB/C mice. Immediately after the injury the animals received intraperitoneal (IP) or intravenous (IV) injections of human MSCs (3 million in Hanks Balanced Salt Solution) or recombinant human TSG-6 protein or vehicle alone. Lung function was monitored by pulse-oximetry until day 4 post-injury. Infiltration of alveolar spaces by inflammatory cells was evaluated by flow-cytometry of bronchoalveolar lavage (BALF). ELISAs were used to

determine concentrations of pro-and anti-inflammatory markers in BALF.

III.1.4 Results

Injury with HCl resulted in sharp decline in gas exchange function as assayed by pulse oximetry. There was a significant drop in the arterial oxygen saturation (SpO_2) levels within 4 hours post-injury, accompanied by significant decrease in heart and breath rates. The changes corresponded to the development of inflammation in the lungs including increases in protein content, amount of infiltrating cells in BALF, and increase in IL6. Intraperitoneal but not intravenous administration of human MSCs prevented decrease of SpO_2 levels below 90%. Both intraperitoneal administration of MSCs and recombinant human TSG-6 significantly reduced total number of infiltrating cells and pro-inflammatory cytokines such as IL6, TNF-α, and CXCL-1 in alveolar spaces.

III.1.5 Conclusions

Intraperitoneal administration of human MSCs prevented decline in lung function and reduced inflammation in mice injured with HCl. Intravenous administration of MSCs failed to produce beneficial effect while administration of human recombinant TSG-6 resulted in inhibition of inflammation in the lungs but did not improve their function.

III.2 Introduction

Acute respiratory distress syndrome is clinically defined by acute onset, bilateral lung opacities, not explained by other factors, respiratory failure of non-cardiogenic

origin, and decreased oxygenation, according to the most recent Berlin classification [129]. Former classification identified ARDS as a severe form of acute lung injury, which had similar definition with lesser extent of reduced oxygenation [130]. Acute respiratory distress syndrome is one of the leading causes in for ICU hospitalizations. Approximately 190,000 patients are hospitalized with ARDS annually with 3.6 million hospital days [131]. The mortality rates for patients with ARDS were estimated to be around 20% in 2005-2006, according to the most recent ARDS Network clinical trials [132].

Various factors can cause ARDS, most common include bacterial pneumonia, sepsis, aspiration of gastric contents and shock [133]. The major underlying pathological mechanism of ARDS is damage to alveolar epithelium either directly from pathogenic factors, such as bacteria or microbial products [134] or by effectors of inflammatory pathways such as neutrophils [135] or platelets [136]. The damage is followed by activation of innate immune system in the lungs and the production of pro-inflammatory cytokines such as TNF-α, IL6 and others. This in turn increases vascular permeability, causing alveolar edema and recruiting immune cells from systemic circulation. The inflammatory response, initially directed to clear the alveolar spaces from the injury becomes excessive and uncontrolled and exacerbates the injury [137].

Clinically, ARDS progresses through several phases that correspond to the development or resolution of underlying inflammation [138]. The early exudative phase is characterized by edema and the development of hallmark hyaline membranes, that

consist mostly of fibrin and detritus. Interstitial inflammation develops concomitant with the appearance of hyaline membranes ultimately progressing into interstitial fibrosis. Inflammation, disruption of alveolar-capillary barrier and edema cause the progression of hypoxemia. The resolution of ALI and ARDS involves proliferation of fibroblasts and regeneration of alveolar epithelium during proliferative phase, which progresses into fibrotic stage characterized by the development of collagen deposits.

Despite significant research in ARDS, only two therapeutic approaches were shown to be effective in reducing the mortality to 26% from 40% - protective low-tidal volume ventilation and fluid conservation therapy [133]. Therefore, there is a need for novel and effective therapeutic approaches.

Recently, human mesenchymal stem cell (MSCs) emerged as potential therapeutic option for treatment of ALI and ARDS. Thus, human MSCs and their products were beneficial in pre-clinical studies of LPS-induced lung injury in mice [59], [86], [139] and in ex-vivo perfused human lungs [140], bleomycin-induced lung injury [18], [94] and ventilator -induced lung injury [141].

The results from these and other studies indicated that human MSCs are being activated in vivo by signals and factors from injured tissues. This activation leads to production of various factors many of which have anti-inflammatory and immunomodulatory activity (reviewed in [62]). TNF-α-stimulated gene/protein 6 (TSG-6) was identified among other factors produced by activated MSCs [54]. TSG-6 is 35 kDa protein originally identified in TNF-α stimulated fibroblasts [142]. It is a potent

anti-inflammatory mediator and its production by MSCs has been shown to partially explain their beneficial effects in models of myocardial infarction [54], corneal injury [91] and lung injury by LPS [86].

Despite the large scope of investigation, the effects of human MSCs have not been studied in models of HCl-induced lung injury. This model mimics the condition known in humans as aspiration-induced lung injury, where alveolar and bronchial epithelium is being injured by acid contents of gastric juice [143]. This condition is acknowledged as one of the leading causes of ARDS [133] and leads to the series of inflammatory events in the lungs described above.

Here, we test the effects of MSCs and human recombinant TSG-6 in a model HCl-induced lung injury. We evaluated the effect of MSCs and TSG-6 on lung function after the injury by pulse-oximetry assay and inflammation by cytokine ELISA assay.

The results demonstrated beneficial effects on lung function and inflammation if MSCs are administered intraperitoneally immediately after the insult with HCl. Human recombinant TSG-6 was shown to improve inflammation in the lungs.

III.3 Material and methods

III.3.1 Mesenchymal stem cells

Mesenchymal stem cells were obtained from the Center for the Preparation and Distribution of Adult Stem Cells (http://medicine.tamhsc.edu/irm/MSCs-distribution.html) Human MSCs were isolated were prepared as previously described [144]. In brief, after thawing about 1 million passage 1 MSCs were plated in complete

culture medium (CCM) consisting of α-minimum essential medium (MEM, Gibco, Grand Island, NY), 17% fetal bovine serum (FBS, Atlanta Biologicals, Lawrenceville, GA), 100 units/mL penicillin (Gibco), 100 mg/mL streptomycin (Gibco), and 2 mM L-glutamine (Gibco) on a 152 cm^2 culture dish (Corning, Acton, MA) for 24 hours. Cells were washed with phosphate buffered saline (PBS) and the adherent viable cells were harvested using 0.25% trypsin and 1 mM ethylenediaminetetraacetic acid (EDTA, Gibco) for 3–4 minutes at 37°C, reseeded at 100–200 cells/cm^2 in CCM and incubated for 6–7 days (with medium change every 2-3 days) before freezing in αMEM containing 30% FBS and 5% dimethylsulfoxide (Sigma, St. Louis, MO). For the experiments, the cells were recovered as passage 2, cultured for 24 hours, and replated at 100–200 cells/cm^2. The cells were cultured for 6–7 days and harvested with trypsin-EDTA, washed once in Hanks Balanced Salt Solution (HBSS, Lonza, Basel, Switzerland) containing 0.1% FBS and then again washed with serum-free HBSS. The cells were finally reconstituted at 1 x 10^4 cells/μl to a total amount of 0.3–3 x 10^6 cells in serum-free HBSS and kept on ice for the injections.

III.3.2 Animals

An animal use protocol was approved by the Texas A&M Health Science Center Institutional Animal Care and Use Committee at Scott and White Hospital. Male 6- to 8-wk-old wild-type (BALB/c) mice obtained from Jackson Laboratories were used for this study. The mice were kept on a 12-h light-dark cycle and fed and watered ad libitum.

III.3.3 Hydrochloric-induced lung injury

Hydrochloric acid (HCl, Sigma-Aldrich) at pH 1.2-1.5 was prepared by slowly adding its concentrated stock solution to 0.3% NaCl (Sigma-Aldrich). The level of acidity was monitored by table-top pH-meter (VWR), that was appropriately calibrated to include the range of pH at 1.3-1.5. The HCl solutions were then filtered via 0.22 micron filter (VWR), aliquoted in sterile tubes and stored at room temperature until the administration into animals. Random tubes of HCl were tested for the acidity before the animal experiment to ensure the pH.

The administration of hydrochloric acid was performed via intubation as previously described [145]. In brief, mice were anesthetized with isoflurane to reach the level of deep anesthesia and placed on the intubation stand facing upward at approximately 45°. With the aid of external light source the trachea was intubated with a 22-G plastic sterile IV catheter (Terumo). Hydrochloric acid or 0.3% sodium chloride alone (sham injury) was instilled through a catheter at volume 4 µl/g body weight in two sets.

At 15 minutes after the injury mice received one of the following treatments: recombinant human TSG-6 (R&D Systems) (50 µg in 50 – 150 µl of sterile PBS) intravenously, human MSCs (250,000-750,000 in 100 µl of HBSS) intravenously or human MSCs (3,000,000 in 300 µl of HBSS) intraperitoneally or appropriate vehicle control.

III.3.4 Blood, tissue and bronchoalveolar lavage fluid collection

Mice were deeply anesthetized with isoflurane and euthanized by intraperitoneal injections of ketamine-xylazine solution at 80 and 8 mg/kg body weight, respectively. Blood, tissue and bronchoalveolar lavage was collected as described in [145]. In brief, blood was collected first from the right heart ventricle into clotting-activator-coated tube (Terumo Medical, Somerset, NJ) and used to prepare serum by centrifuging the tube at 1,500 g for 10 min. To collect bronchoalveolar lavage fluid the lungs were flushed with PBS via 20-G plastic iv catheter placed inside the trachea (Exelint, LosAngeles, CA). Two sets of lavage were obtained. The first set, collected by flushing the lungs with 800 µl of PBS was used for cytokine analysis, while second set, collected by flushing the lungs with 4 ml of PBS was used for cellular analysis and flow cytometry. The lavage fluid was centrifuged at 500 g for 10 min at 4°C to obtain a cell pellet and then spun again at 10,000 g for 10 min to prepare for cytokine analysis. Red blood cells were depleted by incubating the pellets at room temperature with red blood cell lysis buffer (eBioscience, San Diego, CA) for 5 min and then washing with ice-cold PBS twice. The cell pellet was then resuspended in PBS with 1% bovine serum albumin (BSA) (Thermo Fisher Scientific) and used for flow cytometry analysis. The lungs were collected immediately after obtaining BALF, frozen and stored in -80°C.

III.3.5 Flow cytometry

The flow cytometry was performed as previously described [145]. Briefly, the non-specific binding to Fc-receptors was blocked by with anti-CD16/32 antibody

(eBioscience) at concentration 0.5 μg per $1x10^6$ cells in 100 μl of PBS with 1% BSA. The cells were then incubated for 20 min at room temperature with both phycoerythrin-Cy7-conjugated anti-mouse F4/80 antibody (eBioscience) and FITC-conjugated anti-Ly-6G antibody (BD Pharmingen, San Diego, CA) at concentration of 1 μg per $1x10^6$ cells in 100 μl of PBS with 1% BSA. Isotype-matching antibodies at similar concentrations obtained from the same manufacturers and single-color labeling were used as controls for the specificity of labeling. After two washes in PBS, the cells were again resuspended in PBS-1% BSA and analyzed by FC500 flow cytometer (Beckman Coulter, Brea, CA) to determine macrophage (F4/80-positive) and neutrophil (Ly-6G-positive) populations.

III.3.6 Cytokine ELISA in BALF

Cytokine ELISAs in BALF was performed as previously described [145]. In brief, lung protein concentration was determined by using Micro BCA Protein Assay Kit (ThermoFisher Scientific) according to the manufacturer's instructions. Cytokine concentrations were determined by using commercially available ELISA kits for detection of IL-6, TNF-α, IL-1, CCL2/MCP-1, CCL3/MIP-1α, CXCL2/MIP-2, and CXCL1/KC (R&D Systems, Minneapolis, MN) according to the manufacturer's instructions.

III.3.7 Pulse oximetry

Pulse oximetry was performed as previously described [145] using portable mouse pulse oximeter (STARR Life Sciences). Briefly, the collars of experimental

animals were trimmed and extra-small MouseOX collar clip was placed on the animal's neck. SpO_2, heart and breath rates were recorded during "calm" phase [145] at 15-Hz sample rate. The measurements and data extraction and analysis was performed as described before [145].

III.3.8 Statistical analysis

GraphPad Prism software (LaJoia, CA) was used to perform unpaired t-test, one-way ANOVA with Bonferroni's post hoc analysis or log-rank Mantel-Cox test for survival proportions. Null hypotheses were rejected at P values less than 0.05.

III.4 Results

III.4.1 Acidity of HCl solution affects functional outcome after the injury

Acute lung injury in mice was produced by intratracheal instillation of HCl in 0.3% NaCl with pH range of 1.3-1.5. There was a marked difference in survival rate between pH 1.3 and other groups (Fig. 9A). The harshest condition was pH 1.3, where none of the injured animals survived after 24 hours mark. In contrast, animals injured with HCl at pH 1.5 did not show mortality until 3 days after the injury. Furthermore, only 40% of the animals injured with HCl at pH 1.4 survived past 24 hours.

Oxygen saturation levels dropped significantly in the first 8 hours in all groups with the most dramatic drop in pH 1.3 group. These changes were accompanied by pronounced reduction in heart (Fig. 9C) and breath rates (Fig. 9D). The SpO_2 values gradually returned to normal around day 3, while heart and breath rates recovered by day 2 in all groups. No significant changes in SpO_2, heart and breath rates were observed in

control group instilled with 0.3% NaCl.

We chose HCl with pH 1.5 for further experiments because it decreased SpO_2 without affecting survival in the first 24 hours.

Figure 9. Functional changes in hydrochloric acid (HCl)-induced lung injury. HCl in 0.3% NaCl with pH range of 1.3-1.5 was instilled via intubation into the lungs of adult male Balb/C mice. Pulse oximetry was performed over the course of 5 days. (A) Survival rate of mice injured with HCl at indicated pH. Dynamics of oxygen saturation levels (B), heart rate (C) and breath rate (D) after the injury with HCl at indicated pH. Number of animals within each group range between 3 to 6. The values represent arithmetic mean or individual data points, error bars – SEM.

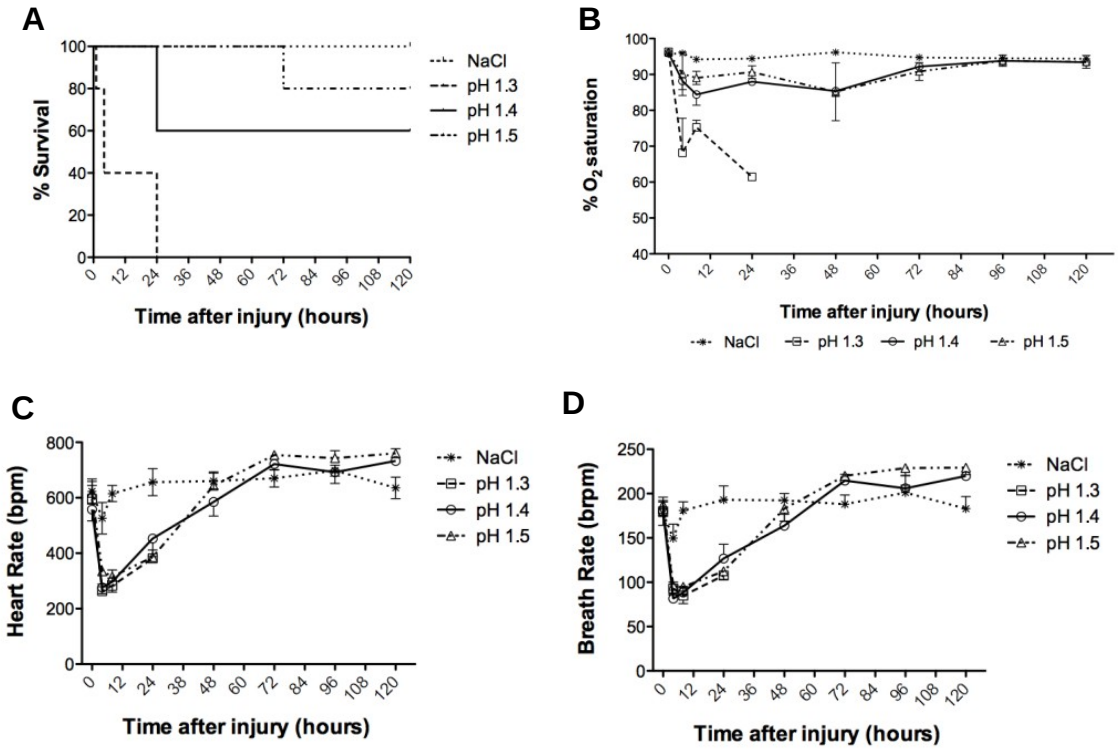

Figure 10. Dynamic changes in BALF following injury with HCl pH 1.5. (A) Total cells, F4/80 positive macrophages and Ly6G-positive neutrophils in BALF after injury with HCl at pH 1.5 (B). Total protein, (C) IL-6 cytokine and (D) IL-10 cytokine levels after HCl injury. Number of animals within each group range between 3 to 6. The values represent arithmetic mean or individual data points, error bars – SEM. * p <0.05, **, p<0.01

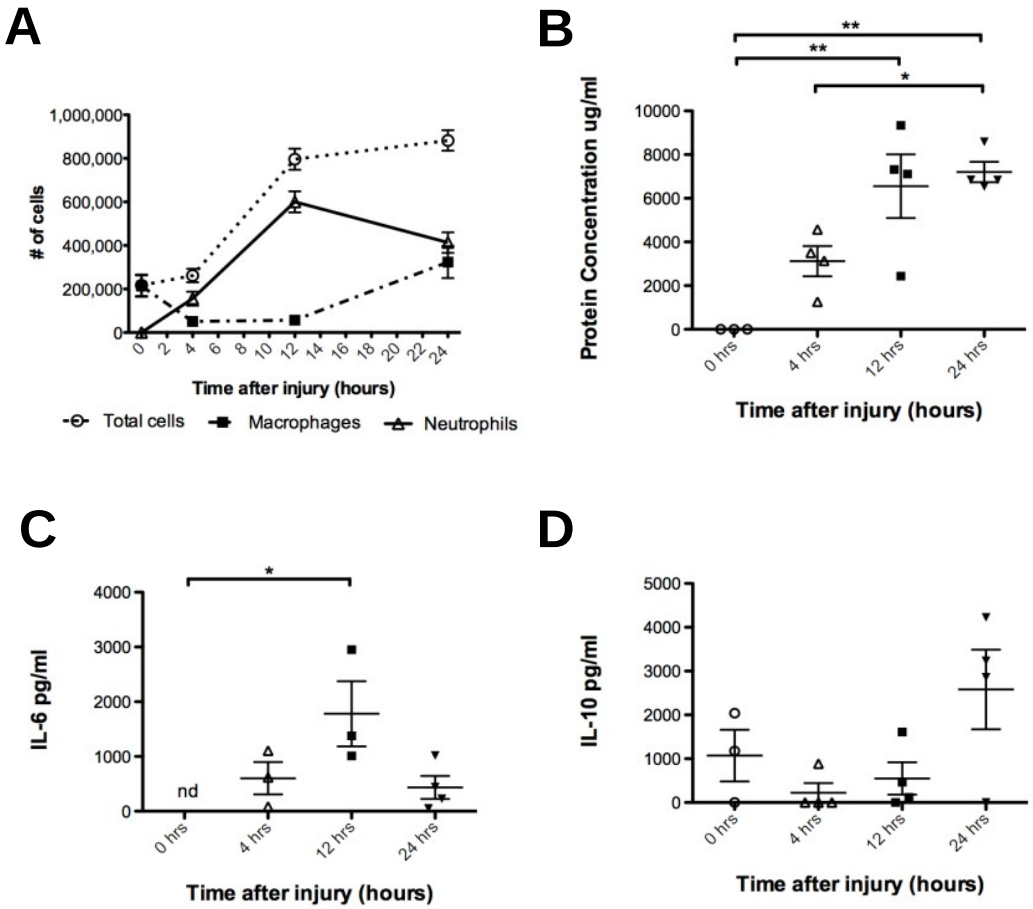

III.4.2 Dynamic changes in BALF following injury with HCl pH 1.5

Following the injury with HCl pH 1.5 we observed increase in total BAL cell number at 4 – 24 hours post injury and highest number of neutrophils at 12 hours (Fig. 10A). Macrophages decreased initially but then gradually increased between 12 – 24 hours (Fig. 10A). Likewise, the highest protein concentration (Fig. 10B) and IL-6 (Fig. 10C) cytokine expression were observed at 12 hrs, while IL-10 (Fig. 10D) levels were lowest at the same time point and increased at 24 hours after the onset of the injury.

III.4.3 Intraperitoneal but not intravenous administration of human MSCs alleviates HCl-induced lung injury

Human MSCs were administered immediately following the injury with HCl. Administration of 3 x 10^6 human MSCs inreaperitoneally resulted in significant improvement in oxygen saturation levels at 24 hours (Fig. 11A). However, mice injected intravenously with various doses of MSCs did not show any improvement in oxygen saturation levels over control group (Fig. 11B).

Analysis of bronchial lavage fluid showed significant decrease in BAL total cell number and neutrophils in animals at 24 hours after administration of MSCs intraperitoneally (Figs. 12A and B). Proinflammatory cytokines TNF-α, IL6 and KC were also reduced in animals after intraperitoneal administration of MSCs (Figs. 12C, D and E). Intravenous administration of MSCs, however, did not have an effect neither on total cells nor neutrophils in BAL (Fig. 13).

Figure 11. Effect of IP and IV administration of human MSCs on SpO_2. Timecourse of SpO_2 changes after administration of human MSCs IP (A) or IV (B).The values are arithmetic mean or individual data points, error bars – SEM. ***, $p<0.001$ at 24 hours between HCL/MSCs and HCL/HBSS groups, ns- non significant changes between HCL/MSCs and HCL/HBSS groups

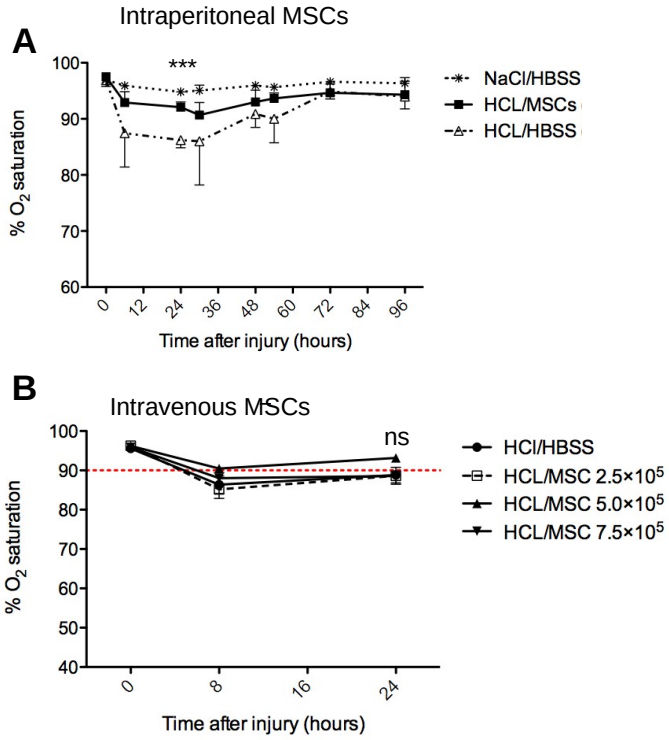

Figure 12. Intraperitoneal MSCs administration reduces inflammation in the lungs. Total cells (A), neutrophils (B) and cytokines TNF-α (C), IL6 (D) and KC/CXCL1 (E) in BAL at 24 hours after the injury with HCl and administration of MSCs intraperitoneally.

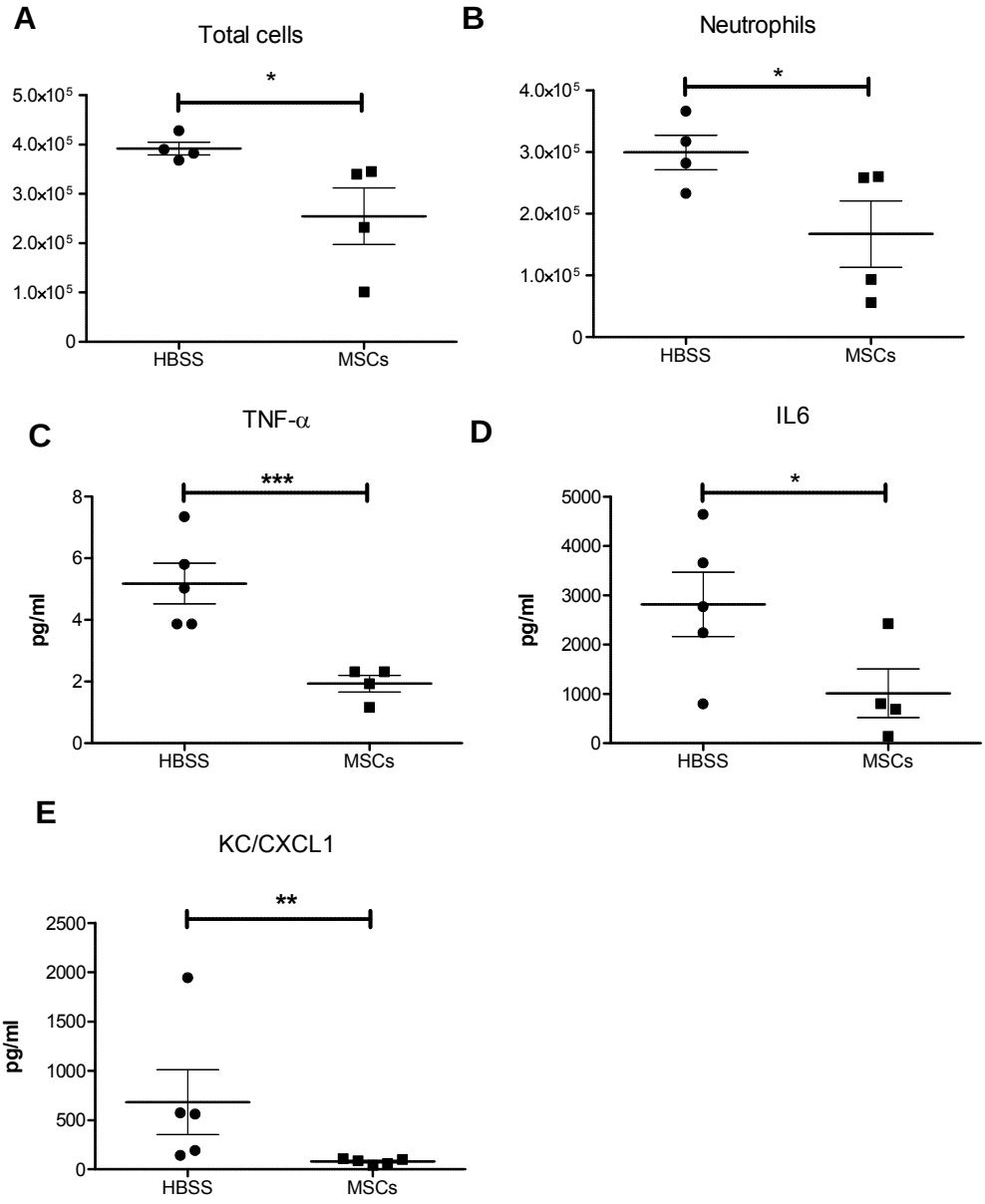

Figure 13. Effect of intravenous administration of MSCs on inflammation in the lungs. Total cells (A) and neutrophils (B) in BAL at 24 hours after the injury with HCl and administration of MSCs intravenously.

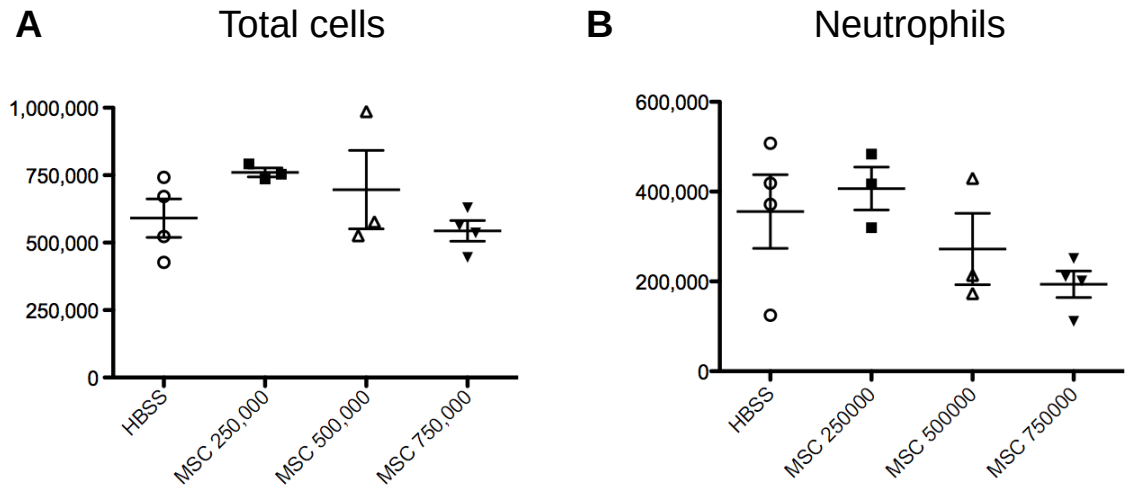

III.4.4 Systemic administration of TSG-6 inhibits inflammation in the HCl-injured lungs

Animals injured with HCl pH 1.5 were treated with TSG-6 protein (50 μg) administered intravenously immediately after injury. Control animals received sham PBS.

There were no significant differences in oxygen saturation levels between TSG-6 treated and control groups at any timepoint after its administration (Fig. 14A). However, there was a significant decrease of total number of cells (Fig. 14B) and neutrophils (Fig. 14C) in BALF at 24 hours in TSG-6 treated animals when compared to controls.

Figure 14. Effect of TSG-6 treatment on SpO_2 and inflammation in the lungs. (A) Dynamics of SpO_2 levels (B) Total cells, (C) Macrophages and (D) Neutrophils in BALF at 24 hours after the injury and TSG-6 administration

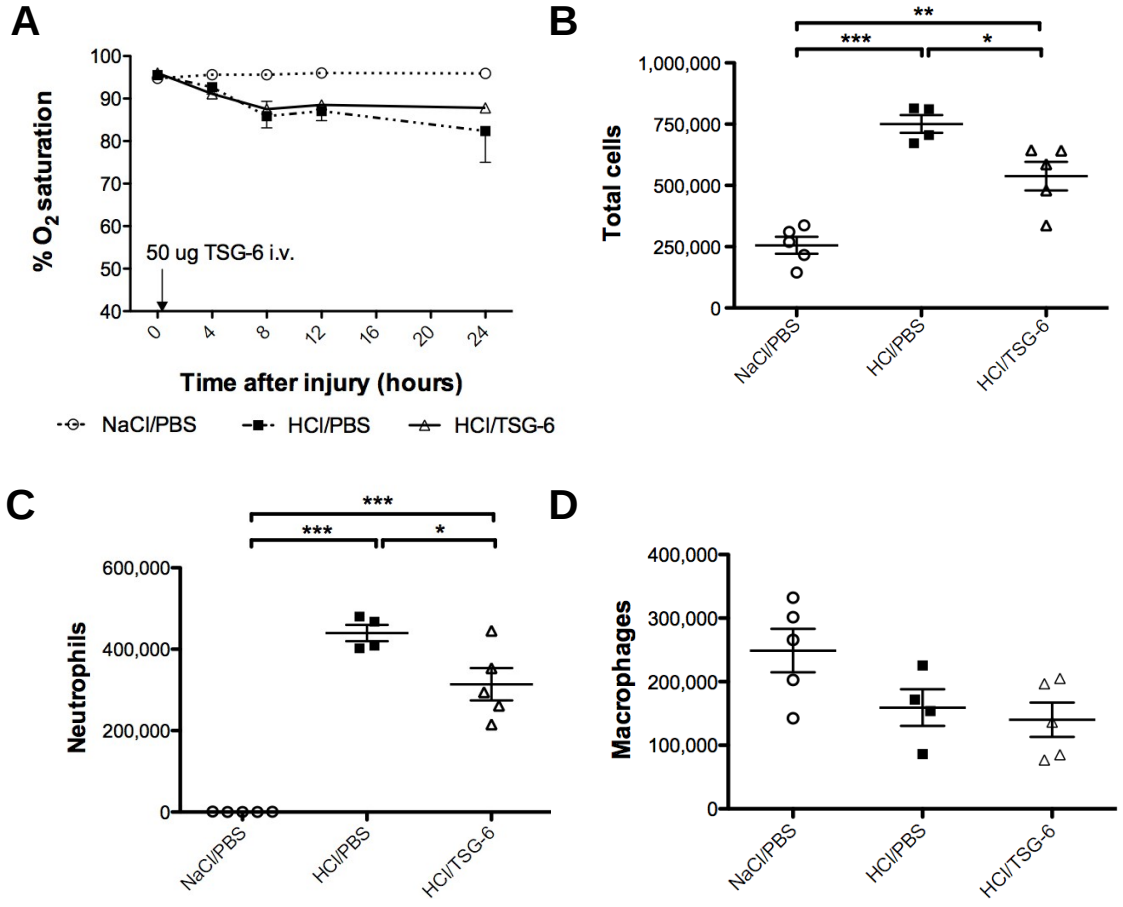

III. 5 Discussion

Acute respiratory distress syndrome is important clinical condition because of high hospitalization, mortality rate and associated health care cost. Currently, there are only two effective therapeutic options that result in reduction in mortality rates: low-tidal volume ventilation and fluid conservation therapy. Together their implementation into

clinical practice reduced the mortality from 40% to 20% in the past decade [133]. Therefore there is a need for therapeutic intervention that will decrease the mortality rate below 20%.

Human MSCs represent viable therapeutic option for ARDS due to their recently discovered anti-inflammatory and immunomodulatory capabilities. Their potential has been demonstrated in various pre-clinical studies [146] and appears to be linked to their activation by the signals from injured tissues to produce anti-inflammatory factors [62].

Here we tested the effects of human MSCs and their secreted protein TSG-6 in a model of HCl-induced lung injury. We used conscious pulse-oximetry as described [145] to evaluate the progression of injury and optimize the acidity of the HCl solution. Among different strengths of the HCl solutions tested pH 1.5 caused sufficient decrease in oxygen saturation levels without causing mortality early during the injury. This strength of HCl was used throughout the study. The dynamic of changes in oxygen saturation levels co-coincided with the changes in BAL. Thus, the peak of cellular infiltration was observed at lowest SpO_2 readings. Surprisingly we observed rapid decline in breathing and heart rate within 30 minutes after the injury.

We used two modes of delivery to test the effect of MSCs. Surprisingly intravenous administration of MSCs immediately after the injury failed to have a beneficial effect on lung function or inflammation. However, intraperitoneal administration of MSCs prevented the drop in SpO_2 levels and reduced the infiltration of neutrophils in the lungs. This finding contradicts results from the studies that showed

positive effects of intravenous MSCs in other models of injury [18], [86], [94], [140]. The discrepancy could be explained by several factors.

First, it has been shown that intravenously injected MSCs get trapped in the microvasculature within minutes after the administration [54], [147], [148]. Moreover, high doses of MSCs caused mortality in the injected mice. HCl directly injures airways which creates large unventilated areas of the lungs, due to compensatory perfusion/ventilation changes [143]. This mechanism is different from other types of injury where lung epithelial or endothelial cells are indirectly injured due to up-regulation of pro-inflammatory pathways. Hence intravenously administered MSCs embolize lung microvasculature in unaffected areas increases overall damage to the lungs.

Second, intraperitoneally administered MSCs are activated in a similar manner to intravenously-injected cells and are able to upregulate genes responsible for the production of anti-inflammatory factors such as TSG-6, PGE_2 and others [65]. This probably explains in part the beneficial effects of MSCs in the model as well as others where intraperitoneally injected MSCs have been shown to be as effective as the intravenous route [86], [91], [95], [149].

Finally, only one donor of MSCs has been tested in this study. The variation between MSCs donors in terms of their activity to produce anti-inflammatory factor TSG-6 has been recently shown by Lee at al. [38]. Donors with lower levels of TSG-6 production performed poorly in models of corneal injury, bleomycin induced lung injury

and zymosan-induced peritonitis. Therefore, donor variability could have contribute to the negative effect of MSCs in this study.

The finding that human recombinant TSG-6 reduced the inflammation in the lungs support previous observations of its effectiveness in models of LPS- and bleomycin induced lung injury [86], [145].

Acute respiratory distress syndrome still remains one of the major causes for hospitalization and has high mortality rate. Present therapeutic options alone are not sufficient in reducing the rate of mortality. The results presented in this study demonstrate the effectiveness of MSCs treatment in reducing inflammation and preventing functional decline in a model of aspiration-induced lung injury. Further studies are necessary to evaluate the mechanism of MSCs and TSG-6 action.

CHAPTER IV

INTRAPERITONEALLY INFUSED HUMAN MSCs FORM AGGREGATES WITH MOUSE MACROPHAGES AND B220+ CELLS LIMITING THEIR ACCESS TO LYMPHATICS BUT PRECONDITION THE MOUSE IMMUNITY

IV.1 Overview

Mesenchymal stem/progenitor cells (MSCs) have shown beneficial effects in many models of diseases in part by modulating excessive inflammatory and immune responses. Frequently the beneficial effects of MSCs persist long after their disappearance from host tissues, suggesting that MSCs interact with intermediate cells in the host that relay or amplify their effects. The cells have usually been injected intravenously (IV) but beneficial effects have also been reported with intraperitoneally (IP) injected MSCs; however, it was not clear how the cells entered the immune system from the peritoneum. Here, the fate of the human MSCs injected IP into immune-competent mice was studied. Within 20 minutes, individual MSCs were no longer detected in peritoneal lavage fluid. Instead they were recovered as aggregates of varying size that contained mouse macrophages and a few B220+ lymphocytes. After 1 day most, of the aggregates containing live MSCs were attached to sites throughout the peritoneal cavity including the omentum and mesentery. Less than 0.05% of the live injected cells were detected in spleen and jejunal lymph nodes. In all locations, MSCs co-localized with mouse macrophages and B220+ lymphocytes. Attachment to omentum

and mesentery was accompanied by the recruitment of immune cells and changes in the production of a series of mouse cytokines. Moreover, the cytokine response to LPS was markedly enhanced in mice preconditioned by IP administration of MSCs 3 days earlier. In effect, the aggregation of IP injected MSCs limited their direct access to the lymphatic system but did not prevent them from preconditioning the immune system.

IV.2 Introduction

Human mesenchymal stem/progenitor cells (MSCs) from bone marrow, adipose tissues, placenta, umbilical cord and other tissues are currently being administered to large numbers of patients. Over 100 clinical trials with MSCs have been registered [150], and five have reached the Phase II or III stage of development [151]. In essentially all the clinical trials and in most experiments in animal models, the cells were administered by intravenous (IV) injection. However, there has also been interest in administration by injection into the peritoneum (IP) [152]–[154]. One advantage of IP injection is that it avoids the highly efficient trapping of the cells in the lung observed with IV injection, trapping that can produce emboli phenomena injuring the lung or even causing death as seen in mice [54]. Also IP injection allows for the administration of larger numbers of the cells. In addition, in direct comparisons with IV administrations, IP injected MSCs were shown to have comparable or even more profound effects in experimental autoimmune encephalitis [149], twitcher mice with globoid cell leukodystrophy [155], mice with cisplatin-induced renal injury [156], mice with experimental intestinal colitis [95], mice with sterile inflammation of the cornea [91],

and mice with zymosan-induced peritonitis [87]. The beneficial effects of MSCs in these and other disease models have been linked to the ability of the cells to modify both the innate and acquired immune systems [25], [157].

The peritoneal cavity provides an unusual setting for immune interactions because it is primed to respond rapidly to bacteria that may be released by intestinal spillage and allergens such as worms that enter the gastro-intestinal tract. The rapidity of the response is obviously critical. It is mediated by at least two special classes of cells. One special class is the B-1ymphocytes, particularly B-1b lymphocytes, found in the peritoneal cavity and other sites such as the omentum that contain an unusual repertoire of receptors that allow them to mount an immediate antibody response to bacteria without being part of the adaptive immune system [158]. The second special class is small cells that are found in mesentery and some other locations in the body and that are triggered by worms and other allergens to mount a rapid Th2 response. The cells are lineage negative and referred to as nuocytes and several other terms [159]–[163]. The cells generate an innate T-helper 2 (Th2) response characterized by secretion of interleukin 4 (IL4) that facilitates production of immunoglobulin (Ig) G_1 and IgE, and by secretion of interleukin 13 (IL13) that contributes to epithelial hypertrophy and recruitment of eosinophils - characteristics of allergic responses [159], [162].

The peritoneal cavity is also an unusual setting for entry into the immune system, because it participates in dynamic exchange of the fluids and cells between the cavity and both the lymphatic system and the general circulation. The exchange occurs through

three or four portals that breach the tight layer of basement membrane and mesothelial cells that forms the peritoneal membrane and that covers all the organs and the walls of the abdomen: (a) “milky spots” that are opaque, highly vascularized clusters of cells on the surface of the omentum, the fatty organ that straddles the spleen, stomach and other organs of the upper abdomen in mice but covers a much more extensive area in man; (b) the draining lymphatic system contained in the stalk of mesenteric arteries and veins that supplies the gastrointestinal tract and in the walls of the peritoneal cavity; (c) punctate regions called lymphatic stomata on the underside of the diaphragm; and (d) the newly discovered small cells in the mesentery and other tissues that mount a rapid Th2 response [159]–[163]. The milky spots of the omentum [163], [164] contain clusters of macrophages and B1 lymphocytes that are similar to the free-floating macrophages and B1 lymphocytes of the peritoneal cavity. The milky spots readily exchange particulate matter and cells between the peritoneal cavity and the general circulation. They may [165] or may not [164] contain resident dendritic cells that can activate lymphocytes, but they can recruit T cells activated at other sites. The draining lymphatics of the mesenteric stalk and peritoneal wall absorb particles from the gastrointestinal tract and both particles and cells from the peritoneal cavity. The lymphatic stomata on the underside of the diaphragm consist of a thin layer of cuboidal cells that overlay large lacunae of lymphatic vessels [166], [167]. The lacunae drain primarily into mediastinal lymph nodes and then to the thoracic duct and eventually the left subclavian vein.

In exploring the fate of MSCs injected into the peritoneal cavity, several groups

of investigators observed engraftment of the cells not only into the peritoneum but also into multiple distal organs [96], [97]. However, the route the cells traveled was not defined. In initial efforts to follow the fate of human MSCs injected into the peritoneum, we recently reported [65] that some of the MSCs aggregated and compacted into spheres similar to the spheres formed after the cells were cultured in hanging drops. Here we report that after IP administration of MSCs into immunocompetent mice, the cells rapidly formed aggregates with macrophages and a few B220+ cells. The aggregates were initially recovered in the peritoneal lavage fluid but then they slowly attached to milky spots in the omentum and to regions of the mesentery. Apparently because of the large size of the aggregates, few of the MSCs appeared in mesenteric lymphatic nodes, a route previously shown to be favored by IP injected splenocytes [168]. The MSCs disappeared in less than a week but prompted recruitment of cells to the omentum and peritoneal cavity that secreted both pro- and anti-immune mouse cytokines. The results indicated therefore that IP injection of MSCs offers an unusual route to the immune system in which the cells are first assembled into aggregates with macrophages and B220+ cells. The large size of the aggregates apparently gives them limited direct access to the lymphatic system but the aggregates precondition the immune system either as free-floating entities in the peritoneal cavity or bound to the omentum and sites in the mesenteric membranes throughout the peritoneal cavity.

IV.3 Materials and methods

IV.3.1 Human Mesenchymal Stem Cell Culture

Passage 1 wild-type MSCs and passage 4 Green-Fluorescent Protein expressing MSCs (GFP-MSCs) were obtained as frozen vials from the Center for the Preparation and Distribution of Adult Stem Cells (http://medicine.tamhsc.edu/irm/MSCs-distribution.html). Human MSCs (donors 7075, 7068, and 7032) were isolated from bone marrow aspirates and cultured as previously described [144]. In vitro growth, differentiation, clonogenicity and epitope markers of MSCs preparations are summarized in Table B-1 according to Reger and Prockop [169]. For the experiments described here, a frozen vial of about 1 million passage 1 MSCs was plated in complete culture medium (CCM) consisting of α-minimum essential medium (MEM, Gibco, Grand Island, NY), 17% fetal bovine serum (FBS, Atlanta Biologicals, Lawrenceville, GA), 100 units/mL penicillin (Gibco), 100 mg/mL streptomycin (Gibco), and 2 mM L-glutamine (Gibco) on a 152 cm^2 culture dish (Corning, Acton, MA) for 24 hours. Cells were washed with phosphate buffered saline (PBS) and the adherent viable cells were harvested using 0.25% trypsin and 1 mM ethylenediaminetetraacetic acid (EDTA, Gibco) for 3–4 minutes at 37°C, reseeded at 100–200 cells/cm^2 in CCM and incubated for 6–7 days (with medium change every 2-3 days) before freezing in αMEM containing 30% FBS and 5% dimethylsulfoxide (Sigma, St. Louis, MO). For the *in vivo* experiments, the cells were recovered as passage 2 (MSCs) and passage 5 (GFP-MSCs), cultured for 24 hours, and replated at 100–200 cells/cm^2. The cells were cultured for 6–7 days and harvested

with trypsin-EDTA, washed once in Hanks Balanced Salt Solution (HBSS, Lonza, Basel, Switzerland) containing 0.1% FBS and then again washed with serum-free HBSS. The cells were finally reconstituted at 1 x 10^4 cells/µl to a total amount of 0.3–3 x 10^6 cells in serum-free HBSS and kept on ice for the injections.

IV.3.2 Single GFP cell measurements in peritoneal cavity

All animal procedures were approved by the Animal Care and Use Committee of Texas A&M University Health Science Center and in accordance with guidelines set forth by the National Institutes of Health.

Male 6 week-old BALB/c mice (Jackson Laboratories, West Grove, PA) were injected IP with 3 x 10^6 GFP-MSCs. At 1 minute, 20 minutes, 4 hours and 72 hours after the administration of MSCs, mice were euthanized by cervical dislocation under deep anesthesia and peritoneal lavage was collected by injecting 5 ml of PBS into the peritoneal cavity followed by harvesting the lavage with a pipette. Ten microliters of the lavage were then placed directly in Neubauer hemocytometer in duplicate and fluorescent and brightfield images were taken using inverted Nikon Eclipse Ti-S microscope (Nikon). The "Analyze Particles" plugin for ImageJ software was used to count total and GFP-positive cells.

IV.3.3 Immunofluorescence of free-floating aggregates

Free-floating GFP+ aggregates were picked with tweezers from the peritoneal cavity 24 hours after the IP injection of GFP-MSCs. The aggregates were washed twice with PBS, and fixed with 2% paraformaldehyde (Affymetrix, Santa Clara, CA) in PBS

for 2 hours. The fixed aggregates were washed twice with PBS, centrifuged at 500 x g for 5 minutes, and incubated at 4°C overnight in 1 mL of 30% sucrose (Sigma) in 0.1 M phosphate buffer (Sigma). After 24 hours, the aggregates were collected in 800 µL of 50% OCT (Sakura Finetek, Torrance, CA) and transferred into a histology mold. The mold was frozen in isopentane (Sigma), chilled by liquid nitrogen and stored at -80°C. Cryosections (6 µm) were prepared with a Microm HM560 cryostat and incubated for 20 minutes at room temperature before storing at -80°C. For the immunfluorescent staining, sections were equilibrated to room temperature, fixed again for 10 minutes in 2% paraformaldehyde and washed twice in Tris-Buffered Saline with Tween (TBST, Cell Signaling, Beverly, MA). Nonspecific antibody binding was blocked by incubating samples for 45 minutes in TBST supplemented with 5% BSA (Thermo Fisher Scientific, Whaltman, MA) and 5% normal serum (Thermo). Following two washes in TBST, samples were incubated for 24 hours at +4°C with primary antibodies to mouse CD11b (catalog #550282;BD Pharmingen, Frankling Lakes, NJ) at 1:100 dilution in blocking solution, or isotype control antibody. Sections were washed three times in TBST, incubated for 1 hour at room temperature with anti-rat Alexa-594 conjugated secondary antibodies (Life Technologies, Grand island, NY) at 2 µg/ml in blocking solution, then counterstained with 0.5 µg/ml of 4,6-diamidino-2-phenylindole (DAPI) (Sigma) in PBS for 10 minutes. The sections were washed three times in TBST and mounted in Prolong Gold antifade reagent (Life Technologies) overnight.

IV.3.4 Whole mount immunofluorescence of aggregates in mesentery and omentum

Whole omenta or portions of mesentery with visible GFP+ clusters were removed from peritoneal cavity 24 hours after GFP-MSCs injection, washed twice with PBS, and fixed with 2% paraformaldehyde in PBS for 2 hours. Fixed tissues were washed twice with PBS and blocked by incubation in TBST with 5% BSA and 5% normal serum for 45 minutes at room temperature. Samples were washed twice with TBST, and incubated for 24 hours at +4°C with primary antibody to mouse CD45R (catalog #550286; BD Pharmingen) or isotype control antibody at 1:100 dilution in blocking solution. Tissues were then washed three times in TBST, incubated for 1 hour at room temperature with anti-rat Alexa-594 conjugated secondary antibodies (Life Technologies) at 2 μg/ml in blocking solution, then counterstained with 0.5 μg/ml of DAPI in PBS for 10 minutes. The tissues were placed on a glass slide and covered with a coverslip.

IV.3.5 Immunofluorescent image acquisition and manipulation

Low magnification (1-2x) bright-field and GFP images were captured with a Nikon Digital Sight DS-2Mv camera attached to a SMZ800 dissecting microscope (Nikon, Japan). Illumatool Bright Light Systems LT 9900 (Lightools Research) with a GFP filter set (470 nm excitation and 515 nm emission), was placed under the objective of the microscope to visualize GFP fluorescence. High magnification images were obtained using a Nikon Eclipse 80i upright microscope and processed using NiS Elements AR3.0 software (Nikon, Japan). All image manipulations (merging, brightness

and contrast adjustment) were performed using ImageJ Version 1.49a (NIH, US).

IV.3.6 Real-time PCR for mouse cytokines

Mouse omenta, jejunal lymph nodes, mesentery, spleen and cell pellet that included MSCs aggregates from peritoneal lavage were obtained as described above and flash-frozen in liquid nitrogen. The tissues were homogenized in Trizol lysis buffer (Qiagen, Germany) and total RNA was isolated using RNeasy Lipid Tissue Mini Kit (Qiagen) with DNA digestion step using DNAse (Qiagen). Isolated RNA was quantified using a Nanodrop specrophotometer (Thermo Fisher Scientific) and 0.3 – 2 µg was converted to cDNA with High-Capacity cDNA RT Kit (Applied Biosystems, Foster City, CA). Real-time PCR for mouse *Il10, Il13, Ifng and Ptgs2* was performed using Taqman Gene Expression Assays (Applied Biosystems) and Taqman Fast Master Mix (Applied Biosystems) in triplicate using 20 ng of cDNA in a 20 µl reaction. Real-time PCR reaction was performed with CFX96 Real-Time PCR Detection System (Biorad, Hercules, CA) by incubating the reactions at 95°C for 20 seconds followed by 40 cycles of 95°C for 1 second and 60°C for 20 seconds. Calculated delta-Ct values between gene of interest and *Gapdh* were used to obtain relative expression values ($2^{-\Delta Ct}$).

IV.3.7 Real-time PCR for assay of human cell number

To estimate the total number of human cells in omentum, jejunal lymph nodes, mesentery, spleen and peritoneal lavage, human Glyceraldehyde 3-phosphate dehydrogenase (GAPDH) expression was measured [54], [91]. Standard curves were prepared by combining known amounts of MSCs with tissues and peritoneal resident

cells from naïve BALB/c mice. Total RNA was isolated using RNeasy Lipid Tissue Mini Kit (Qiagen) with DNA digestion step using DNAse (Qiagen). Isolated RNA was quantified using Nanodrop specrophotometer (Thermo Fisher Scientific) and 0.3 – 2 μg was converted to cDNA with High-Capacity cDNA RT Kit (Applied Biosystems, Foster City, CA). Real-time polymerase chain reaction (PCR) for eukaryotic 18S ribosomal RNA and human GAPDH was performed using Taqman Gene Expression Assays (Applied Biosystems) and Taqman Fast Master Mix (Applied Biosystems) in triplicate using 20 ng of cDNA in a 20 μl reaction. Real-time PCR was performed with a CFX96 Real-Time PCR Detection System (Biorad, Hercules, CA) by incubating the reactions at 95°C for 20 seconds followed by 40 cycles of 95°C for 1 second and 60°C for 20 seconds. Delta Ct values between human GAPDH and 18S were calculated and used to generate standard curves (Fig. B-1A). Microsoft Excel was used to perform a non-linear regression fit and obtain formulas for human cell number calculations (Table B-2). Delta Ct values between human GAPDH and eukaryotic 18S were then obtained for samples from MSCs -injected animals and used to calculate total cell numbers based on formulas provided in Table B-2.

IV.3.8 Preparation of dead MSCs

Total of 3 x 10^6 MSCs in HBSS at 1x10^4 cells/μl were frozen by immersion into liquid nitrogen followed by thawing at 37°C. These steps were repeated 3 times. The cells were then placed on ice for injections. The viability of the cells was assayed by trypan blue staining (Gibco) and more than 99% of the cells were positive for uptake of

the dye.

IV.3.9 Whole tissue, blood, and peritoneal lavage fluid collection

Experimental and control mice were euthanized by cervical dislocation under deep anesthesia. The rib cage was opened and blood was collected from the right ventricle of the heart and placed in a tube containing clotting activators (Terumo Medical Corporation, Somerset, NJ) for 20 minutes and then stored on ice until further processing. Serum was separated by centrifugation at 1500 x g for 10 minutes and stored at -80°C until further analysis. To obtain lavage fluid for assays of cytokines, 1 ml of PBS containing Halt Protease inhibitor Cocktail (Thermo) was injected IP, followed by gentle massaging and collection of fluid with a sterile pipette. Complete harvest of the peritoneal cells was obtained by another injection of PBS (5 ml) followed by lavage harvest. The cell suspension from both collections were separately centrifuged at 500 x g for 10 minutes at 4°C. Supernatant from the first wash was further clarified by centrifugation at 10,000 x g for 10 minutes at 4°C, aliquoted and stored for further cytokine analysis at -80°C. The supernatant from the second wash was discarded and cell pellets were combined and homogenized with Trizol lysis buffer (Qiagen, Germany), flash frozen in liquid nitrogen, and stored at -80°C until further processing. Mouse omentum, jejunal lymph nodes, mesentery, and spleen were collected and either flash-frozen in liquid nitrogen for later RNA isolation, or placed in sterile HBSS for enzymatic digestion.

IV.3.10 Assays of cells in omentum

Omenta were excised from the animals and placed in HBSS with calcium- and magnesium-containing 0.8 mg/ml dispase/collagenase, 0.2 mg/ml collagenase P and 0.1 mg/ml DNAse II (Roche Molecular Diagnostics, USA, Pleasanton, CA). The omenta were minced and incubated at 37°C for 60 minutes with gentle pipetting every 15 minutes. The digest was then diluted 10 times with calcium and magnesium-free HBSS, strained via 70 μm nylon mesh and centrifuged at 500 x g for 5 minutes at room temperature. Supernatant was discarded and cell pellet was resuspended in calcium- and magnesium-free HBSS, centrifuged again, resuspended in HBSS containing 2% BSA, followed by cell counting with hemocytometers. The cells were then incubated for 10 min at 4°C with anti-CD16/32 antibody at a concentration 0.5 μg per $1x10^6$ cells in 100 μl (eBioscience) to block nonspecific binding to Fc-receptors. After one wash with PBS supplemented with 1% BSA, the cells were incubated for 20 min at room temperature with fluorescently conjugated antibody against mouse F4/80 (eBioscience), Ly6G, CD19, CD3, CD8, CD45R (BD Pharmingen). The antibodies were used at a concentration of 1 μg per $1x10^6$ cells in 100 μl of PBS- supplemented with 1% BSA. Isotype-matching antibodies at similar concentrations obtained from the same manufacturers and single-color labeling, were used as controls for the specificity of labeling. After two washes in PBS, the cells were resuspended in PBS supplemented with 1% BSA and analyzed by flow cytometer (Model FC500; Beckman Coulter, USA, Brea, CA) to determine macrophage (F4/80-positive), neutrophil (Ly-6G-positive), T-cell

(CD3 or CD8 positive) and B-cell (CD19 or CD45R positive) populations.

IV.3.11 In Vivo Tracking of GFP-MSCs

We used male BALB/c mice that were 6–8 weeks of age and housed on a 12-hour light/dark cycle. Total of 2-3 x 10^6 GFP-MSCs were injected IP with 28G needle under isoflurane anesthesia. At 4, 24, 72 and 168 hours the animals were euthanized and their peritoneal cavities exposed. For the visualization of GFP-MSCs in omentum, the organs were excised from peritoneal cavities and placed on a plate with white background. Lumina IVIS II System (Perkin Elmer, Waltham, MA) was used to obtain fluorescent images of whole peritoneal cavity and individual omenta. Living Image Software version 4.1 (Perkin Elmer) was used for GFP fluorescence analysis. To aid in visualization, the GFP signal was pseudocolored by applying logarithmic grayscale to the whole peritoneal cavity image or by applying reverse logarithmic grayscale to the images of omenta.

IV.3.12 Assays for mouse secreted cytokines

Mouse interleukin (IL) 6, IL10, IL12p70, interferon gamma (IFNγ), monocyte chemotactic protein 1 (MCP1), chemokine (C-X-C motif) ligand 1 (CXCL1), transforming growth factor beta 1 (TGFβ1), and tumor necrosis factor alpha (TNF-α) and prostaglandin E_2 (PGE_2), in peritoneal lavage and/or serum, were assayed with commercial ELISA kits (R&D Systems Inc, Minneapolis, MN). Mouse IL13 was assayed with commercial ELISA kit from Life Technologies. For all assays, optical density was determined on a plate reader (FLUOstar Omega; BMG Labtech, Germany)

at an absorbency of 450 nm with wavelength correction at 540 nm for the optical imperfections on the plate.

IV.3.13 LPS injury model in mice

Male 6 week-old BALB/c mice were injected IP with $3x10^6$ MSCs or dead MSCs, prepared as described above. Sterile HBSS injections were used as controls. At 3 days after the MSCs delivery, the animals were injected with LPS (Sigma) at 0.1 mg/kg of body weight via tail vein. After 3 hours after the administration of LPS, tissues were harvested and lavage fluid collected.

IV.3.14 Data analysis and presentation

When comparing two groups, unpaired *t*-test was used, whereas one-way ANOVA with Bonferroni's post hoc analysis was used in multiple comparisons. One-way ANOVA with Dunett's post-hoc analysis was used to compare groups to a control. Null hypotheses were rejected at *P* values less than 0.05. All statistical analyses and chart preparations were performed with GraphPad Prism 6 software (GraphPad Software, Inc., USA, La Jolla, CA). Curve fitting was performed using Microsoft Excel Software. Images and charts were combined and annotated using Inkscape Software.

IV.4 Results

IV.4.1 Fate of human MSCs in peritoneal cavity

To study the fate of MSCs injected into the peritoneal cavity, 3 x 10^6 GFP-labeled human MSCs were used in wild-type male BALB/C mice. To detect single GFP-labeled cells in the peritoneal cavity, 5 ml of PBS was injected IP and the harvested lavage fluid

was examined in a hemocytometer (Figs. 15A and B). One minute after injection, 75% of the injected GFP-labeled cells were accounted for (Fig. 15A). Surprisingly, the number fell to less than 10% after 20 minutes. At the same time, there was a marked decrease in the total number of mouse cells in the lavage fluid, apparently because macrophages and some lymphocytes in the peritoneal cavity had aggregated with the MSCs [65]. The number of murine single cells increased by 4 hours and it continued to increase for at least 72 hours (Fig. B-1B).

Aggregation of the injected MSCs was demonstrated by assays of the pellet obtained by low speed centrifugation (500 x g for 10 min) of the peritoneal lavage. Four hours after injection of the MSCs, assays by real-time-PCR for human GAPDH mRNA demonstrated that about 50% of the injected human cells were recovered in the pellet (Fig. 15C, B-1A, Tables B-2 and B-3). However, at 1 day, only about 1 % of the injected cells were recovered in the pellet of the peritoneal lavage (Fig. 15C), apparently because the aggregates had attached to the mesentery, omentum and other surfaces of the peritoneal cavity. Of special interest was that less than 1,500 or 0.05% of the injected 3 x 10^6 cells were found in the spleen and jejunal lymph nodes at any of the time points examined.

Figure 15. Fate of the IP injected MSCs in the peritoneal cavity. (A) Changes in the numbers of single GFP-positive cells and total single cells in the peritoneal cavity after intraperitoneal administration of GFP-MSCs into BALB/c mice. The cells were recovered by a 5 ml wash of peritoneal cavity with PBS. Resulting lavage was gently mixed and the single cells counted in a hemocytometer (n=4, mean +/- SEM). (B) Fluorescent images of single GFP-MSCs in hemocytometer chamber. Magnification 20X, (C) Total number of human cells in pellets of peritoneal lavage (PLP), random sampling of about 25 mg or about 10% of mesentery (MT), omentum (OM), jejunal lymph nodes (JLN) and spleen (SP). To collect PLP, peritoneal lavage was collected by washing the peritoneal cavity first with 1 ml and then with 5 ml of sterile PBS. The two samples of lavage were centrifuged at 500 x g for 5 min and the pellets were combined. Human cells in the samples were assayed by real-time PCR for human GAPDH normalized to total eukaryotic 18S. Data points represent arithmetic means +/- SEM, n=3 – 5. Insert indicates human cell numbers in the spleen and jejunal lymph nodes. Note dramatic differences in cell numbers between inset and large panel.

Figure 15 (continued)

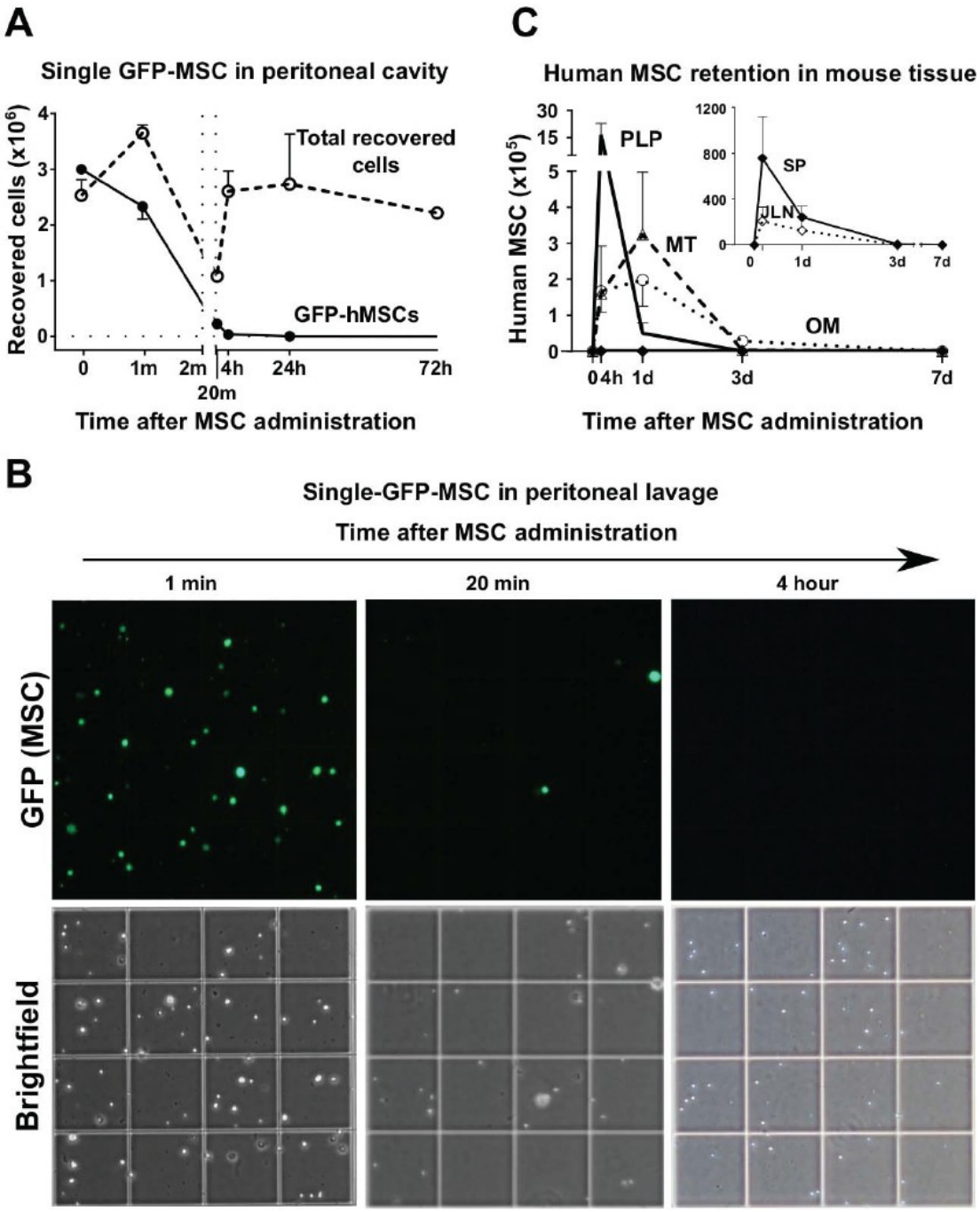

To examine the fate of the injected cells further, we injected GFP-MSCs IP and opened the peritoneal cavity to follow the distribution of the cells by *in vivo* fluorescent imaging (Fig. 16). As expected from the assays of the lavage pellet (Fig. 15C), numerous aggregates of GFP-positive cells were found as free-floating in peritoneal cavity at 4 hours (Fig. 16A, B). At 1 day, the GFP-positive aggregates appeared to have increased in size and become attached to multiple surfaces within the peritoneal cavity. Many were easily detached by flushing with PBS or lifting with a tweezers. However the aggregates that attached to the omentum and to sites within the mesentery were firmly adherent and appeared to be embedded within the tissues. At 3 days, there was a decrease in GFP-labeled aggregates and at 7 days they were no longer detected.

Figure 16. In vivo fluorescent imaging of GFP-MSCs in peritoneal cavity. (A) Depiction of GFP-MSCs distribution in the peritoneal cavity of BALB/c mice 24 hours after IP administration. Yellow dashed lines outline GFP-positive areas (bright white) corresponding to omentum, aggregates and portions of mesentery. (B) Representative images of the peritoneum of BALB/c mice injected IP with GFP-MSCs and followed by *in vivo* fluorescent imaging. Bright white areas correspond to the areas of GFP-positive cells. Logarithmic grayscale was applied to panels (A) and (B) to help in visualization of GFP signal.

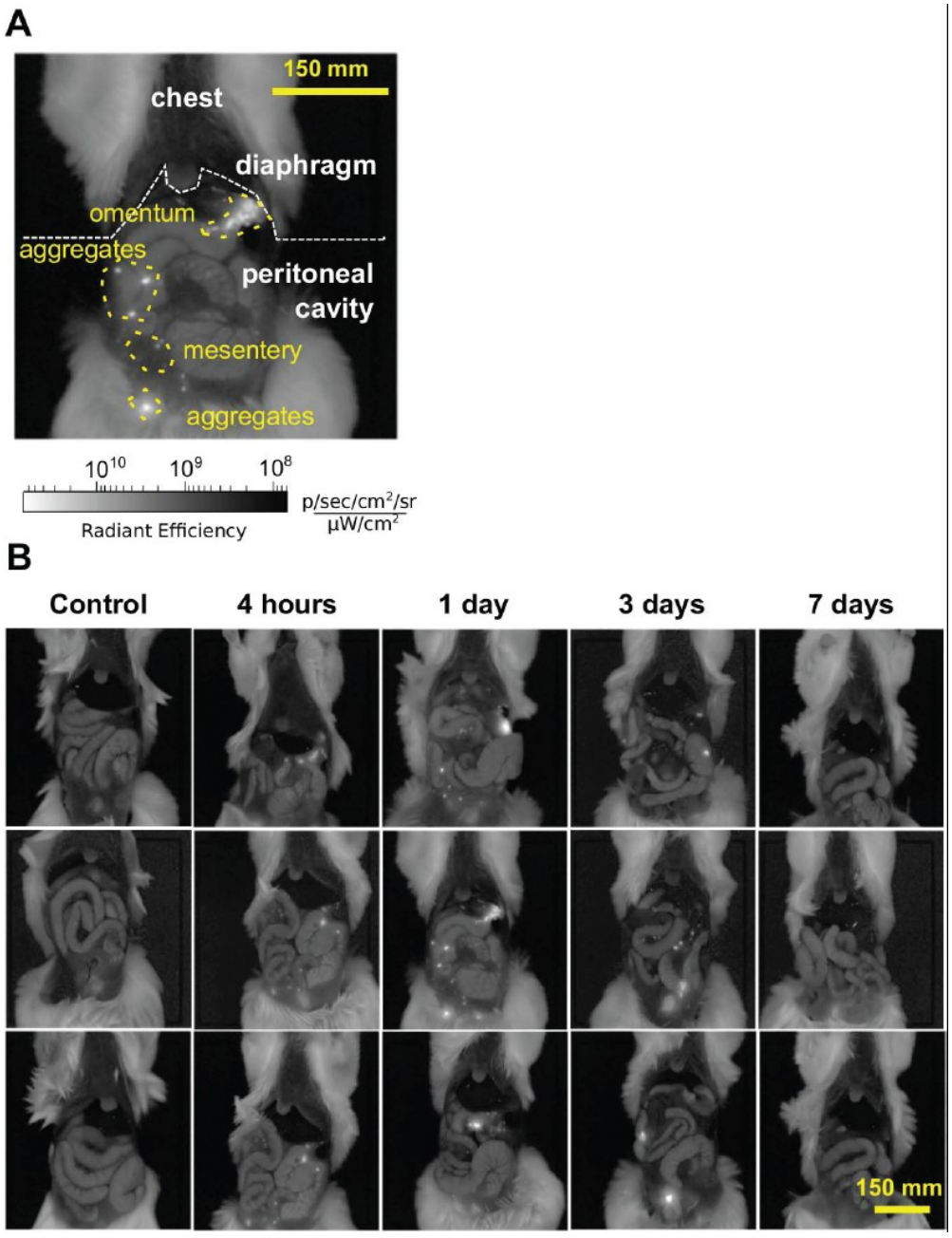

To examine the composition of the aggregates, GFP-MSCs were injected IP and GFP-positive aggregates in the peritoneal lavage, mesenteric sites, and the omentum were isolated after 24 hours and examined (Fig. 17A). Immunofluorescent images of sections of aggregates from the peritoneal lavage demonstrated that they were rich in cells positive for CD11b+ (Fig. 17B), a marker for macrophages. Immunohistochemistry of whole mounts of aggregates from mesenteric sites and the omentum demonstrated that they were rich in B220+ cells (Fig. 17C), a marker, expressed in various immune cells including B1 lymphocytes that are the predominant lymphocytes of the peritoneal cavity and the omentum, macrophages, T-cells and dendritic cells. The micrographs and a z-stack video of an aggregate from the omentum demonstrated that the GFP-MSCs were at the center of the aggregates without any specific orientation (Video 1).

IV.4.2 The MSCs-aggregates in the omentum recruit macrophages and lymphocytes

Since the omentum was a major site for the firm attachment of the aggregates, the organ was excised and examined. Fluorescence assays indicated that the content of GFP-MSCs increased sharply by 4 hours, decreased by 3 days and were not detected by 7 days (Fig. 18A). As the MSCs decreased, there was a marked increase in the weight of the omentum (Fig. 18B), the total cell content (Fig. 18C), and macrophage content (Fig. 18D), observations suggesting recruitment of macrophages and lymphocytes into the omentum that continued after most of the MSCs had disappeared (Fig. B-1B).

Figure 17. Co-localization of human GFP-MSCs with immune cells in the peritoneal cavity. Representative immunofluorescent images of human GFP-MSCs in free-floating aggregates, and aggregates attached to mesentery and omentum 24 hours after their IP administration (A) *In vivo* low-magnification (1.5x) images. (B) GFP-positive aggregates as shown in (A) were obtained from peritoneal cavity, cryosectioned and stained with CD11b antibody (magnification 20x). (C) GFP-positive aggregates attached to mesentery and omentum were isolated with tweezers, fixed, labeled with B220 antibody, and examined as whole mounts (magnification 20x).

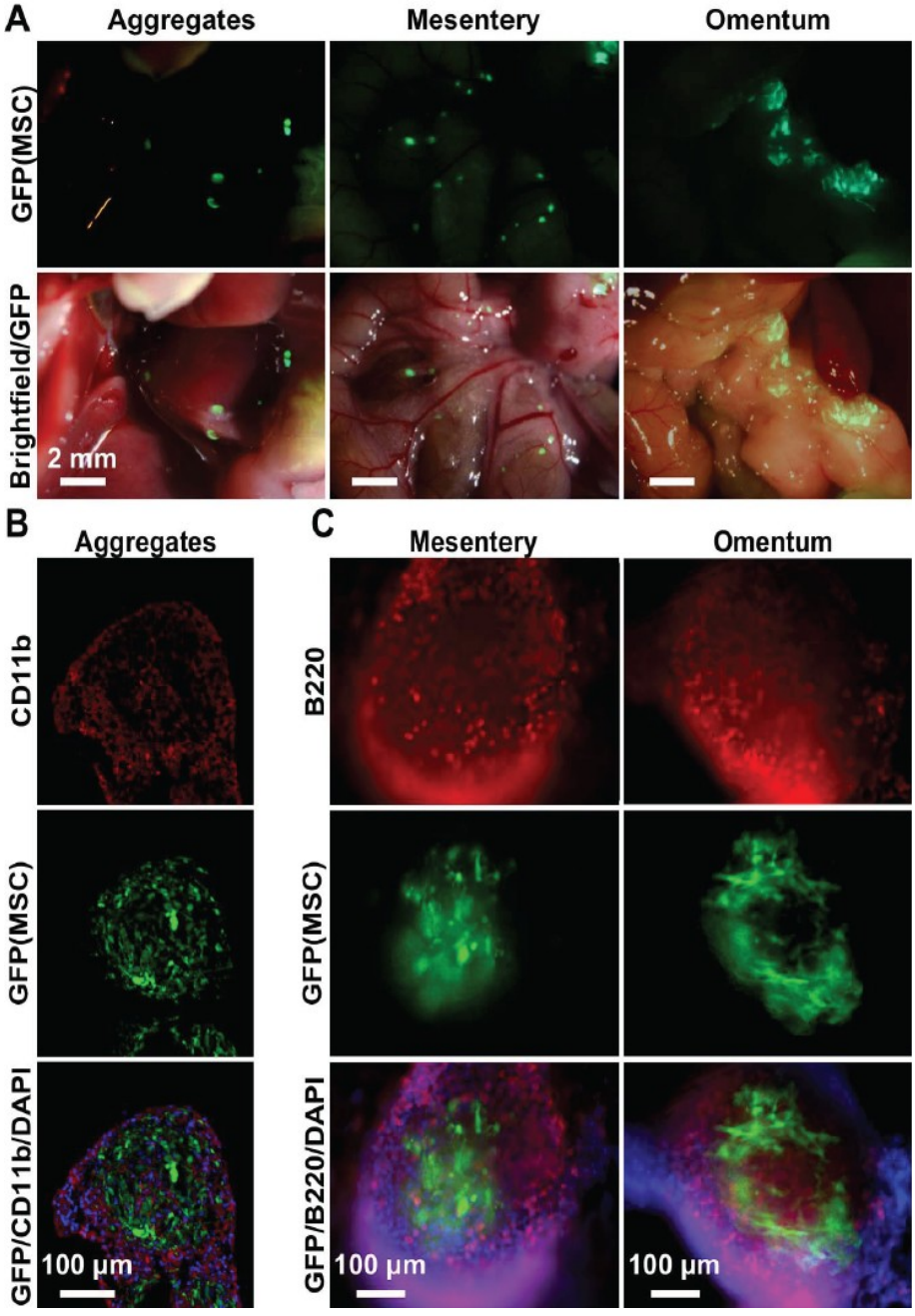

Figure 18. IP injected MSCs localized to omentum and recruit immune cells. (A) *Ex-vivo* fluorescent images of omenta excised from GFP-MSCs-injected BALB/c mice. To help in visualization of GFP signal, reversed logarithmic grayscale was applied to the images. Black areas correspond to GFP-positive signal. Omenta were isolated from MSCs or HBSS-injected animals, weighed, digested and analyzed by flow cytometry. (B) Scatter plots represent weights of individual omenta. (C) Total cells after digestion and (D) total macrophages at 3 days after injections. Error bars are +/- SEM. *, $p<0.05$; **, $p<0.01$; ***, $p<0.001$ compared to HBSS.

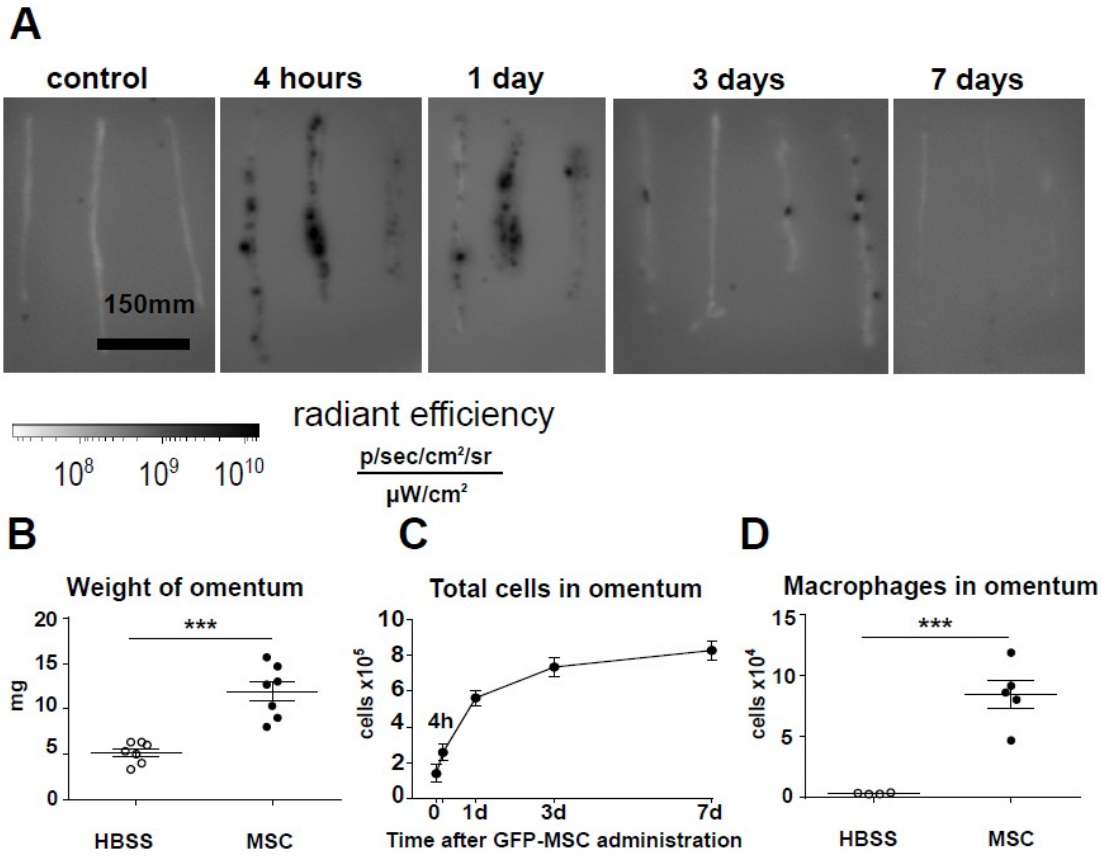

IV.4.3 IP injection of MSCs triggers increased expression of murine cytokines

The IP infusion of MSCs stimulated increased secretion of a series of mouse cytokines in a time-dependent manner (Fig. 19). Among the early responses was a peak in IL12p70 at 4 hours that decayed slowly, a peak of TGFβ1 at 4 hours that slowly decayed, and a sharp peak of IL6 at 4 hours (Fig. 19A). Among the intermediate responders, IL10 had a small peak at 4 hours and then a larger peak at 3 days that paralleled the very large peak of IFNγ (Fig. 19B). TNF-α remained at very low levels but had small peaks at 4 hours and 3 days. The late responders IL13 and PGE_2 slowly increased and then remained at high levels for at least 13 days (Fig. 19C). Small increases in the systemic levels of IL10 and IL13 were detected at 3 days after MSCs administration (Fig. B-2).

To examine effect of different MSCs preparations on the production of cytokines in the peritoneal cavity, we examined cells isolated and expanded from three donors of bone marrow with the standard protocol employed by our NIH-sponsored center for preparation and distribution of MSCs. After IP injection of the cells, all three MSCs preparations increased the levels of mouse IL10, IL13, and PGE_2 in the lavage (Fig. B-3A). Dose response data from one donor demonstrated that IP administration of 3 million MSCs was more effective than lower amounts (Fig. B-3B).

IV.4.4 Mouse omentum is a major source of cytokines

To define the source of the cytokines detected in the lavage after injection of MSCs, we used real-time PCR assays of omentum, mesentery, cells from peritoneal lavage, and jejunal lymph nodes (Fig. 19D). The results suggested that the omentum was the major source of the increases in expression of mouse *Il10, Ifng* and *Il13* but both the omentum and the cells in the peritoneal lavage made major contributions to the increase in *Cox2* (cyclooxygenase; prostaglandin-endoperoxide synthase).

Human MSCs showed distinct change in their gene expression profiles after administration inside peritoneal cavity. Real-time PCR assays showed upregulation of human *TGFβ1*, *COX2* and *TSG6* in injected cells in peritoneal cavity in comparison to unstimulated in vitro cultures of MSCs (Fig. 19E).

Figure 19. Production of mouse cytokines in the peritoneal cavity after MSCs administration. Mouse cytokines were assayed in peritoneal lavage of MSCs-injected BALB/c mice. Based on the timing of the cytokine production, they were categorized into (A) early- , (B) intemediate-, or (C) late-responding cytokines. Data are representative of 2 independent experiments. Values are arithmetic means +/- SEM, n= 4 – 6. (D) Relative gene expression of selected mouse cytokines in omentum (OM), mesentery (MT), peritoneal lavage pellet (PLP) and jejunal lymph nodes (JLN). Values are average gene expression values normalized to mouse *Gapdh* using $2^{-\Delta Ct}$ method +/- SEM, n= 4 to 5. *, $p<0.05$; **, $p<0.01$; ***, $p<0.001$ compared to baseline expression levels. (E) Relative gene expression of human cytokines in omentum, mesentery, peritoneal lavage pellet and jejunal lymph nodes. Values are fold change of gene expression in vivo over corresponding gene expression in unstimulated in vitro cultures of MSCs prior to the injection into mice represented on the graph by dotted line. The expression values were obtained using $2^{-\Delta\Delta Ct}$ method with human GAPDH as housekeeping control.

Figure 19 (continued)

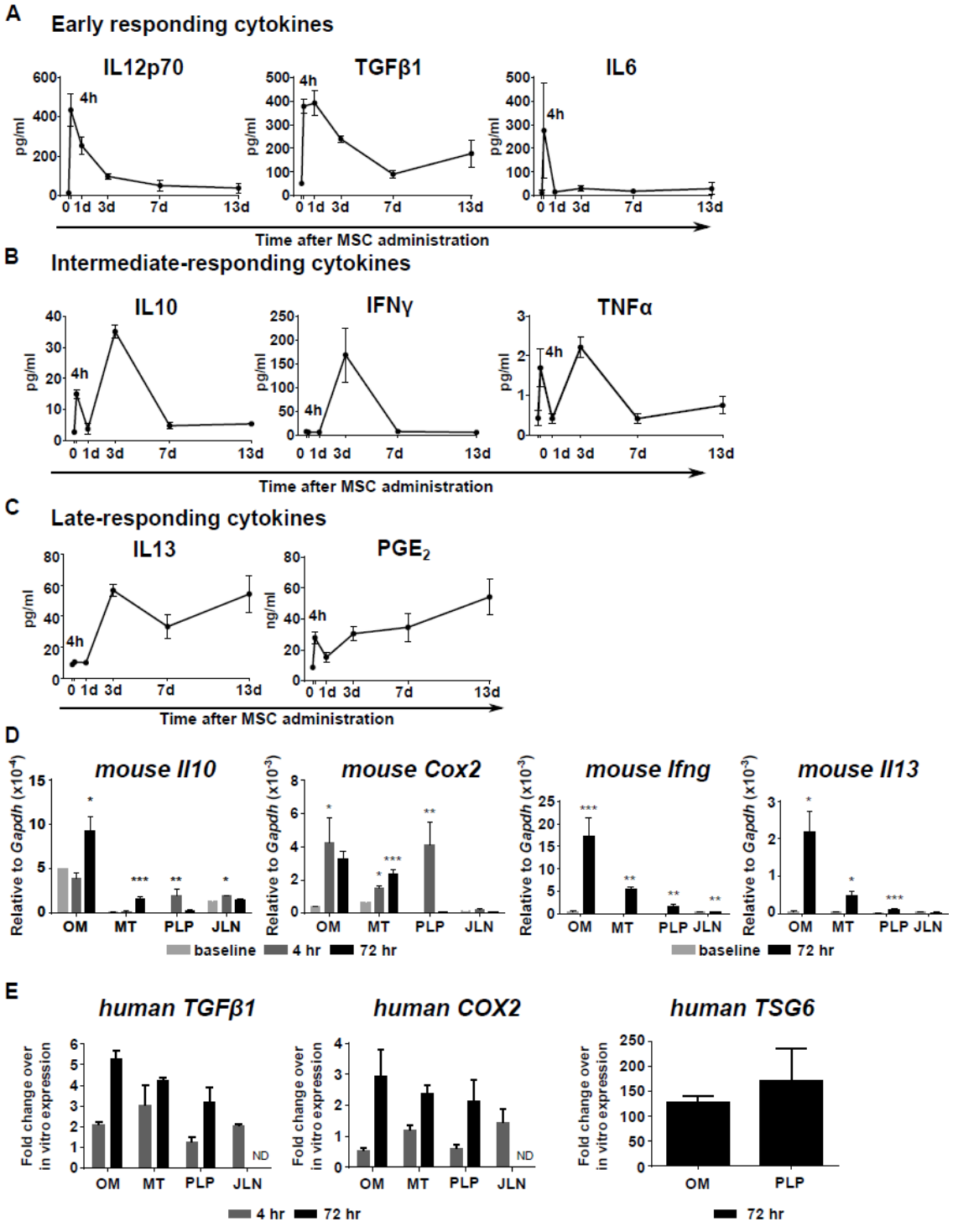

IV.4.5 Pre-conditioning of the mouse immune system by IP injection of MSCs

The persistence of changes in the peritoneum suggested that the IP infusion of MSCs had pre-conditioned the immune system of the mouse. Therefore we tested the effects of challenging the mice with the bacterial extract LPS. Mice received an IP injection of MSCs followed by IV infusion of LPS 3 days later. Three hours after the LPS injections, the mice were sacrificed and the lavage fluid was collected for cytokine measurements (Fig. 20). Among the early responding cytokines, the pre-conditioning enhanced the expression of IL12p70, MCP1, and CXCL1 (Fig. 20A). Among the intermediate responding cytokines, pre-conditioning enhanced the levels of IL10 and greatly enhanced the levels of IFNγ and TNF-α (Fig. 20B). MSCs pre-conditioning had no effect on the levels of the late responding cytokines PGE_2 and IL13 (Fig. 20C). Of special importance was the observation that MSCs killed by repeated cycles of freezing and thawing had little effect in preconditioning the immune system, an observation that suggested an active rather than passive role of the IP delivered MSCs.

Figure 20. Preconditioning of the mouse immune system by IP injected MSCs. Live or dead MSCs were injected IP into BALB/c mice 3 days prior to systemic administration of LPS. Identical experiments without LPS administration were performed in naïve mice. Mouse cytokines in the peritoneal lavage were measured at 3 days after MSCs administration and 3 hours after LPS administration. Based on the timing of the cytokine production, they were categorized into (A) early- , (B) intermediate- , or (C) late-responding cytokines. Values represent mean +/- SEM, n = 4 – 7. *, $p<0.05$; **, $p<0.01$; ***, $p<0.001$ compared to vehicle controls in each experimental setting. The Y-scale is logarithmically transformed.

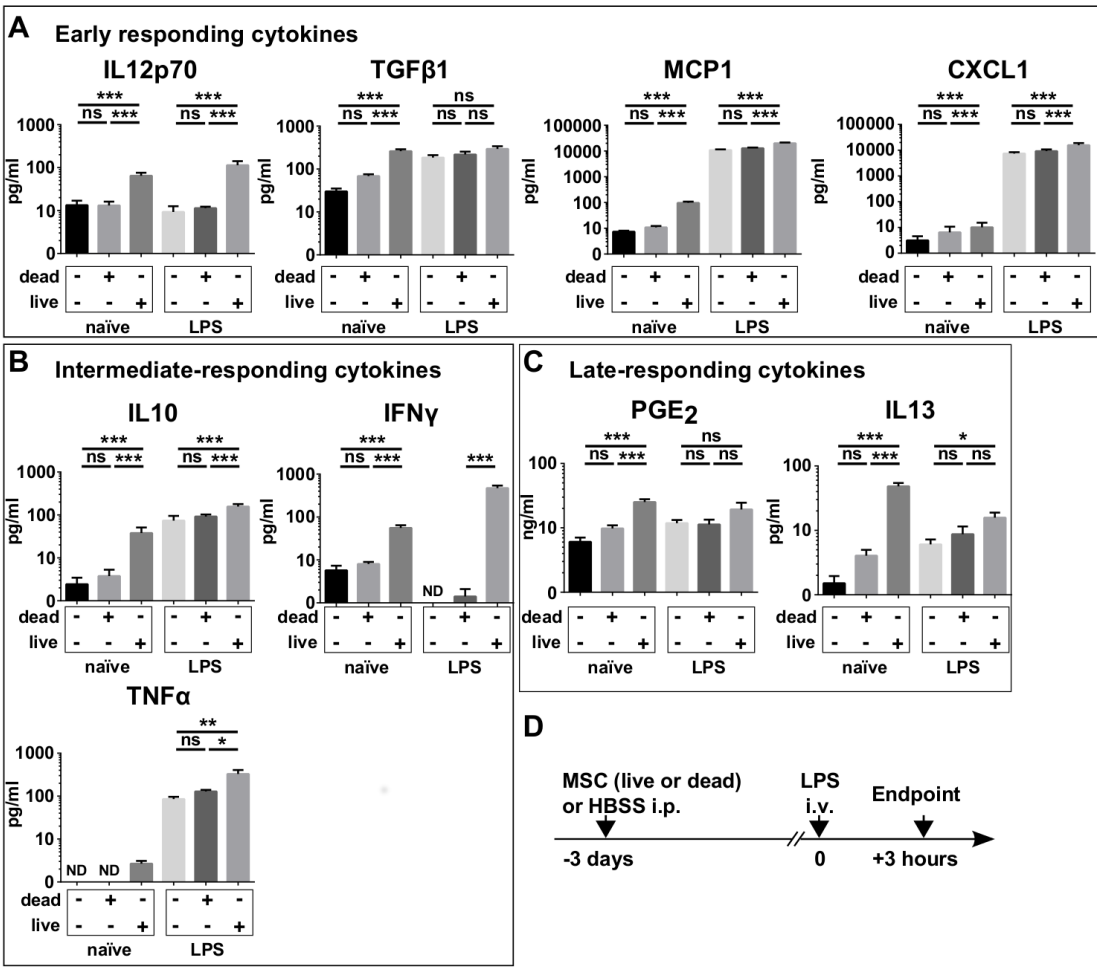

IV.5 Discussion

The results demonstrated that after human MSCs were injected into peritoneum of immune-competent mice, they quickly formed aggregates with the resident macrophages and the B220+ cells of the peritoneal cavity. The aggregation was so rapid that less than 10% of the MSCs were recovered as single cells in the peritoneal lavage after 20 minutes. At 4 hours, about half of the injected MSCs were recovered in the peritoneal lavage fluid as aggregates that were readily isolated by low speed centrifugation. At 1 day, only few of the aggregates containing MSCs were found in the peritoneal lavage. Instead they were found as aggregates attached to multiple sites in the peritoneal cavity. Most of the aggregates were loosely attached but those attached to the omentum and sites within the mesentery were embedded within the tissues. The survival and viability of the human cells was assessed by real-time PCR for human specific GAPDH and measuring levels of GFP fluorescence emitted by GFP-MSCs. Both signals indicated that the cells survived transiently and most disappeared after about 3 days.

Surprisingly, less than 1 in 3,000 (0.003%) of the injected cells were recovered in jejunal lymph nodes or the spleen. The results present a contrast to previous observations with IP injections of splenocytes in which most of the cells passed into the lymphatic system and accumulate in lymph nodes [168]. The results indicated therefore that apparently because of the rapid aggregation, the MSCs had limited direct access to lymphatics.

One interesting observation was that although the number of MSCs in the

omentum rapidly decreased after 3 days, they initiated a cascade whereby large numbers of mouse cells were recruited to the omentum and the organ doubled in weight. The observations are probably explained by the peaks of the pro-inflammatory mouse cytokines IL6 and IL12p70 at 4 hours and IFNγ and TNF-α at 72 hours that probably attracted and activated macrophages.

However, the pattern of cytokines was mixed with a peak of the regulatory cell cytokine IL10 at 4 hours, and later more sustained secretion of the Th2 cytokine IL13. Real-time PCR assays suggested that the aggregated cells in omentum were a major source of the cytokines with large increases in message levels for *Il10, Ifng,* and *Il13*. The increases in cytokines in the peritoneum were reflected by more modest increases in serum levels of IL10 and IL13. The recruitment of immune cells inside peritoneal cavity resulted in net precondition the immune system. The recruited cells readily responded to the challenge with LPS which resulted in the enhanced production of several pro-inflammatory cytokines such as CXCL1, TNF-α and others in mice that received IP MSCs 3 days earlier.

Dose response curves demonstrated that a large dose of 3 million MSCs was required to produce maximal increases in the peritoneal cytokines. Surprisingly, however, the samples of MSCs from three donor preparations of bone marrow were not equally effective. The variability among preparations of MSCs may have important implications for clinical trials with the cells [157].

The rapid aggregation of MSCs with macrophages and B220+ cells explains

some of the therapeutic effects previously observed with IP administration of MSCs in animal models. As reported previously [65], the MSCs in the aggregates formed in the peritoneum within 4 hours were activated to express high levels of potentially therapeutic human genes such as the genes for the natural anti-inflammatory protein TSG-6, for COX2 that is a critical enzyme in the synthetic pathway for PGE_2, and for STC-1 that can reduce reactive oxygen species. The activation was more rapid than seen with human MSCs cultured as hanging drops under conditions in which the cells condense into spheres and it is probably accelerated by the presence of the macrophages and B220+ cells in the aggregates. The rapid activation of human MSCs injected IP into immuno-competent mice probably explains the effectiveness of this route of administration of human MSCs in two models of sterile inflammation: ethanol injury to the cornea [91] and zymosan-induced peritonitis [88]. In cornea model, the window for effective therapy is less than 6 hours [87] and in the peritonitis model, the beneficial effects were seen within 4 hours [88]. In both models, the therapeutic responses were linked to expression of TSG-6, since MSCs with a silencing-RNA knock down of the TSG-6 gene were ineffective and most of the effects of MSCs were reproduced by administration of recombinant TSG-6. In present study we also show the upregulation of TSG-6 in injected MSCs. Increase in COX2 and TGFβ1 mRNA in MSCs and COX2, IL10 mRNAs in mouse tissues could provide an insight to anti-inflammatory effects of MSCs.

Similar rapid activations of IP MSCs may also explain some of the therapeutic

effects observed in other models [95], [149], [155], [156]. The MSCs used in the experiments were either isogeneic or allogeneic but could have invoke the rapid reactions of the peritoneal macrophages and B1 lymphocytes because the MSCs acted as foreign bodies in the peritoneum, or because they had acquired foreign antigens during their isolation and expansion in culture. As shown previously [170], MSCs rapidly internalize large amounts of fetal bovine proteins from the medium used to culture the cells and the internalized proteins stimulate immune responses after IV infusions of the cells into mice. The isogeneic mouse MSCs used by Yousefi et al.[149], Scruggs et al. [155], and Cheng et al. [156], were all isolated and expanded in medium containing high concentrations of fetal bovine serum. In the Wistar rat model for induced colitis study, Castelo-Branco et al. [95] used bone marrow and adipose derived MSCs that were isolated and expanded in 15% or 20% fetal calf serum. Therefore either the cells themselves or the foreign proteins they carried could have prompted rapid aggregation with peritoneal macrophages and B220+ cells, and the subsequent activation of therapeutic genes in the MSCs. Sorting out these possibilities is technically challenging because of the tendency of mouse MSCs to undergo spontaneous transformation during expansion in culture [171], [172], and the extensive manipulations of MSCs in culture required to remove internalized fetal calf proteins [170].

The longer-term effects of the IP MSCs in preconditioning the immune system speak to a complex phenomenon seen frequently with MSCs in which their effects persist long after the cells can no longer be detected. Such “hit and run” effects have

been seen with injection of MSCs into the hippocampus of uninjured mice [173], and in mouse models for transient global ischemia [174], acute myocardial infarction [54], diabetes [175], repair of meniscus [176], bleomycin-induced lung injury [145] and many others (see [157]). Under some circumstances the longer-term effects on the immune system can be explained by the MSCs suppressing an early inflammatory phase that is essential in triggering the acquired immunity. In others, it appears to be linked to the MSCs suppressing antigen-presenting cells or other regulatory cells of the immune system [175]. The results here demonstrate that one route to establishing longer-term effects on the immune system is through aggregates of MSCs, macrophages and B220+cells that bind to milky spots on the omentum and probably to similar sites on the peritoneal membranes in the mesentery.

The finding that MSCs triggered production of pro-inflammatory cytokines after challenge with systemic LPS contrasts with the previous observations of anti-inflammatory activity of MSCs in vivo [25], [54], [91], [155]. We suggest that the differences can be explained by a combination of factors including the time of MSCs administration relative to the challenge, the microenviromental conditions at the site at which the MSCs engraft, and the nature of the challenge. In the current study, the MSCs were injected 3 days prior to the injury in contrast with the majority of the studies where MSCs are administered at the same time or after the injury.

One of the limitations of the present study is that human MSCs were employed in immuno-competent mice. Therefore some of the effects can be ascribed to inflammatory

and immune reactions to xenogeneic cells. However, comparable experiments with mouse MSCs are limited by the inability of the cells to be expanded significantly without undergoing spontaneous transformation [171], [172]. Another limitation is that the data did not establish whether the MSCs were more effective in preconditioning the immune system than cells such as fibroblasts. However, the data demonstrated that three preparations of human MSCs isolated and expanded with the same protocols varied in their efficacy. Therefore it will probably be necessary to compare large numbers of different preparations of MSCs and large numbers of control cells to establish which are the most effective. The results did establish that live MSCs were far more effective than dead MSCs in preconditioning the mice in their response to LPS. Therefore the results were not explained by inflammatory or immune reactions to human cellular proteins or cell debris.

IV.6 Conclusions

In conclusion, we demonstrated that IP injected human MSCs quickly aggregate and the aggregates attach to mesentery, omentum and other sites in the peritoneal cavity. In contrast, only small amounts of the cells also migrate to spleen and jejunal lymph nodes. Aggregation and attachment to tissues was accompanied by the recruitment of immune cells and sequential changes in the production of mouse cytokines. In effect, the aggregation of IP injected MSCs appeared to limit their direct access to the lymphatic system but did not prevent them from preconditioning the immune system.

CHAPTER V

PHASE-DIRECTED THERAPY: TSG-6 TARGETED TO EARLY INFLAMMATION IMPROVES BLEOMYCIN-INJURED LUNGS*

V.1 Overview

Previous reports demonstrated that bleomycin-induced injury of lungs in mice can be improved by the administration of murine multipotent adult stem/progenitor cells (MSCs) from the bone marrow. Recently some of the beneficial effects of MSCs have been explained by the cells being activated by signals from injured tissues to express the inflammation modulating protein TNF-α-stimulated gene/protein 6 (TSG-6). In this study, we elected to test the hypothesis that targeting the early phase of bleomycin-induced lung injury with systemic TSG-6 administration may produce therapeutic effects such as preventing the deterioration of lung function and increasing survival by modulation of the inflammatory cascade. Lung injury in C57Bl/6J mice was induced by intratracheal administration of bleomycin. Mice then received intravenous injections of TSG-6 or sham controls. Pulse oximetry was used to monitor changes in lung function. Cell infiltration was evaluated by flow cytometry, cytokine expression was measured by ELISA assays, and lungs were assessed for histological attributes. The results demonstrated that intravenous infusion of TSG-6 during the early inflammatory phase

*Reprinted with permission from "Phase-directed therapy: TSG-6 Targeted to Early Inflammation Improve Bleomycin-Injured Lungs" by Andrea M. Foskett, Nikolay Bazhanov, Xinyu Ti, April Tiblow, Thomas J. Bartosh, Darwin J Prockop, 2014, Am J Physiol Lung Cell Mol Physiol, Volume 306, Issue 2, Pages L120-L131, Copyright 2008 by American Physiological Society.

decreased cellular infiltration into alveolar spaces. Most importantly, it improved both the subsequent decrease in arterial oxygen saturation levels and the survival of the mice. These findings demonstrated that the beneficial effects of TSG-6 in a model of bleomycin-induced lung injury are largely explained by the protein modulating the early inflammatory phase. Similar phase-directed strategy with TSG-6 or other therapeutic factors that MSCs produce may be useful for other lung diseases and diseases of other organs.

V.2 Introduction

Bleomycins are a family of antibiotics that are currently used as chemotherapeutic agents to treat germ-cell cancers, lymphomas, and malignancies of head and neck [177]. Unfortunately, bleomycin chemotherapy is a frequent cause of interstitial pneumonitis, a complex lung disease that can progress into interstitial pulmonary fibrosis with a poor clinical prognosis and high rate of mortality [178], [179]. Up to 46% of bleomycin-treated patients develop some form of lung toxicity leading to death in 3% of treated patients [180].

Bleomycin exerts its toxic effects by intercalating into double-stranded DNA to degrade the DNA and trigger the intrinsic apoptotic pathway [181]. Within the initial 48 h after administration, bleomycin produces damage/necrosis of the alveolar epithelium, capillary congestion, perivascular permeability leading to edema, and the formation of hyaline membranes [182]–[184]. Concomitantly, there is an increase in inflammatory cell infiltrates in the bronchoalveolar lavage fluid (BALF) [184], [185]. There is also a

marked influx of immune cells such as lymphocytes during this acute phase [183], [184]. As the injury progresses, pulmonary fibrosis develops with an excessive deposition of extracellular matrix deposition in the lung interstitium [185]–[187]. In the long term, there is compromised lung function with impaired transfer of oxygen and carbon dioxide gases.

Several reports demonstrated that bleomycin-induced injury of lungs in mice can be improved by administration of multipotent adult stem/progenitor cells referred to as mesenchymal stem or stromal cells (MSCs). Ortiz et al. [17], [94] demonstrated that murine bone marrow-derived MSCs decreased inflammation and collagen deposition in lung by expression of IL-1R antagonist. Rojas et al. [18] reported that the murine bone marrow-derived MSCs localized to lung and assumed the phenotypes of lung cells, but they also suppressed inflammation and triggered production of growth factors. In other models of acute lung injury, MSCs were shown to suppress proinflammatory cytokines, edema, and the influx of neutrophils [188], [189]. They improved clearance of bacteria [190], [191]. The beneficial effects of MSCs were largely explained by the ability of the cells to modulate immune and inflammatory reactions via several different mechanisms [25], [48], [192]. Similar beneficial effects of MSCs were also observed in other disease models, such as sepsis [193], myocardial infarction [54], [55], [194], and acute kidney injury [195], [196].

Accordingly, a common theme in recent reports is that MSCs produce their beneficial effects by being activated by signals from injured tissues to express genes that

modulate inflammatory and immune responses [188], [192]. Among the anti-inflammatory factors MSCs are activated to express is TNF-α stimulated gene/protein-6 (TSG-6) [54]. TSG-6 was first discovered in the early 1990s and was shown to have multiple anti-inflammatory effects [85], [197]. It cross-links proinflammatory fragments of hyaluronan [198] and catalytically transfers a heavy chain from inter-α-inhibitor to hyaluronan, thereby inhibiting the cascade of proteases released by inflammation [198], [199]. It also inhibits transport of leukocytes through endothelial cells [200]. Administration of recombinant TSG-6 was shown to reproduce most of the beneficial effects of MSCs administration in models of myocardial infarction [54], peritonitis [88], and corneal injury [87], [91]. Also, Danchuk et al. [86] demonstrated that the beneficial effects of MSCs in a model of LPS-induced lung injury were partly explained by the secretion of TSG-6 by MSCs.

Here we tested the hypothesis that beneficial effects can be produced by administration of TSG-6 to target the early inflammatory phase of bleomycin-induced lung injury. In effect, administration of the protein during the early inflammatory phase of the injury might be more effective than administration of MSCs. Therapies with MSCs are complex because the cells undergo a lag period of 10–12 h before they are activated by signals from injured cells to express potentially therapeutic factors such as TSG-6, and after intravenous (IV) infusion they disappear from the lung after 24 h [54]. We used a rapid and real-time assay for arterial oxygen saturation (SpO_2) to follow the deleterious effects of bleomycin on gaseous exchange in the lung. The results

demonstrated that administration of TSG-6 on 2 and 4 days after bleomycin exposure decreased the initial cellular infiltration into alveolar spaces and improved both the subsequent decrease in SpO_2 levels and the survival of the mice.

V.3 Materials and methods

V.3.1 Animals

Animal use protocol was approved by the Texas A&M Health Science Center Institutional Animal Care and Use Committee at Scott and White Hospital. Female 6- to 8-wk-old wild-type (C57BL/6J) mice and female transgenic mice with a CD44 gene knockout (B6.Cg-Cd44tm1Hbg/J) obtained from Jackson Laboratories were used for this study. The mice were kept on a 12-h light-dark cycle and fed and watered ad libitum.

V.3.2 Bleomycin-induced lung injury

Mice were anesthetized with 4% isoflurane in 100% oxygen for 4 min to reach the level of deep anesthesia and placed on the intubation stand facing upward at a 45° tilt by using sterile elastic string positioned under the animal's front incisors. The tongue was retracted with forceps and the trachea was intubated with a 22-G plastic sterile iv catheter (Terumo). An external high-power light source was used to visualize the tracheal opening. Bleomycin sulfate from *Streptomyces verticillus* (Sigma-Aldrich) at 2.25 U/kg body wt in 0.9% sodium chloride (Sigma-Aldrich) or 0.9% sodium chloride alone (sham injury) was instilled through a catheter at volume 4 μl/g body wt in two sets. The dose per mouse varied from 0.036 to 0.047 U. Mice were kept on the board for an

additional 90 s with the continued 4% isoflurane in 100% oxygen anesthesia via facemask.

Intravenous administration of recombinant human TSG-6 (R&DSystems) was performed on days 2 and 4 after bleomycin administration. Mice were anesthetized with 3% isoflurane, the tail vein was visualized by warming the tail, and a 28-G needle was used to inject rhTSG-6 (50 μg in 50 –150 μl of sterile PBS) or sterile PBS (50 –150 μl).

V.3.3 End point tissue, blood, and bronchoalveolar lavage fluid collection

At the indicated time points after bleomycin administration, mice were anesthetized with 3% isoflurane in 100% oxygen for 3 min and euthanized by intraperitoneal injections of ketamine-xylazine solution at 80 and 8 mg/kg body wt, respectively. The rib cage was opened without damaging the lungs. Blood was collected from the right heart ventricle and placed in a tube containing activators of clotting (Terumo Medical, Somerset, NJ) for 20 min and then stored on ice until further processing. Care was used to prevent bleeding into the rib cage. Serum was separated by centrifuging the tube at 1,500 g for 10 min and stored at 80°C until further analysis. Immediately following the collection of blood, the trachea was cannulated with a 20-G plastic IV catheter (Exelint, LosAngeles, CA). Two fractions of BALF were obtained. The first fraction was obtained by flushing the lungs back and forth fourtimes with a single volume of 800 μl of PBS containing Halt Protease Inhibitor Cocktail (Thermo Fisher Scientific, Rockford, IL). The second fraction was obtained by flushing the lung four additional times each with a volume of 800 μl of PBS without protease inhibitor

cocktail. The first BALF fraction was centrifuged at 500 g for 10 min at 4°C to obtain a cell pellet, which was later combined with the cell pellet from the second fraction. The supernatant was then spun again at 10,000 g for 10 min and stored at 80°C until further analysis. The cell pellet from the second wash was obtained by centrifugation at 500 g for 10 min and combined with the cell pellet from the first fraction. To lyse erythrocytes, the combined pellets were incubated at room temperature with red blood cell lysis buffer (eBioscience, San Diego, CA) for 5 min, centrifuged at 500 g for 5 min at 4°C, resuspended with 10 ml of ice-cold PBS, and centrifuged again. The supernatant was discarded and the cells were then resuspended in PBS containing 1% bovine serum albumin (BSA) (Thermo Fisher Scientific), counted by use of disposable Improved Neubauer Hemocytometers (INCYTO, Cheonan-si, Chungcheongnam-do, South Korea), and used later for flow cytometry analysis. After obtaining BALF, the lungs were excised, washed once in ice-cold PBS and immediately frozen and stored in 80°C until further processing.

V.3.4 Flow cytometry

The cells from BALF were prepared as described in the previous section, counted, resuspended in 100 µl of PBS with 1% BSA, and incubated for 10 min at 4°C with anti-CD16/32 antibody at a concentration 0.5 µg per $1x10^6$ cells in 100 µl (eBioscience) to block nonspecific binding to Fc-receptors. After being washed once with PBS-1% BSA, the cells were incubated for 20 min at room temperature with both phycoerythrin-Cy7-conjugated anti-mouse F4/80 antibody (eBioscience) and FITC-

conjugated anti-Ly-6G antibody (BD Pharmingen, San Diego, CA). The antibodies were used at a concentration of 1 μg per $1x10^6$ cells in 100 μl of PBS-1% BSA. Isotype-matching antibodies at similar concentrations obtained from the same manufacturers and single-color labeling were used as controls for the specificity of labeling. After two washes in PBS, the cells were again resuspended in PBS-1% BSA and analyzed by FC500 flow cytometer (Beckman Coulter, Brea, CA) to determine macrophage (F4/80-positive) and neutrophil (Ly-6G-positive) populations.

V.3.5 Cytokine ELISA in BALF and lung tissues

BALF was prepared as described in the previous section and frozen lungs were homogenized with RIPA buffer (ThermoFisher Scientific). Appropriate dilutions were used in the assays. Lung protein concentration was determined by using Micro BCA Protein Assay Kit (ThermoFisher Scientific) according to the manufacturer's instructions. Cytokine concentrations were determined by using commercially available ELISA kits for detection of IL-6, TNF-a, IL-1, CCL2/MCP-1, CCL3/MIP-1a, CXCL2/MIP-2, and CXCL1/KC (R&D Systems, Minneapolis, MN) according to the manufacturer's instructions.

V.3.6 Histology

Mice were anesthetized with 3% isoflurane in 100% oxygen for 3 min and euthanized by intraperitoneal injections of ketamine-xylazine solution as described previously. The rib cage was opened and the blood flow was stopped by placing a

permanent silk suture between atria and ventricles of the heart. The trachea was then cannulated with 20-G IV catheter and the lungs were excised, immediately washed with PBS, and fixed with 4% paraformaldehyde at pressure 20 cm H_2O for 24 h. The lungs were then dehydrated with graded ethanol solutions and embedded in paraffin. Five-micrometer sections were cut with Leitz 1512 microtome (Leitz, Germany) and stained with a Masson TriChrome Kit (Richard-Allan Scientific, Kalamazoo, MI). The bright-field images were taken with Nikon Eclipse 80i upright microscope (Nikon, Kawasaki, Japan), and linear adjustments were made in Adobe Photoshop CS3 (Adobe Systems, San Jose, CA).

V.3.7 Pulse oximetry

A portable mouse pulse oximeter (STARR Life Sciences) was used to monitor SpO_2 and other physiological parameters (heart and breath rates, pulse distention) in free-roaming nonanesthetized mice. The collars of experimental animals were trimmed of fur at least a day before the beginning of pulse oximetry monitoring. At indicated experimental time points, mice were anesthetized with 3% isoflurane in 100% oxygen for 2 min and an extra-small MouseOX collar clip was placed on the animal's neck. Mice were allowed to recover from anesthesia (1–2 min) and pulse oximetry readings were recorded as a Windaq Waveform file at 15-Hz sample rate. After placing the collar clip, we observed two sequential behavioral states in mice: 1) an agitated state, characterized by frequent movements resulting in an unstable signal, and 2) a relatively calm state with improved signal quality. The measurements were continued to allow

recording of 3–5 min of stable signal. Using Windaq Waveform Browser (DATAQ Instruments), we extracted data from only the calm state. An in-house Microsoft Excel (Microsoft) VBAbased script was then used to filter values associated with error-free signals implementing formulas provided by the manufacturer. With the same script, arithmetic means for each reading were obtained and later used for statistical analysis.

V.3.8 Statistical analysis

Unpaired t-test or one-way ANOVA with Bonferroni's post hoc analysis was used to compare two or more groups, respectively. Null hypotheses were rejected at P values less than 0.05. Survival of animals between groups was compared by log-rank (Mantel-Cox) test. All statistical analyses were performed with GraphPad Prism software.

V.4 Results

V.4.1 Functional oxygen saturation correlates with changes in cellular infiltrates and cytokines in BALF

To monitor in real-time the bleomycin-induced injury to the lung, we used a pulse oximeter to assay SpO_2 in mice (Fig. 21A and B). Placing a collar clip on the necks of the mice agitated them and distorted the reading. However, with care in handling, the mice became calm so that reliable values with minimum associated errors were readily obtained. Intratracheal administration of 2.25 U/kg of bleomycin produced a progressive decrease in SpO_2 below 90% reflecting hypoxemia beginning on day 8 (Fig. 21A).

Figure 21. Pulse oximetry in the bleomycin model of lung injury. A: dynamics of oxygen saturation (SpO_2) levels in bleomycin-injured and uninjured (sham-injured with NaCl) mice over the course of 12 days following injury. Only bleomycin-injured mice dropped SpO_2 levels below 90% (dashed line) that were significantly lower than in uninjured mice beginning on day 8. B: SpO_2 curves extracted from Windaq files of bleomycin-injured and uninjured mice prior to the beginning of the experiment and 12 days after injury. Note visible changes in the SpO_2 curve of injured animals (bleomycin day 12). C and D: although no significant changes from pre-injury baseline recordings (day 0) were detected, heart rates of bleomycin-injured mice were significantly lower on day 12 and breath rates were significantly lower on days 4, 6, and 12 compared with uninjured mice. E: weight changes normalized to pre-injury (day 0). Significant weight changes were noted on day 6 and constituted ~20% weight loss in injured mice. P values were calculated between uninjured and bleomycin-injured groups at each time point by 1-tailed t-test. *P < 0.05, **P < 0.01.

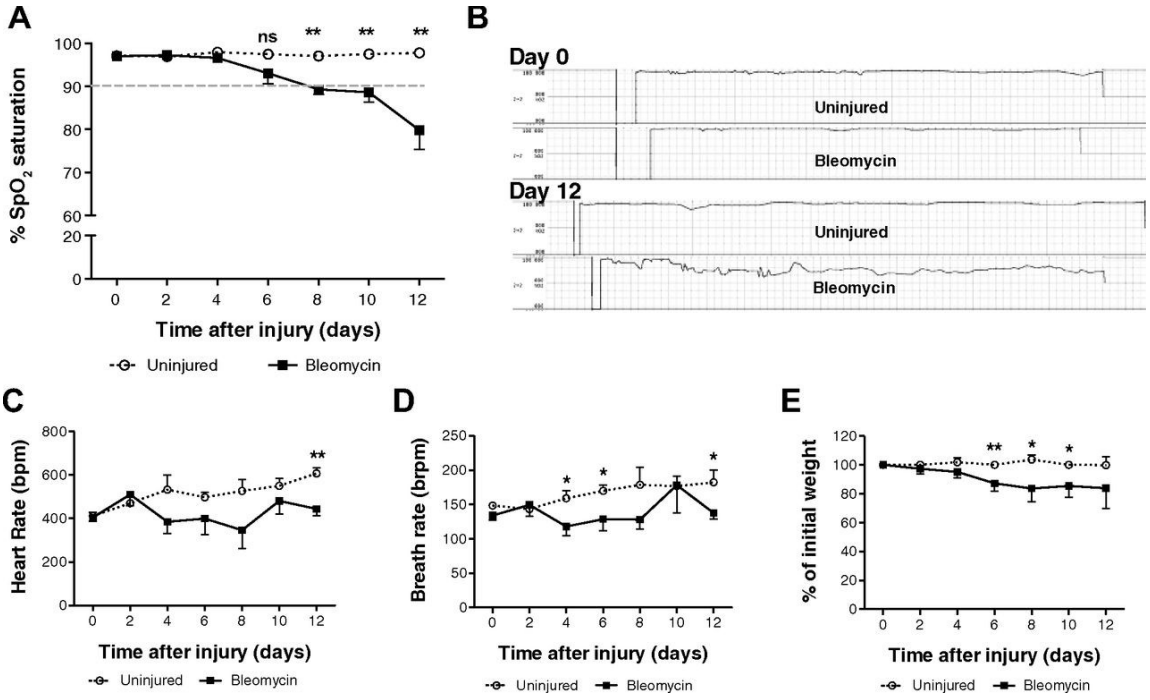

As expected, the decrease in SpO_2 paralleled changes in the BALF. There were progressive increases in total cells and protein concentration (Fig. 22, A and D). Macrophages in the BALF showed an initial decrease and then increased on day 6 and day 12 (Fig. 22B). Neutrophils were more variable but showed increases vs. a control in the number of neutrophils from days 2 to 12 (Fig. 22C). As also expected, the major changes in cytokine and chemokine levels occurred earlier than the decrease in SpO_2 (Fig. 23). Levels of the proinflammatory cytokines IL-6 and TNF-α in the BALF were increased on day 2 and then decreased. Similarly, the chemokines CCL2 and CXCL1 were increased on day 2 and then decreased.

In addition, the decrease in SpO_2 roughly paralleled a decrease in body weight (Fig. 21E) and pathological changes in lung morphology (Fig. 22E). There were more variable decreases in heart rate and respiration rate (Fig. 21, C and D).

V.4.2 Intravenous administration of TSG-6 improved functional oxygen saturation and survival of bleomycin-injured mice

We elected to test the potential effectiveness of TSG-6 in suppressing the early inflammatory phase in the bleomycin model. Day 8 post injury was chosen for performing last end point assays in further experiments. This was based on the findings from the optimization of the bleomycin model (Fig. 21-23) in which SpO_2 levels in bleomycin-injured mice were significantly different from uninjured mice on day 8 and the extent of inflammation paralleled SpO_2 levels. Additionally, the bleomycin-injured mice were observed until day 21 for long-term survival.

Figure 22. Temporal changes in cell composition of bronchoalveolar lavage fluid (BALF) and histological changes in the lungs following bleomycin injury. BALF was collected at 2, 4, 6, and 12 days following bleomycin injury and at 12 days from uninjured mice (A–D); for histology, lungs were collected at day 8 (E). A and D: total number of cells in BALF was counted with a disposable hemocytometer. Protein concentration (Conc) in BALF was determined by the BCA assay. Both total BALF cell number and protein concentration increased temporally. Both parameters were the highest by day 12 postinjury and were significantly higher than in the uninjured controls. Significant differences in total cells and protein concentration between groups were also observed at various time points as indicated in the figure. B and C: the cells were labeled with antibodies against macrophage (F4/80) and neutrophil (Ly6G) markers and analyzed by flow cytometry. Macrophages and neutrophils also increased temporally following bleomycin injury. However, on days 2 and 4, whereas total cells and macrophages were either similar to or lesser in number compared with uninjured mice, neutrophil numbers on those days were higher than the uninjured mice. E: representative images of Masson's trichrome-stained lung sections from bleomycin-injured and uninjured mice from day 8. Lower row represents magnification of area inside orange frame in upper row. Area of inflammation and fibrosis is clearly visible in bleomycin-injured lungs. Values are represented as arithmetic means ± SE (n = 3 mice per group). P values were calculated by 1-way ANOVA with a post hoc Bonferroni's multiple comparison analysis performed between all the groups. *P < 0.05, **P < 0.01, and ***P < 0.001.

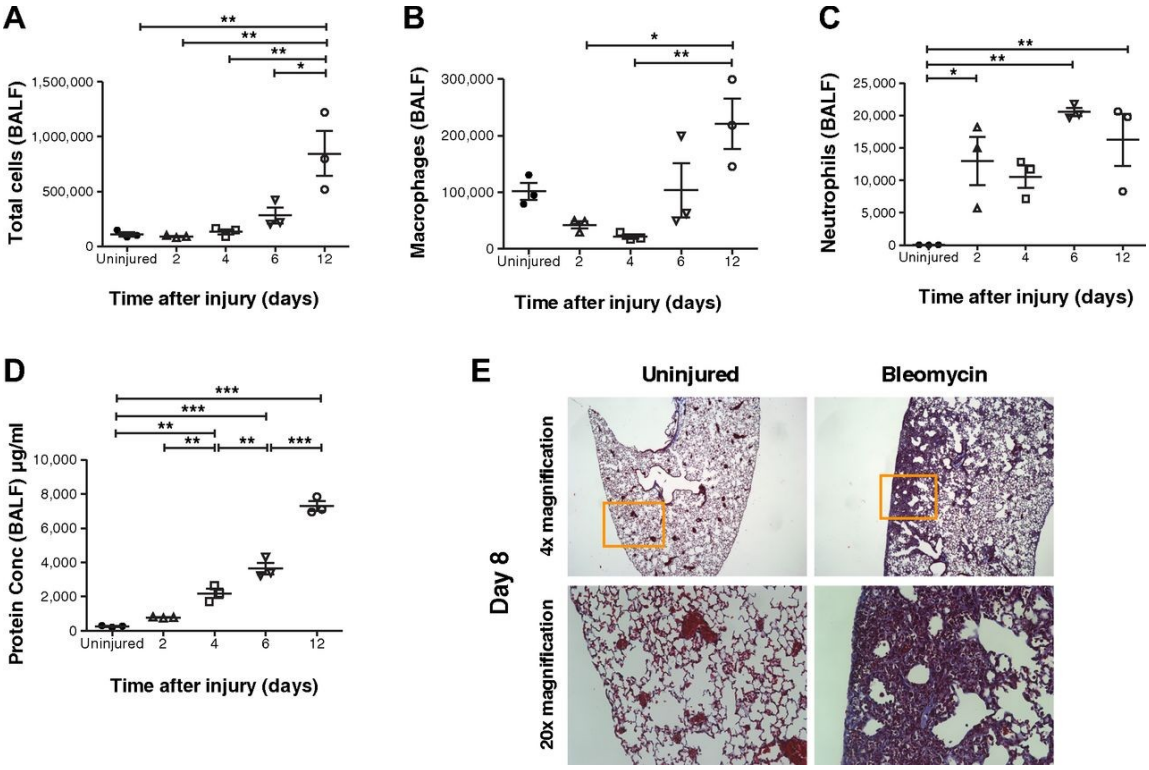

Figure 23. Temporal changes in cytokine expression of BALF in the bleomycin model of lung injury. Cytokine expression levels on days 2, 4, 6, and 12 were assayed in BALF by use of ELISA. IL-6 (A), TNF-α (B), CCL2/MCP-1 (C), and CXCL1/KC (D) expression levels were the highest on day 2 and were significantly higher than those in uninjured mice. Expression levels of all the cytokines tested returned to close to uninjured levels by days 6 and 12. Significant differences in cytokine levels between groups on the individual days tested are indicated. Values are represented as arithmetic means ± SE (n = 3 mice per group). P values were calculated by 1-way ANOVA with a post hoc Bonferroni's multiple comparison analysis performed between all the groups. *P < 0.05, **P < 0.01, and ***P < 0.001.

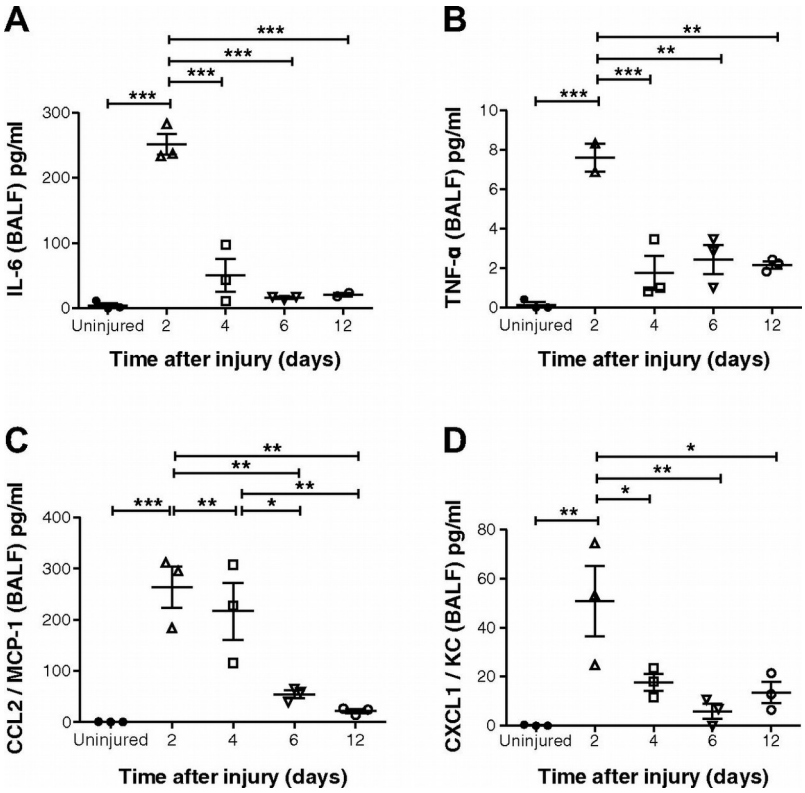

A high (50 μg) and a low dose (12.5 μg) of TSG-6 were tested to determine the most effective dose. The functional SpO_2 data on day 8 (Fig. 24, A and B) and the cellular infiltrates on day 5 (Fig. 24, C-H) suggested that the high 50 μg dose would be most beneficial in reducing early inflammation and improving function in the bleomycin lung injury model. Hence the high dose (50 μg) was used for the rest of the study. The TSG-6 protein (50 μg) was infused intravenously on day 2 and day 4 to target the early inflammatory stage. As expected, there was a decrease in early signs of inflammation by a decrease in total cells, macrophages, and neutrophils in BALF on day 5 (Fig. 25). There was also a decrease in the proinflammatory cytokines TNF-α on day 2 and IL-6 on day 3 (Fig. 26, A and B). However, IL-1β expression in lung tissues was increased in TSG-6-treated mice on day 2 (Fig. 26C). In addition, administration of TSG-6 increased the BALF levels of the chemokines CCL2, CCL3, CXCL1, and CXCL2 on day 2 (Fig. 26, D-G). Protein concentration levels were not significantly different between TSG-6- and PBS-treated mice (Fig. 26H) at all examined end points.

Figure 24. TNF-α-stimulated gene/protein 6 (TSG-6) dose response on SpO_2 and cellular infiltrates. A: effect of TSG-6 dose response on the dynamics of SpO_2 levels over the course of 8 days following bleomycin (Bleo) injury. A high dose (50 µg) and a low dose (12.5 µg) were administered on days 2 and 4 following bleomycin injury. B: dot plot represents the distribution of SpO2 levels on day 8. Significant differences between high dose of TSG-6 and PBS groups was observed on day 8. For the analysis of cellular infiltrates, BALF was collected on days 2, 3, 5, and 8 following bleomycin injury. From day 3 onward following injury of the lungs with bleomycin, total cells (C) and macrophages (D) in BALF increased in the low-dose TSG-6 mice compared with PBS control mice. F and G: the high dose of TSG-6 lowered these parameters compared with PBS-treated mice with statistically significant differences between these 2 groups observed only on day 5. E and H: the low dose of TSG-6 increased neutrophil numbers early on day 2, whereas the high dose of TSG-6 maintained the neutrophil infiltration lower than PBS mice at all time points. Values are represented as arithmetic means ± SE (n = 5–8 mice per group). For the SpO_2 data, P value was calculated between PBS and TSG-6 groups by 1-tailed t-test. For the cellular infiltrates data, P values were calculated by 1-way ANOVA with a post hoc Bonferroni's multiple comparison analysis performed between all the groups. *P < 0.05, **P < 0.01.

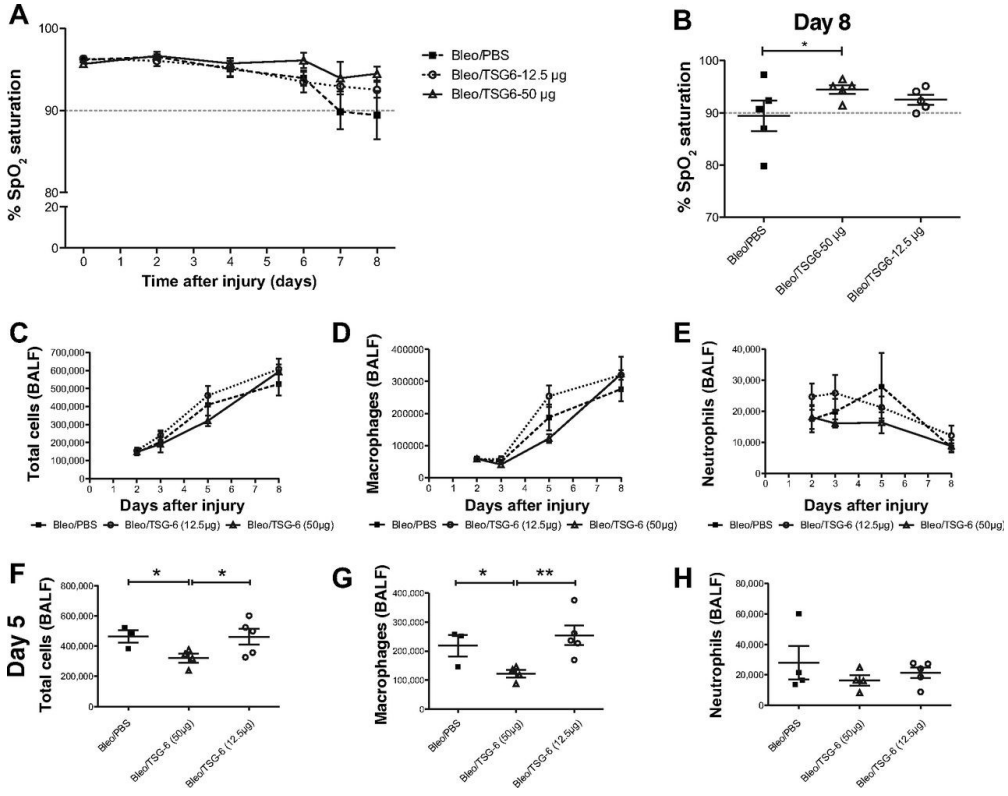

Figure 25. TSG-6 treatment reduces cellular infiltration in the lungs during the early inflammatory phase. BALF was collected at 12 h and on days 2, 3, 4, 5, and 8 following bleomycin injury. On days 2 and 4 alone, BALF was collected 4 h after TSG-6 (50 μg) administration. From day 4 onward following injury of the lungs with bleomycin, total cells (A), macrophages (B), and neutrophils (C) in BALF increased compared with uninjured mice. TSG-6 treatment lowered these parameters compared with PBS-treated mice with statistically significant differences between these 2 groups observed only on day 5. Insets represent changes on day 5 in individual mice from the 3 groups. Note that on days 2 and 3 following bleomycin injury, macrophages (B) were significantly lower in PBS and TSG-6 groups (√√ = $P < 0.01$, √√√ = $P < 0.001$) compared with uninjured mice. Values are represented as arithmetic means ± SE (n = 5–8 mice per group). P values were calculated by 1-way ANOVA with a post hoc Bonferroni's multiple comparison analysis performed between all the groups. P values represented in the larger panels only indicate significant differences between PBS and TSG-6 groups following bleomycin injury. P values represented in the insets indicate significant differences between all 3 groups. *$P < 0.05$ and **$P < 0.01$.

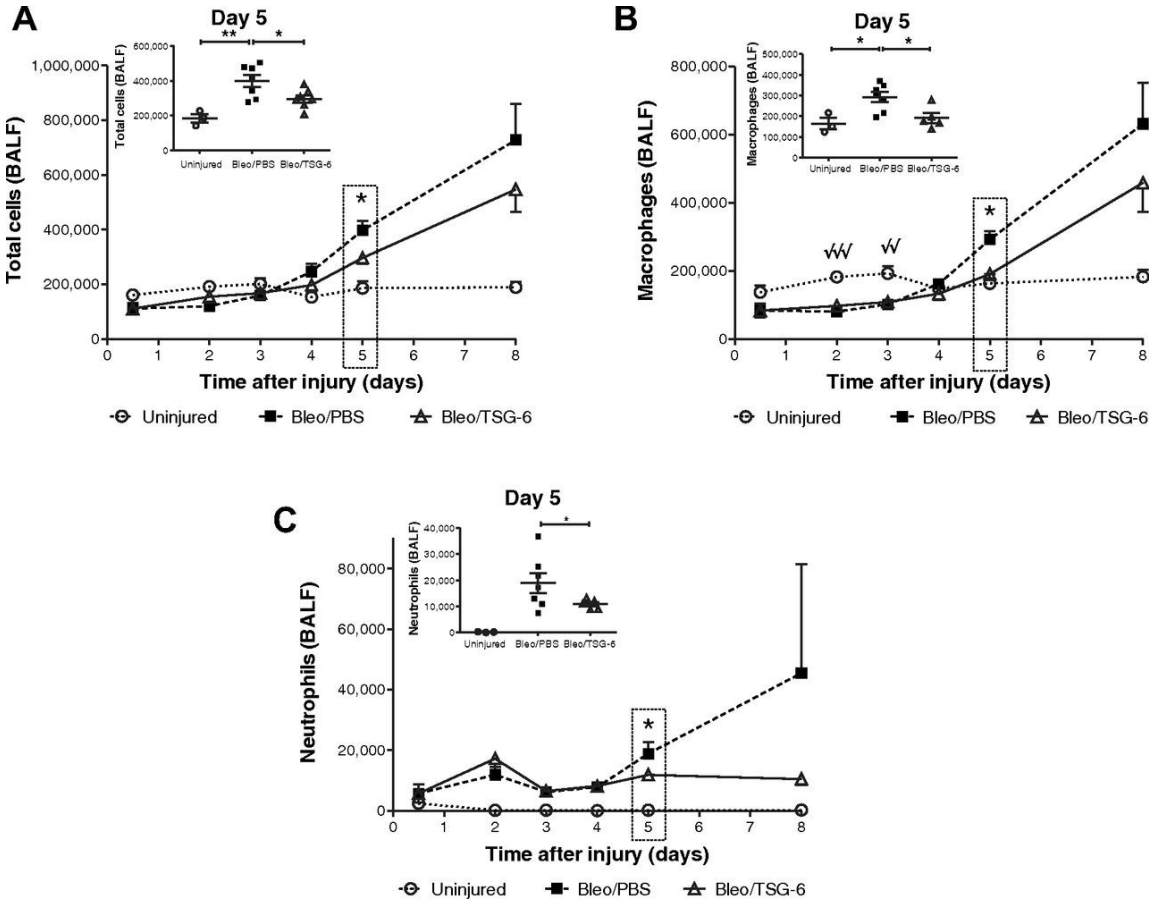

Figure 26. Temporal changes in cytokine/chemokine expression following TSG-6 treatment in the bleomycin model of lung injury. TSG-6 (50 μg) treatment significantly decreased TNF-α (A) expression on both days 2 and 3, whereas decreasing IL-6 (B) only on day 3 in comparison with PBS-treated mice. Surprisingly, TSG-6 initially increased IL-1β (C) expression on day 2 but decreased it significantly by day 8. TSG-6 treatment significantly increased expression of CCL2/MCP-1 (D), CCL3/MIP-1α (E), and CXCL2/MIP-2 (G) chemokines on day 2, whereas significantly increasing CXCL1/KC (F) on both days 2 and 4. No significant differences in protein concentration (H) were observed after TSG-6 treatment. Values are represented as arithmetic means ± SE (n = 5–8 mice per group). P values were calculated by 1-way ANOVA with a post hoc Bonferroni's multiple comparison analysis performed between all the groups. Only significant differences between bleomycin-injured (PBS and TSG-6) groups are indicated in the figure: *P < 0.05, **P < 0.01, and ***P < 0.001.

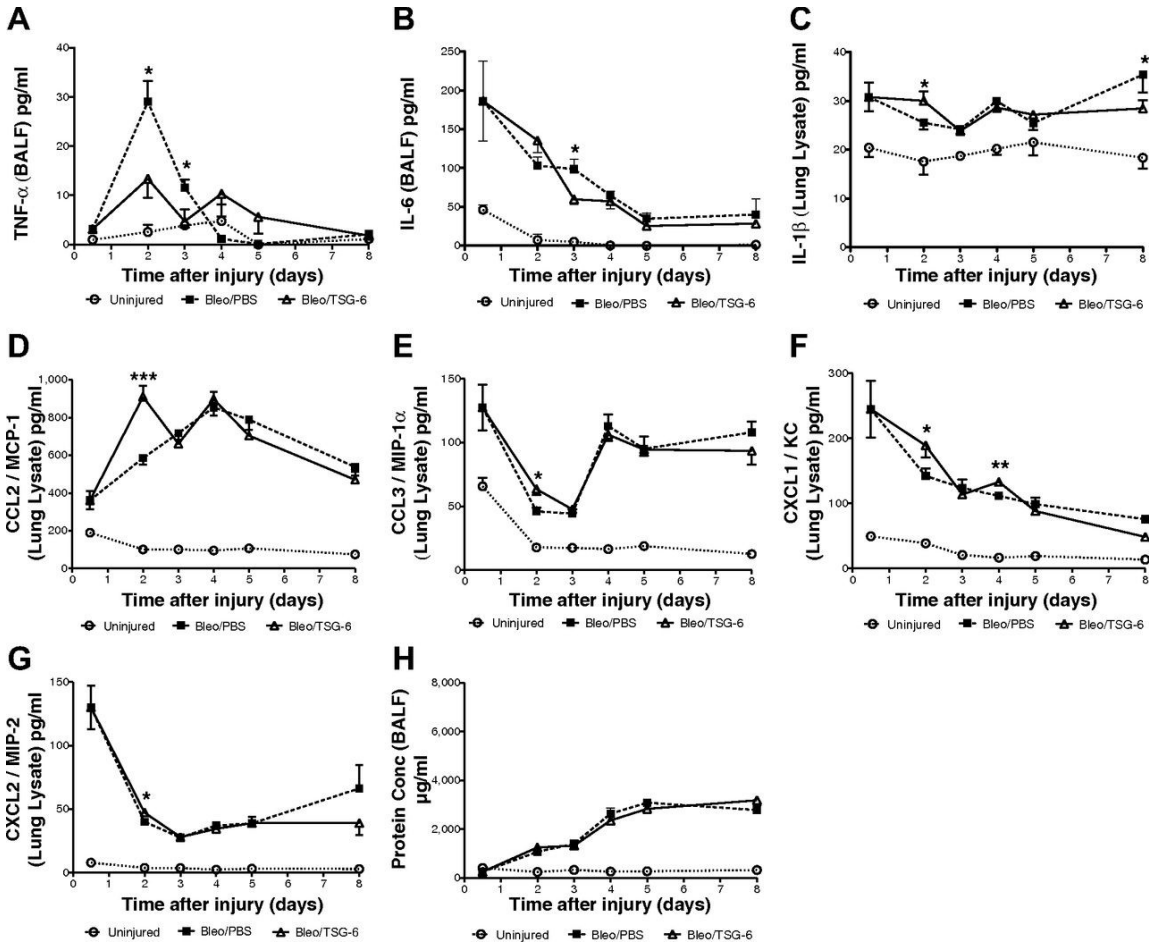

These changes were accompanied by an improvement in both the SpO_2 and survival of the bleomycin injured mice (Fig. 27A and B). Furthermore, there was a significant improvement in percent change of initial weight on days 7 and 8 following TSG-6 treatment (Fig. 27E), whereas there were no significant changes in heart and breath rates between groups (Fig. 27C and D). However, there was no significant reduction in fibrosis in TSG-6-treated lungs as measured by hydroxyproline content in the lungs on day 8 (data not shown), suggesting that there was no increase in fibrosis at this time.

V.4.4 The effects of TSG-6 are not observed in mice that do not express CD44

Previous reports demonstrated that some of the anti-inflammatory effects of TSG-6 involved its interaction with CD44 either by directly binding to the receptor or in a complex with hyaluronan (7, 24, 51). Therefore we elected to test the hypothesis that the beneficial effects of TSG-6 observed in the bleomycin model would not be observed in transgenic mice that did not express CD44 (42). As expected, TSG-6 administration had no effect in bleomycin-treated mice on SpO_2 (Fig. 28, A and B), or on BALF content of total cells, macrophages or neutrophils (Fig. 28, C–E). Also, administration of TSG-6 had no effect on the BALF levels of the cytokines IL-6, TNF-α, and IL-1β (Fig. 29, A–C). Similarly it had no effect on the BALF levels of the chemokines CCL2, CCL3, CXCL1, or CXCL2 (Fig. 29, D–G) and protein concentration (Fig. 29H).

Figure 27. TSG-6 improves functional SpO_2 and survival following bleomycin injury. A: effect of TSG-6 (50 μg) treatment on the dynamics of SpO_2 levels over the course of 8 days following bleomycin injury (representative of 3 independent experiments). Significant differences between TSG-6 and PBS groups were observed on days 5, 6, and 8. Note that TSG-6 treatment prevented the drop of SpO_2 levels below 90% threshold (dashed line) through day 8. P values represented in panel (A) only indicate significant differences between PBS and TSG-6 groups following bleomycin injury. B: Kaplan-Meier curves depicting survival proportions after administration of bleomycin. TSG-6 administration significantly improved survival compared with PBS-treated mice [P = 0.0363, log-rank (Mantel-Cox) test]. Dynamics of heart rate (C) and breath rate (D) following bleomycin injury and TSG-6 administration. No significant changes from preinjury baseline recordings (day 0) were detected. E: weight changes normalized to preinjury (day 0). Significant weight changes between bleomycin-injured (PBS and TSG-6) groups was noted on days 5, 7, and 8 and constituted ~20% weight loss in injured mice. Values are represented as arithmetic means ± SE (n = 5–8 mice per group). P values were calculated by 1-way ANOVA with a post hoc Bonferroni's multiple comparison analysis performed between all the groups. *P < 0.05 and **P < 0.01.

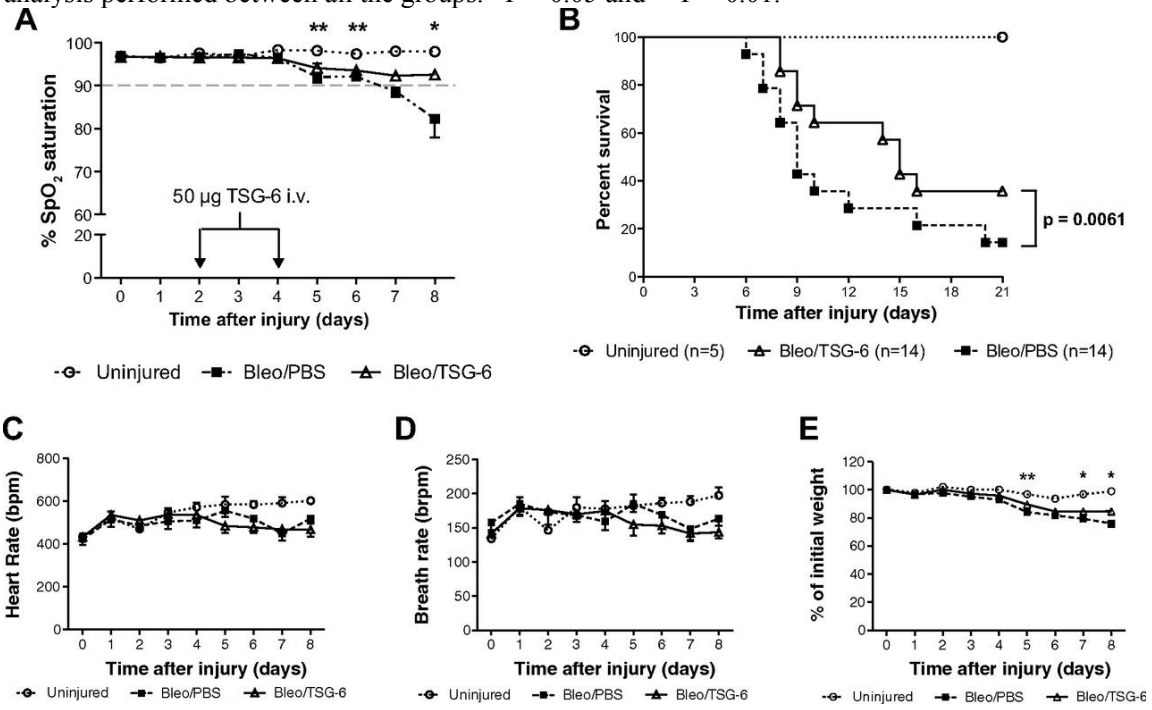

Figure 28. CD44 partly mediates beneficial effect of TSG-6 in vivo. A: effect of TSG-6 (50 μg) treatment on the dynamics of SpO_2 levels over the course of 8 days following bleomycin injury (representative of 2 independent experiments) in CD44 knockout mice. No significant differences between TSG-6 and PBS groups were observed on any of the days tested. Note that SpO_2 levels of both TSG-6 and PBS groups remained slightly above 90% threshold (dashed line) through day 8. B: dot plot represents the distribution of SpO_2 levels on day 8 following bleomycin injury. Significant differences were observed between bleomycin-injured and uninjured mice, although, in the absence of CD44, TSG-6 failed to improve SpO_2 levels over the PBS-treated group. C–E: BALF was collected in a similar manner as described above for the wild-type mice. No significant differences were observed between total cells, macrophages, and neutrophil numbers between TSG-6 and PBS-treated groups. Values are represented as arithmetic means ± SE (n = 5–8 mice per group). P values were calculated by 1-way ANOVA with a post hoc Bonferroni's multiple comparison analysis performed between all the groups. *P < 0.05.

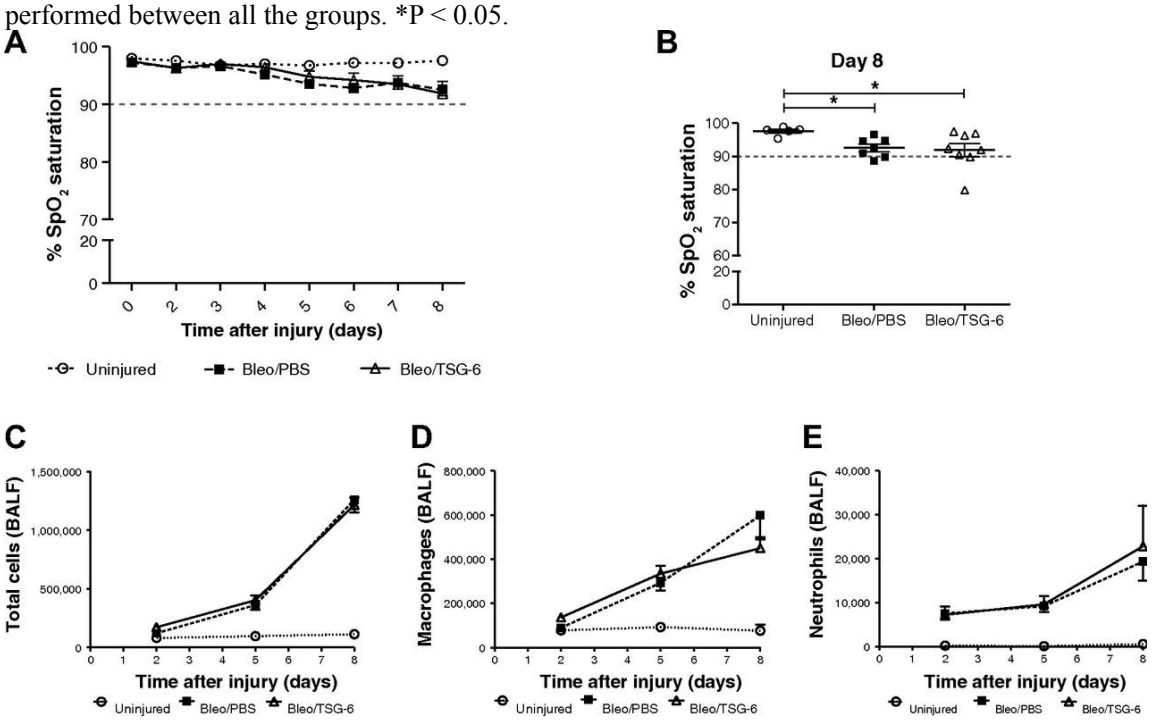

Figure 29. Temporal changes in cytokine/chemokine expression following TSG-6 treatment in CD44 knockout mice. No significant changes were observed in CD44 knockout mice after TSG-6 (50 μg) treatment in any of the proinflammatory cytokines examined such as IL-6 (A), TNF-α (B), and IL-1β (C), or in the expression of chemokines such as CCL2/MCP-1 (D), CCL3/MIP-1α (E), and CXCL2/MIP-2 (G), or in protein concentration (H) levels. However, TSG-6 treatment significantly decreased CXCL1/KC (F) levels only on day 5 compared with the PBS group. Values are represented as arithmetic means ± SE (n = 5–8 mice per group). P values were calculated by 1-way ANOVA with a post hoc Bonferroni's multiple comparison analysis performed between all the groups. No P values are indicated on this figure since there were no statistical differences between the bleomycin-injured (PBS and TSG-6) groups in most of the cytokines/chemokines tested and at any of the time points examined.

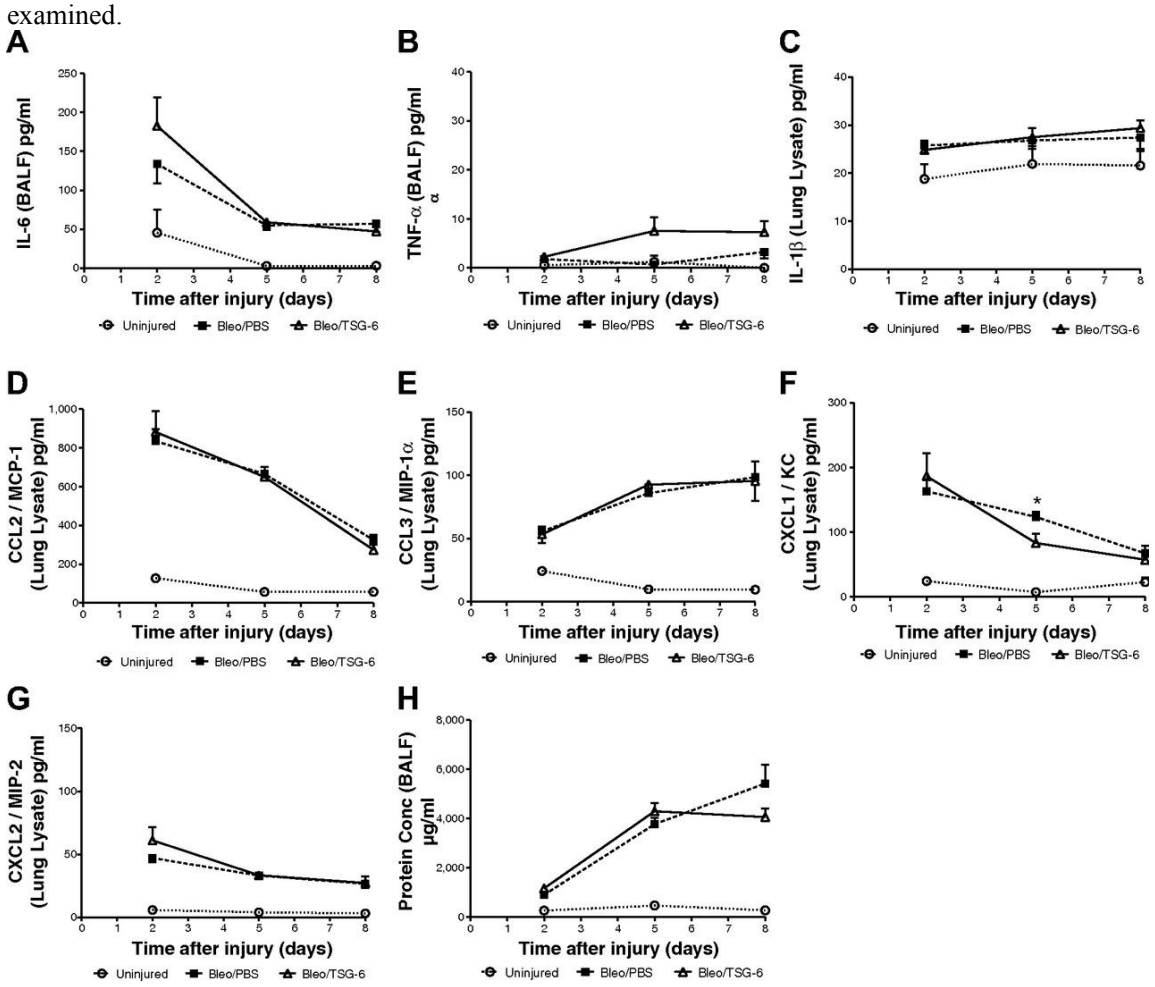

V.5 Discussion

The assay of SpO_2 with pulse oximeter provided a useful measure of the deleterious effects of bleomycin on the lungs of mice. The data are obtained in a rapid, quantitative, and real-time manner without the need to euthanize the mice. Therefore this assay has many advantages both in following the natural progression of the injury and for testing potential therapies for lung injury.

The response of the lung to injury by bleomycin is complex and occurs in several relatively distinct phases [181]–[185]. The beneficial effects previously observed with administration of MSCs may in fact reflect the plasticity of the cells in responding to injured tissues in a manner that is appropriate to the type and phase of the injuries [17], [94]. For example, MSCs were shown to produce beneficial effects [25], [48], [189], [192], [201] in various injury models by expressing factors that enhance vascularization (VEGF and IL-6), enhance cell proliferation (TGF-β, KGF), modulate immune responses (indoleamine 2,3-dioxygenase in human MSCs, iNOS with mouse MSCs, CCL2, MMP-9), reduce reactive oxygen species and apoptosis (stanniocalcin-1), and are antibacterial (peptide LL-37).

The characterization of the bleomycin model gave us an exact timeline of cellular and morphological events that occurred after the injury. Hence it allowed us to target specific inflammatory and functional events to examine whether TSG-6 had positive effects on reducing cytokine storm and infiltration of inflammatory cells and finally whether these early reductions translated to functional improvement and improved

survival. In the experiments described here, we elected to use iv administration of TSG-6 over intratracheal administration for several reasons: 1) clinical relevance, 2) increased risk of physical insult resulting from the repeated intubation required, and 3) oxygen-exacerbated damage to the lung during anesthesia [183], [202]–[204]. Under the conditions employed in this study, we reached therapeutic effect in the lungs by iv infusion of 50 μg TSG-6 protein. This was demonstrated by an improvement in oxygen saturation, increased survival, and modulation of cytokines following bleomycin injury.

To test TSG-6 in the bleomycin model, we infused the protein during the early inflammatory phase marked by the appearance of neutrophils and proinflammatory cytokines (IL-6 and TNF-α) in the BALF (day 2 and day 4). The TSG-6 decreased the inflammatory phase as indicated by a decrease in BALF on day 5 of total cells, macrophages, and neutrophils. It also decreased proinflammatory cytokine TNF-α on day 2, and IL-6 on day 3. At the same time, administration of TSG-6 increased the levels in BALF of chemokines (CCL2/MCP-1, CCL3/MIP-1α, CXCL1/KC, and CXCL2/MIP-2) that attract macrophages to resolve inflammation. The potential beneficial effects of the increase in chemokines is consistent with the observations by Liang et al. [205] that mice with lung-specific overexpression of CCL2/MCP-1 were protected from bleomycin-induced lung injury because of increased recruitment of cells capable of clearing apoptotic cells.

However, our data on day 5 demonstrate that the early increases in MCP-1 after TSG-6 administration only translated to a modest increase in macrophage recruitment

between days 2 and 5 but that these increases were still significantly lower than the number of macrophages recruited in the PBS-treated group. To explain this discrepancy, we speculate here that the macrophages recruited to alveolar spaces in TSG-6-treated animals possibly contained a larger proportion of alternatively activated or regulatory M2 macrophages. This could result in decrease of inflammation and subsequent decrease in the recruitment of proinflammatory monocytes from the circulation. In support of this theory, Roca et al. [206] have demonstrated that CCL2 (MCP-1) in the lungs can induce M2-type macrophage polarization. Furthermore, employing models of gastric aspiration and lung contusion, there is evidence for the protective effect of CCL2 and its receptor CCR2 in the pathogenesis of acute lung injury (ALI) by attenuating the inflammatory response, decreasing neutrophil infiltration, increasing macrophage recruitment, activation of the M2 polarized macrophages, and improved survival [187], [207]. In a pneumonia model of ALI, Amano et al. [208] also demonstrated that CCL2 was critical in decreasing neutrophil infiltration and increasing the phagocytosis of apoptotic neutrophils by alveolar macrophages. Thus this study might also help explain why there was decreased neutrophil recruitment on day 5 in our model following TSG-6 treatment despite elevated levels of MIP-2 and KC chemokines on day 2. We speculate that TSG-6 treatment of mice that were injured with bleomycin results in a complex interaction between different types of cells and their corresponding cytokines, which needs further investigation. However, the combined results from these studies lead us to conclude that the early elevated chemokine levels following TSG-6 treatment in our model could

partly explain the overall beneficial effects that we observed such as resolution of inflammation and reduced neutrophil numbers due to either reduced recruitment of neutrophils or their increased phagocytosis, thus resulting in improved oxygenation and survival. In addition, decrease in levels of TNF-α by TSG-6 could have resulted in decreased levels of apoptosis in alveolar epithelium as indicated by Wang et al. [209], although apoptosis was not addressed in our study. Thus the cumulative effects of TSG-6 on the early inflammatory stage in part explained the subsequent increase in SpO_2 and survival seen in treated mice compared with controls (Fig. 30). However, in this model, there was some mortality in bleomycin-injured mice treated with PBS, with the earliest occurrence beginning on day 6. Thus, had these mice survived to day 8, the average SpO_2 levels would have been much lower and accordingly the numbers of cellular infiltrates in BALF would have been much higher compared with the bleomycin/TSG-6 group than what is represented. Although not explored here, more frequent or larger doses on TSG-6 may have been even more effective.

Figure 30. Modulatory effects of TSG-6 in bleomycin-injured lungs. The beneficial effects of TSG-6 on modulating the early inflammatory phase in bleomycin-injured lungs is indicated by 1) a decrease in proinflammatory cytokines IL-6 and TNF-α (days 2 and 3), 2) an increase in chemokines CCL2, CCL3, KC, and CXCL2 (days 2 and 4), and 3) a corresponding decrease in total cells and infiltrating cells such as macrophages and neutrophils (day 5). These early modulatory events promoted by TSG-6 lead to functional improvement by preventing the drop of SpO_2 levels below 90% (day 8) and decreased mortality (weeks 1-3).

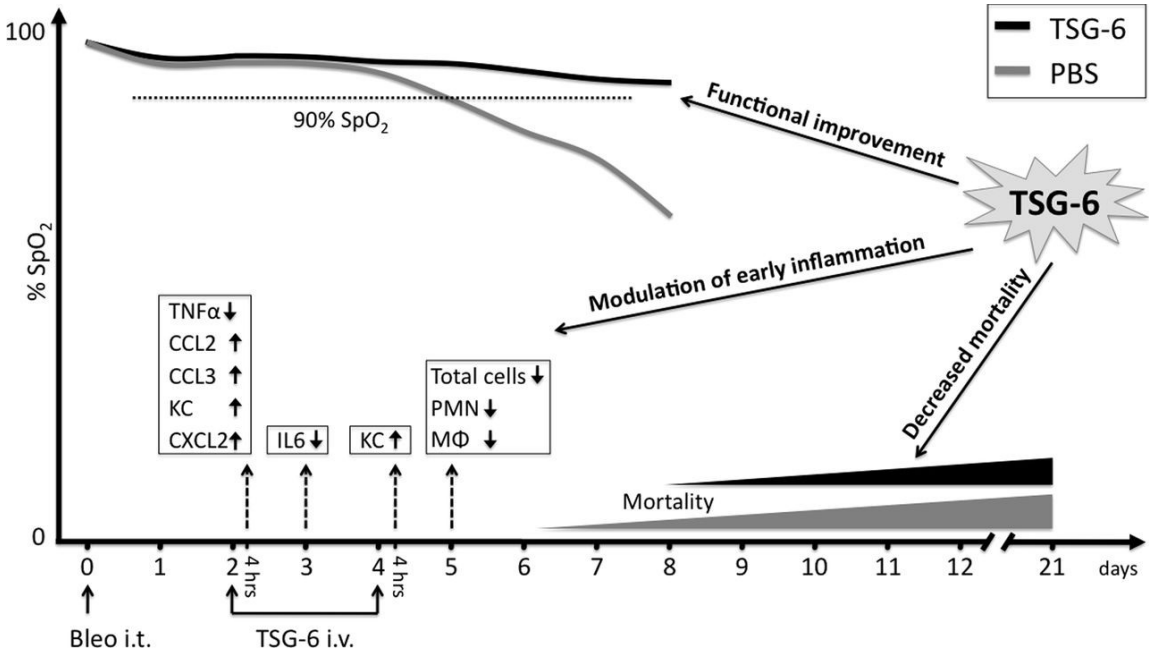

TSG-6 has been previously shown to have multiple interactions that can be anti-inflammatory [85], [197], [198], [200]. Particularly, in a recently published study by Choi et al. [88], it was shown that at least part of the inflammatory action of TSG-6 in the peritonitis model could be explained by its direct or indirect interaction with CD44 on resident macrophages. TSG-6 bound to CD44, either directly or in a complex with hyaluronan, to dissociate CD44 from TLR2 and thereby limit TLR2-driven NF-κB

signaling. In CD44 knockout mice, bleomycin induced an unrelenting inflammatory response in a TLR2- and TLR4-dependent manner [210], [211]. TSG-6 was also effective in wild-type mice but ineffective in CD44 knockout mice employed in a mouse model for sterile injury to the cornea [212]. In the present study, we employed the CD44 knockout mouse model, similar to that used in the study by Choi et al. In these mice, CD44 expression is constitutively knocked out in all cell lineages and not restricted to only macrophages. Also, on the basis of previous publications [87], [88] we hypothesized that resident macrophages with functional CD44 could be important in mediating the effects of TSG-6 in bleomycin-injured lungs. Since TSG-6 was not effective in reducing inflammation and improving bleomycin-induced injury in the CD44 knockout mice, the results were consistent with the conclusion that TSG-6 decreased inflammation by interacting with functional CD44 on resident macrophages in a manner previously demonstrated in zymosan-induced peritonitis [88] and chemical injury to the cornea [87].

Toxic agents such as bleomycin trigger a cascade of destructive events in the lung. It seems unlikely that any single therapy can halt all of them. The results presented in this study demonstrate that the systemic administration of TSG-6 improved functional outcome and survival of bleomycin-injured mice by modulating inflammation at early stages. Hence these data suggest that it may be useful to target specific phases in the cascade with agents such as TSG-6 for the early inflammatory phase. Similar phase-specific strategies may be useful for other diseases of the lung.

CHAPTER VI

CONCLUSIONS

Mesenchymal stem cells represent an attractive therapeutic option based on the results from preclinical studies. Most of beneficial effects of MSCs, such as modulation of immunity, tissue regeneration, inhibition of inflammation is attributed to their ability to actively respond to the surroundings and produce therapeutic factors [48], [62]. There is a need to investigate both, basic MSCs biology, and their therapeutic potential.

The dissertation focused on studying basic biology of MSCs in vitro and the effects of the cells and their secreted factor TSG-6 in vivo models of diseases.

VI.1 In vitro biology of single-cell-derived MSCs colony

In vitro single-cell colony formation was chosen as an object to study the heterogeneity of MSCs in culture. It was hypothesized previously that different parts of the colony exhibit different microenvironments that might affect their fate [33]. We used laser-capture microdissection to specifically isolate two distinct parts of MSCs colony – densely packed inside (IN) and outside (OUT). Using comparative microarray analysis we showed that OUT cells expressed many cell-cycle, division and motility genes, while IN cells expresses ECM-related genes. These findings were also confirmed by immunofluorescence of different parts of the colonies. Not surprisingly we found that IN region of the colonies differentiated into fat and bone more readily than OUT region. However the functional assays did not produce expected results. We sub-cloned IN and

OUT regions and showed virtually no difference in growth and clonogenicity of the cells regardless of the origin. This result suggests that in vitro colony of MSCs represents a unique niche-like structure that contains distinct microenviroments but able to preserve the characteristics of cells, such as ability to differentiate and self renew.

VI.2 In vivo effects of MSCs

We chose mouse model of HCl-induced lung injury to test the effects of MSCs. The chosen model mimics one of the leading causes of deaths in ICU patients – acute respiratory distress syndrome. We utilized two treatment approaches – administration of MSCs intravenously and intraperitoneally. To our surprise, intravenous injection of the cells did not produce beneficial results. On the contrary, there was an increase in inflammatory cell in the bronchial lavage fluid after intravenous MSCs administration. Intraperitoneal injections, however, improved lung function and reduced inflammation in the lungs. Intraperitoneal administration of MSCs has been shown beneficial in several models of diseases [86], [91], [95], [99], moreover, intraperitoneal administration was shown to be superior to intravenous in certain models [95]. The negative effect of MSCs after intravenous administration could be attributed to several factors, including the lung embolization [54], [55], donor variation [37]–[39] and the model itself. Further investigation is needed to address these issues.

Little is known about the fate of MSCs after the administration inside peritoneal cavity. We followed the fate of human MSCs administered i.p. using several methods. As we reported previously [65] we also observed the aggregation of MSCs within minutes

after the injection. When the aggregates of MSCs were analyzed by immunofluorescence, we discovered the presence of CD11b and B220 positive cells, possibly B1 cells and peritoneal macrophages. The aggregates of MSCs were free-floating or adhered to various tissues in peritoneal cavity. Particularly we showed the preferential adherence of the aggregates to mouse omentum. Very few MSCs were found in mesentery, lymph nodes and spleen. The omentum has gained attention in scientific literature recently. Thus, it was shown that it contains clusters of immune cells that include macrophages and B-cells [213]–[215]. These clusters participate in mounting the immune response to viruses [164] and also respond to pathogens such as LPS. Importantly omental milky spots participate in transport of lymphocytes from and into systemic circulation and serve as site of migration and adherence for cancer cells originating in peritoneal cavity [165], [215], [216].

Aggregated and adhered MSCs survived for less than a week and recruited the cells to omentum and peritoneal cavity. The aggregation and recruitment of immune cell pre-conditioned the immune system in peritoneal cavity. Analysis of cytokines inside peritoneal cavity showed mixed response with early peak of type-1 related cytokines (IL12p70, TNF-α) and prolonged peaks of type-2 cytokines (IL13, PGE_2). Systemic administration of LPS unexpectedly resulted in increase of production of pro-inflammatory cytokines.

The responses of naive mice to MSCs could be attributed to interaction of human cells with mouse immune cells or reactivity of host to the antigens from bovine serum

used to culture the cells and carried by MSCs [170]. In addition to conventional immune cells, peritoneal cavity contains special class of recently discovered innate lymphoid cells [159]–[161]. Their characteristics is lack of T- or B-cell markers and the ability to produce type-2-associated cytokines earlier than canonical Th2 cells [217]. Interestingly we showed early cytokine production, including Th2-related cytokines IL13, PGE_2 in response to MSCs. It will be important to investigate in future studies whether MSCs communicate with these cells in peirtoneal cavity or elsewhere in a body.

VI.3 In vivo effects of TSG-6

To study the effects of TSG-6 in models of lung injury we administered the protein intravenously in HCl-injured and bleomycin-injured mice. While TSG-6 treatment of bleomycin-injured mice prevented functional decline, there was no significant effect of TSG-6 on lung function in HCl-induced lung injury. In both models TSG-6 was effective in diminishing the inflammation in the lungs, in support of previous studies in lung injury [86] and other models [54], [87], [175]. As proposed by Choi et al, TSG-6 could inhibit inflammatory pathways in macrophages by acting through CD44 receptor and preventing TLR-2-induced NFkB translocation [88]. Similarly we showed that CD44 knockout mice failed to respond to TSG-6 treatment. Future studies are necessary to determine the effectiveness of TSG-6 in other models of lung injury and in clinical settings.

REFERENCES

[1] A. J. Friedenstein, I. I. Piatetzky-Shapiro, and K. V Petrakova, "Osteogenesis in transplants of bone marrow cells.," *J. Embryol. Exp. Morphol.*, vol. 16, no. 3, pp. 381–390, Dec. 1966.

[2] US National Institutes of Health, "US National Library Of Medicine." [Online]. Available: www.ncbi.nlm.nih.gov. [Accessed: 20-Feb-2015].

[3] US National Instututes of Health, "Research Portfolio Online Reporting Tools (RePORT)," 2015. [Online]. Available: projectreporter.nih.gov. [Accessed: 01-Feb-2015].

[4] US National Instututes of Health, "ClinicalTrials.gov." [Online]. Available: www.clinicaltrials.gov. [Accessed: 01-Feb-2015].

[5] M. F. Pittenger, A. M. Mackay, S. C. Beck, R. K. Jaiswal, R. Douglas, J. D. Mosca, M. A. Moorman, D. W. Simonetti, S. Craig, and D. R. Marshak, "Multilineage potential of adult human mesenchymal stem cells.," *Science*, vol. 284, no. 5411, pp. 143–147, Apr. 1999.

[6] C. M. Digirolamo, D. Stokes, D. Colter, D. G. Phinney, R. Class, and D. J. Prockop, "Propagation and senescence of human marrow stromal cells in culture: A simple colony-forming assay identifies samples with the greatest potential to propagate and differentiate," *Br. J. Haematol.*, vol. 107, no. 2, pp. 275–281, Nov. 1999.

[7] L. Jackson, D. R. Jones, P. Scotting, and V. Sottile, "Adult mesenchymal stem cells: differentiation potential and therapeutic applications.," *J. Postgrad. Med.*, vol. 53, pp. 121–127.

[8] G. Chamberlain, J. Fox, B. Ashton, and J. Middleton, "Concise review: mesenchymal stem cells: their phenotype, differentiation capacity, immunological features, and potential for homing.," *Stem Cells*, vol. 25, pp. 2739–2749, 2007.

[9] I. Sekiya, B. L. Larson, J. T. Vuoristo, J.-G. Cui, and D. J. Prockop, "Adipogenic differentiation of human adult stem cells from bone marrow stroma (MSCs).," *J. Bone Miner. Res.*, vol. 19, pp. 256–264, 2004.

[10] D. C. Colter, I. Sekiya, and D. J. Prockop, "Identification of a subpopulation of rapidly self-renewing and multipotential adult stem cells in colonies of human marrow stromal cells.," *Proc. Natl. Acad. Sci. U. S. A.*, vol. 98, no. 14, pp. 7841–7845, Jul. 2001.

[11] A. M. Mackay, S. C. Beck, J. M. Murphy, F. P. Barry, C. O. Chichester, and M. F. Pittenger, "Chondrogenic differentiation of cultured human mesenchymal stem

cells from marrow.," *Tissue Eng.*, vol. 4, pp. 415–428, 1998.

[12] I. Sekiya, D. C. Colter, and D. J. Prockop, "BMP-6 enhances chondrogenesis in a subpopulation of human marrow stromal cells.," *Biochem. Biophys. Res. Commun.*, vol. 284, pp. 411–418, 2001.

[13] I. Sekiya, B. L. Larson, J. T. Vuoristo, R. L. Reger, and D. J. Prockop, "Comparison of effect of BMP-2, -4, and -6 on in vitro cartilage formation of human adult stem cells from bone marrow stroma," *Cell Tissue Res.*, vol. 320, pp. 269–276, 2005.

[14] A. Hermann, R. Gastl, S. Liebau, M. O. Popa, J. Fiedler, B. O. Boehm, M. Maisel, H. Lerche, J. Schwarz, R. Brenner, and A. Storch, "Efficient generation of neural stem cell-like cells from adult human bone marrow stromal cells.," *J. Cell Sci.*, vol. 117, pp. 4411–4422, 2004.

[15] J. Lu, S. Moochhala, X.-L. Moore, K. C. Ng, M. H. Tan, L. K. H. Lee, B. He, M. C. Wong, and E.-A. Ling, "Adult bone marrow cells differentiate into neural phenotypes and improve functional recovery in rats following traumatic brain injury.," *Neurosci. Lett.*, vol. 398, pp. 12–17, 2006.

[16] D. N. Kotton, B. Y. Ma, W. V Cardoso, E. A. Sanderson, R. S. Summer, M. C. Williams, and A. Fine, "Bone marrow-derived cells as progenitors of lung alveolar epithelium.," *Development*, vol. 128, pp. 5181–5188, 2001.

[17] L. A. Ortiz, F. Gambelli, C. McBride, D. Gaupp, M. Baddoo, N. Kaminski, and D. G. Phinney, "Mesenchymal stem cell engraftment in lung is enhanced in response to bleomycin exposure and ameliorates its fibrotic effects.," *Proc. Natl. Acad. Sci. U. S. A.*, vol. 100, no. 14, pp. 8407–8411, Jul. 2003.

[18] M. Rojas, J. Xu, C. R. Woods, A. L. Mora, W. Spears, J. Roman, and K. L. Brigham, "Bone marrow-derived mesenchymal stem cells in repair of the injured lung.," *Am. J. Respir. Cell Mol. Biol.*, vol. 33, no. 2, pp. 145–52, Aug. 2005.

[19] S. Arnhold, P. Heiduschka, H. Klein, Y. Absenger, S. Basnaoglu, F. Kreppel, S. Renke-Fahle, S. Kochanek, K. U. Bartz-Schmidt, K. Addicks, and U. Schraermeyer, "Adenovirally transduced bone marrow stromal cells differentiate into pigment epithelial cells and induce rescue effects in RCS rats," *Investig. Ophthalmol. Vis. Sci.*, vol. 47, pp. 4121–4129, 2006.

[20] S. Arnhold, Y. Absenger, H. Klein, K. Addicks, and U. Schraermeyer, "Transplantation of bone marrow-derived mesenchymal stem cells rescue photoreceptor cells in the dystrophic retina of the rhodopsin knockout mouse," *Graefe's Arch. Clin. Exp. Ophthalmol.*, vol. 245, pp. 414–422, 2007.

[21] X. Fu, L. Fang, X. Li, B. Cheng, and Z. Sheng, "Enhanced wound-healing quality with bone marrow mesenchymal stem cells autografting after skin injury," *Wound Repair Regen.*, vol. 14, pp. 325–335, 2006.

[22] H. Nakagawa, S. Akita, M. Fukui, T. Fujii, and K. Akino, “Human mesenchymal stem cells successfully improve skin-substitute wound healing,” *Br. J. Dermatol.*, vol. 153, pp. 29–36, 2005.

[23] M. B. Herrera, B. Bussolati, S. Bruno, V. Fonsato, G. M. Romanazzi, and G. Camussi, “Mesenchymal stem cells contribute to the renal repair of acute tubular epithelial injury.,” *Int. J. Mol. Med.*, vol. 14, pp. 1035–1041, 2004.

[24] M. Morigi, B. Imberti, C. Zoja, D. Corna, S. Tomasoni, M. Abbate, D. Rottoli, S. Angioletti, A. Benigni, N. Perico, M. Alison, and G. Remuzzi, “Mesenchymal stem cells are renotropic, helping to repair the kidney and improve function in acute renal failure.,” *J. Am. Soc. Nephrol.*, vol. 15, pp. 1794–1804, 2004.

[25] D. J. Prockop and J. Youn Oh, “Mesenchymal Stem/Stromal Cells (MSCs): Role as Guardians of Inflammation,” *Molecular Therapy*, vol. 20, no. 1. pp. 14–20, Jan-2012.

[26] TAMHSC, “MSC Distribution Center.” [Online]. Available: medicine.tamhsc.edu/irm/msc-distribution.html.

[27] A. J. Friedenstein, J. F. Gorskaja, and N. N. Kulagina, “Fibroblast precursors in normal and irradiated mouse hematopoietic organs.,” *Exp. Hematol.*, vol. 4, no. 5, pp. 267–274, 1976.

[28] H. Castro-Malaspina, R. E. Gay, G. Resnick, N. Kapoor, P. Meyers, D. Chiarieri, S. McKenzie, H. E. Broxmeyer, and M. A. Moore, “Characterization of human bone marrow fibroblast colony-forming cells (CFU-F) and their progeny.,” *Blood*, vol. 56, no. 2, pp. 289–301, 1980.

[29] A. I. Caplan, “Mesenchymal stem cells.,” *J. Orthop. Res.*, vol. 9, no. 5, pp. 641–650, Sep. 1991.

[30] M. Dominici, K. Le Blanc, I. Mueller, I. Slaper-Cortenbach, F. Marini, D. Krause, R. Deans, A. Keating, D. Prockop, and E. Horwitz, “Minimal criteria for defining multipotent mesenchymal stromal cells. The International Society for Cellular Therapy position statement.,” *Cytotherapy*, vol. 8, no. 4, pp. 315–317, Jan. 2006.

[31] K. C. Russell, M. R. Lacey, J. K. Gilliam, H. A. Tucker, D. G. Phinney, and K. C. O’Connor, “Clonal analysis of the proliferation potential of human bone marrow mesenchymal stem cells as a function of potency,” *Biotechnol. Bioeng.*, vol. 108, no. 11, pp. 2716–2726, May 2011.

[32] K. C. Russell, D. G. Phinney, M. R. Lacey, B. L. Barrilleaux, K. E. Meyertholen, and K. C. O’Connor, “In vitro high-capacity assay to quantify the clonal heterogeneity in trilineage potential of mesenchymal stem cells reveals a complex hierarchy of lineage commitment.,” *Stem Cells*, vol. 28, no. 4, pp. 788–98, Apr. 2010.

[33] C. A. Gregory, J. Ylostalo, and D. J. Prockop, “Adult bone marrow stem/progenitor cells (MSCs) are preconditioned by microenvironmental ‘niches’ in culture: a two-stage hypothesis for regulation of MSC fate.,” *Sci. STKE*, vol. 2005, no. 294, p. pe37, Jul. 2005.

[34] B. L. Larson, J. Ylöstalo, and D. J. Prockop, “Human multipotent stromal cells undergo sharp transition from division to development in culture.,” *Stem Cells*, vol. 26, no. 1, pp. 193–201, Jan. 2008.

[35] R. H. Lee, M. J. Seo, A. A. Pulin, C. A. Gregory, J. Ylostalo, and D. J. Prockop, “The CD34-like protein PODXL and {alpha}6-integrin (CD49f) identify early progenitor MSCs with increased clonogenicity and migration to infarcted heart in mice,” *Blood*, vol. 113, no. 4, pp. 816–826, 2009.

[36] H. L. Ryang, C. H. Shu, J. Munoz, S. J. Jin, N. R. Lee, R. Pochampally, and D. J. Prockop, “A subset of human rapidly self-renewing marrow stromal cells preferentially engraft in mice,” *Blood*, vol. 107, no. 5, pp. 2153–2161, Mar. 2006.

[37] D. G. Phinney, G. Kopen, W. Righter, S. Webster, N. Tremain, and D. J. Prockop, “Donor variation in the growth properties and osteogenic potential of human marrow stromal cells.,” *J. Cell. Biochem.*, vol. 75, no. 3, pp. 424–436, 1999.

[38] R. H. Lee, J. M. Yu, A. M. Foskett, G. Peltier, J. C. Reneau, N. Bazhanov, J. Y. Oh, and D. J. Prockop, “TSG-6 as a biomarker to predict efficacy of human mesenchymal stem/progenitor cells (hMSCs) in modulating sterile inflammation in vivo.,” *Proc. Natl. Acad. Sci. U. S. A.*, vol. 111, no. 47, pp. 16766–71, 2014.

[39] D. G. Phinney, “Biochemical heterogeneity of mesenchymal stem cell populations: Clues to their therapeutic efficacy,” *Cell Cycle*, vol. 6, no. 23. pp. 2884–2889, 2007.

[40] D. G. Phinney, G. Kopen, R. L. Isaacson, and D. J. Prockop, “Plastic adherent stromal cells from the bone marrow of commonly used strains of inbred mice: Variations in yield, growth, and differentiation,” *J. Cell. Biochem.*, vol. 72, no. 4, pp. 570–585, Mar. 1999.

[41] I. R. Murray, C. C. West, W. R. Hardy, A. W. James, T. S. Park, A. Nguyen, T. Tawonsawatruk, L. Lazzari, C. Soo, and B. Péault, “Natural history of mesenchymal stem cells, from vessel walls to culture vessels,” *Cellular and Molecular Life Sciences*, vol. 71, no. 8. pp. 1353–1374, 2014.

[42] P. Bianco, M. Riminucci, S. Gronthos, and P. G. Robey, “Bone marrow stromal stem cells: nature, biology, and potential applications.,” *Stem Cells*, vol. 19, no. 3, pp. 180–192, 2001.

[43] M. Crisan, S. Yap, L. Casteilla, C.-W. Chen, M. Corselli, T. S. Park, G. Andriolo, B. Sun, B. Zheng, L. Zhang, C. Norotte, P.-N. Teng, J. Traas, R. Schugar, B. M.

Deasy, S. Badylak, H.-J. Buhring, J.-P. Giacobino, L. Lazzari, J. Huard, and B. Péault, “A perivascular origin for mesenchymal stem cells in multiple human organs.,” *Cell Stem Cell*, vol. 3, no. 3, pp. 301–313, 2008.

[44] D. T. Covas, R. A. Panepucci, A. M. Fontes, W. A. Silva, M. D. Orellana, M. C. C. Freitas, L. Neder, A. R. D. Santos, L. C. Peres, M. C. Jamur, and M. A. Zago, “Multipotent mesenchymal stromal cells obtained from diverse human tissues share functional properties and gene-expression profile with CD146 + perivascular cells and fibroblasts,” *Exp. Hematol.*, vol. 36, no. 5, pp. 642–654, 2008.

[45] Y. Takashima, T. Era, K. Nakao, S. Kondo, M. Kasuga, A. G. Smith, and S. I. Nishikawa, “Neuroepithelial Cells Supply an Initial Transient Wave of MSC Differentiation,” *Cell*, vol. 129, no. 7, pp. 1377–1388, 2007.

[46] S. Méndez-Ferrer, T. V Michurina, F. Ferraro, A. R. Mazloom, B. D. Macarthur, S. A. Lira, D. T. Scadden, A. Ma’ayan, G. N. Enikolopov, and P. S. Frenette, “Mesenchymal and haematopoietic stem cells form a unique bone marrow niche.,” *Nature*, vol. 466, no. 7308, pp. 829–834, Aug. 2010.

[47] V. L. Battula, K. W. Evans, B. G. Hollier, Y. Shi, F. C. Marini, A. Ayyanan, R. Y. Wang, C. Brisken, R. Guerra, M. Andreeff, and S. A. Mani, “Epithelial-mesenchymal transition-derived cells exhibit multilineage differentiation potential similar to mesenchymal stem cells,” *Stem Cells*, vol. 28, no. 8, pp. 1435–1445, 2010.

[48] D. J. Prockop, D. J. Kota, N. Bazhanov, and R. L. Reger, “Evolving paradigms for repair of tissues by adult stem/progenitor cells (MSCs).,” *J. Cell. Mol. Med.*, vol. 14, no. 9, pp. 2190–9, Sep. 2010.

[49] E. M. Horwitz, D. J. Prockop, L. A. Fitzpatrick, W. W. Koo, P. L. Gordon, M. Neel, M. Sussman, P. Orchard, J. C. Marx, R. E. Pyeritz, and M. K. Brenner, “Transplantability and therapeutic effects of bone marrow-derived mesenchymal cells in children with osteogenesis imperfecta.,” *Nat. Med.*, vol. 5, no. 3, pp. 309–313, 1999.

[50] E. M. Horwitz, D. J. Prockop, P. L. Gordon, W. W. Koo, L. A. Fitzpatrick, M. D. Neel, M. E. McCarville, P. J. Orchard, R. E. Pyeritz, and M. K. Brenner, “Clinical responses to bone marrow transplantation in children with severe osteogenesis imperfecta.,” *Blood*, vol. 97, no. 5, pp. 1227–1231, 2001.

[51] F. Tögel and C. Westenfelder, “Stem cells in acute kidney injury repair.,” *Minerva Urol. Nefrol.*, vol. 61, no. 3, pp. 205–213, 2009.

[52] R. H. Lee, M. J. Seo, R. L. Reger, J. L. Spees, A. A. Pulin, S. D. Olson, and D. J. Prockop, “Multipotent stromal cells from human marrow home to and promote repair of pancreatic islets and renal glomeruli in diabetic NOD/scid mice.,” *Proc.*

Natl. Acad. Sci. U. S. A., vol. 103, no. 46, pp. 17438–17443, 2006.

[53] U. Krause, C. Harter, A. Seckinger, D. Wolf, A. Reinhard, F. Bea, T. Dengler, S. Hardt, A. Ho, H. A. Katus, H. Kuecherer, and A. Hansen, "Intravenous delivery of autologous mesenchymal stem cells limits infarct size and improves left ventricular function in the infarcted porcine heart.," *Stem Cells Dev.*, vol. 16, no. 1, pp. 31–37, 2007.

[54] R. H. Lee, A. A. Pulin, M. J. Seo, D. J. Kota, J. Ylostalo, B. L. Larson, L. Semprun-Prieto, P. Delafontaine, and D. J. Prockop, "Intravenous hMSCs Improve Myocardial Infarction in Mice because Cells Embolized in Lung Are Activated to Secrete the Anti-inflammatory Protein TSG-6," *Cell Stem Cell*, vol. 5, no. 1, pp. 54–63, Jul. 2009.

[55] Y. Iso, J. L. Spees, C. Serrano, B. Bakondi, R. Pochampally, Y.-H. H. Song, B. E. Sobel, P. Delafontaine, and D. J. Prockop, "Multipotent human stromal cells improve cardiac function after myocardial infarction in mice without long-term engraftment," *Biochem. Biophys. Res. Commun.*, vol. 354, no. 3, pp. 700–706, Mar. 2007.

[56] S. T. Lee, J. H. Jang, J. W. Cheong, J. S. Kim, H. Y. Maemg, J. S. Hahn, Y. W. Ko, and Y. H. Min, "Treatment of high-risk acute myelogenous leukaemia by myeloablative chemoradiotherapy followed by co-infusion of T cell-depleted haematopoietic stem cells and culture-expanded marrow mesenchymal stem cells from a related donor with one fully mismatched hu," *Br. J. Haematol.*, vol. 118, no. 4, pp. 1128–1131, 2002.

[57] H. M. Lazarus, O. N. Koc, S. M. Devine, P. Curtin, R. T. Maziarz, H. K. Holland, E. J. Shpall, P. McCarthy, K. Atkinson, B. W. Cooper, S. L. Gerson, M. J. Laughlin, F. R. Loberiza, A. B. Moseley, and A. Bacigalupo, "Cotransplantation of HLA-identical sibling culture-expanded mesenchymal stem cells and hematopoietic stem cells in hematologic malignancy patients," *Biol. Blood Marrow Transplant.*, vol. 11, no. 5, pp. 389–398, 2005.

[58] J. L. Spees, S. D. Olson, J. Ylostalo, P. J. Lynch, J. Smith, A. Perry, A. Peister, M. Y. Wang, and D. J. Prockop, "Differentiation, cell fusion, and nuclear fusion during ex vivo repair of epithelium by human adult stem cells from bone marrow stroma.," *Proc. Natl. Acad. Sci. U. S. A.*, vol. 100, no. 5, pp. 2397–2402, 2003.

[59] M. N. Islam, S. R. Das, M. T. Emin, M. Wei, L. Sun, K. Westphalen, D. J. Rowlands, S. K. Quadri, S. Bhattacharya, and J. Bhattacharya, "Mitochondrial transfer from bone-marrow–derived stromal cells to pulmonary alveoli protects against acute lung injury," *Nature Medicine*, vol. 18, no. 5. Nature Publishing Group, pp. 759–765, 15-Apr-2012.

[60] A. P. Robinson, J. E. Foraker, J. Ylostalo, and D. J. Prockop, "Human

Stem/Progenitor Cells from Bone Marrow Enhance Glial Differentiation of Rat Neural Stem Cells: A Role for Transforming Growth Factor β and Notch Signaling.," *Stem Cells Dev.*, vol. 20, no. 2, pp. 289–300, Feb. 2011.

[61] K. Németh, A. Leelahavanichkul, P. S. T. Yuen, B. Mayer, A. Parmelee, K. Doi, P. G. Robey, K. Leelahavanichkul, B. H. Koller, J. M. Brown, X. Hu, I. Jelinek, R. A. Star, and E. Mezey, "Bone marrow stromal cells attenuate sepsis via prostaglandin E(2)-dependent reprogramming of host macrophages to increase their interleukin-10 production.," *Nat. Med.*, vol. 15, no. 1, pp. 42–49, 2009.

[62] R. H. Lee, J. Y. Oh, H. Choi, and N. Bazhanov, "Therapeutic factors secreted by mesenchymal stromal cells and tissue repair," *J. Cell. Biochem.*, vol. 112, no. 11, pp. 3073–3078, Nov. 2011.

[63] G. J. Block, S. Ohkouchi, F. Fung, J. Frenkel, C. Gregory, R. Pochampally, G. Dimattia, D. E. Sullivan, and D. J. Prockop, "Multipotent Stromal Cells (MSCs) are Activated to Reduce Apoptosis in Part by Upregulation and Secretion of Stanniocalcin-1 (STC-1).," *Stem Cells*, pp. 670–681, Dec. 2008.

[64] S. Ohkouchi, G. J. Block, A. M. Katsha, M. Kanehira, M. Ebina, T. Kikuchi, Y. Saijo, T. Nukiwa, and D. J. Prockop, "Mesenchymal Stromal Cells Protect Cancer Cells From ROS-induced Apoptosis and Enhance the Warburg Effect by Secreting STC1," *Mol. Ther.*, vol. 20, no. 2, pp. 417–423, Feb. 2012.

[65] T. J. Bartosh, J. H. Ylöstalo, N. Bazhanov, J. Kuhlman, and D. J. Prockop, "Dynamic compaction of human mesenchymal stem/precursor cells into spheres self-activates caspase-dependent Il1 signaling to enhance secretion of modulators of inflammation and immunity (PGE2, TSG6, and STC1)," *Stem Cells*, vol. 31, no. 11, pp. 2443–2456, Nov. 2013.

[66] X. Y. Yu, Y. J. Geng, X. H. Li, Q. X. Lin, Z. X. Shan, S. G. Lin, Y. H. Song, and Y. Li, "The effects of mesenchymal stem cells on c-kit up-regulation and cell-cycle re-entry of neonatal cardiomyocytes are mediated by activation of insulin-like growth factor 1 receptor," *Mol. Cell. Biochem.*, vol. 332, no. 1–2, pp. 25–32, 2009.

[67] T. Tsubokawa, K. Yagi, C. Nakanishi, M. Zuka, A. Nohara, H. Ino, N. Fujino, T. Konno, M. Kawashiri, H. Ishibashi-Ueda, N. Nagaya, and M. Yamagishi, "Impact of anti-apoptotic and anti-oxidative effects of bone marrow mesenchymal stem cells with transient overexpression of heme oxygenase-1 on myocardial ischemia.," *Am. J. Physiol. Heart Circ. Physiol.*, vol. 298, no. 5, pp. H1320–H1329, 2010.

[68] D. Angoulvant, F. Ivanes, R. Ferrera, P. G. Matthews, S. Nataf, and M. Ovize, "Mesenchymal stem cell conditioned media attenuates in vitro and ex vivo myocardial reperfusion injury.," *J. Heart Lung Transplant.*, vol. 30, no. 1, pp. 95–

102, 2011.

[69] B. Imberti, M. Morigi, S. Tomasoni, C. Rota, D. Corna, L. Longaretti, D. Rottoli, F. Valsecchi, A. Benigni, J. Wang, M. Abbate, C. Zoja, and G. Remuzzi, "Insulin-like growth factor-1 sustains stem cell mediated renal repair.," *J. Am. Soc. Nephrol.*, vol. 18, no. 11, pp. 2921–2928, 2007.

[70] Y. Bin Deng, W. B. Ye, Z. Z. Hu, Y. Yan, Y. Wang, B. F. Takon, G.-Q. Zhou, and Y. F. Zhou, "Intravenously administered BMSCs reduce neuronal apoptosis and promote neuronal proliferation through the release of VEGF after stroke in rats.," *Neurol. Res.*, vol. 32, no. 2, pp. 148–156, 2010.

[71] K. Wakabayashi, A. Nagai, A. M. Sheikh, Y. Shiota, D. Narantuya, T. Watanabe, J. Masuda, S. Kobayashi, S. U. Kim, and S. Yamaguchi, "Transplantation of human mesenchymal stem cells promotes functional improvement and increased expression of neurotrophic factors in a rat focal cerebral ischemia model," *J. Neurosci. Res.*, vol. 88, no. 5, pp. 1017–1025, 2010.

[72] F. Wang, T. Yasuhara, T. Shingo, M. Kameda, N. Tajiri, W. J. Yuan, A. Kondo, T. Kadota, T. Baba, J. T. Tayra, Y. Kikuchi, Y. Miyoshi, and I. Date, "Intravenous administration of mesenchymal stem cells exerts therapeutic effects on parkinsonian model of rats: focusing on neuroprotective effects of stromal cell-derived factor-1alpha.," *BMC Neurosci.*, vol. 11, p. 52, 2010.

[73] B. Bakondi, I. S. Shimada, B. M. Peterson, and J. L. Spees, "SDF-1α secreted by human CD133-derived multipotent stromal cells promotes neural progenitor cell survival through CXCR7.," *Stem Cells Dev.*, vol. 20, no. 6, pp. 1021–1029, 2011.

[74] K. Le Blanc, L. Tammik, B. Sundberg, S. E. Haynesworth, and O. Ringdén, "Mesenchymal Stem Cells Inhibit and Stimulate Mixed Lymphocyte Cultures and Mitogenic Responses Independently of the Major Histocompatibility Complex," *Scand. J. Immunol.*, vol. 57, no. 1, pp. 11–20, Jan. 2003.

[75] A. Bartholomew, C. Sturgeon, M. Siatskas, K. Ferrer, K. McIntosh, S. Patil, W. Hardy, S. Devine, D. Ucker, R. Deans, A. Moseley, and R. Hoffman, "Mesenchymal stem cells suppress lymphocyte proliferation in vitro and prolong skin graft survival in vivo," *Exp. Hematol.*, vol. 30, no. 1, pp. 42–48, Jan. 2002.

[76] R. Meisel, A. Zibert, M. Laryea, U. Göbel, W. Däubener, and D. Dilloo, "Human bone marrow stromal cells inhibit allogeneic T-cell responses by indoleamine 2,3-dioxygenase-mediated tryptophan degradation," *Blood*, vol. 103, no. 12, pp. 4619–4621, 2004.

[77] J. L. Harden and N. K. Egilmez, "Indoleamine 2,3-Dioxygenase and Dendritic Cell Tolerogenicity," *Immunological Investigations*, vol. 41, no. 6–7. pp. 738–764, 2012.

[78] F. C. Popp, E. Eggenhofer, P. Renner, P. Slowik, S. A. Lang, H. Kaspar, E. K. Geissler, P. Piso, H. J. Schlitt, and M. H. Dahlke, "Mesenchymal stem cells can induce long-term acceptance of solid organ allografts in synergy with low-dose mycophenolate," *Transpl. Immunol.*, vol. 20, no. 1–2, pp. 55–60, 2008.

[79] W. Ge, J. Jiang, J. Arp, W. Liu, B. Garcia, and H. Wang, "Regulatory T-cell generation and kidney allograft tolerance induced by mesenchymal stem cells associated with indoleamine 2,3-dioxygenase expression.," *Transplantation*, vol. 90, no. 12, pp. 1312–1320, 2010.

[80] G. Ren, L. Zhang, X. Zhao, G. Xu, Y. Zhang, A. I. Roberts, R. C. Zhao, and Y. Shi, "Mesenchymal Stem Cell-Mediated Immunosuppression Occurs via Concerted Action of Chemokines and Nitric Oxide," *Cell Stem Cell*, vol. 2, no. 2, pp. 141–150, 2008.

[81] J. H. Ylöstalo, T. J. Bartosh, K. Coble, and D. J. Prockop, "Human mesenchymal stem/stromal cells cultured as spheroids are self-activated to produce prostaglandin E2 that directs stimulated macrophages into an anti-inflammatory phenotype.," *Stem Cells*, vol. 30, no. 10, pp. 2283–96, Oct. 2012.

[82] C. Bouffi, C. Bony, G. Courties, C. Jorgensen, and D. Noël, "IL-6-dependent PGE2 secretion by mesenchymal stem cells inhibits local inflammation in experimental arthritis," *PLoS One*, vol. 5, no. 12, 2010.

[83] M. Najar, G. Raicevic, H. I. Boufker, H. F. Kazan, C. D. Bruyn, N. Meuleman, D. Bron, M. Toungouz, and L. Lagneaux, "Mesenchymal stromal cells use PGE2 to modulate activation and proliferation of lymphocyte subsets: Combined comparison of adipose tissue, Wharton's Jelly and bone marrow sources," *Cell. Immunol.*, vol. 264, no. 2, pp. 171–179, 2010.

[84] K. English, J. M. Ryan, L. Tobin, M. J. Murphy, F. P. Barry, and B. P. Mahon, "Cell contact, prostaglandin E2 and transforming growth factor beta 1 play non-redundant roles in human mesenchymal stem cell induction of CD4+CD25Highforkhead box P3+ regulatory T cells," *Clin. Exp. Immunol.*, vol. 156, no. 1, pp. 149–160, 2009.

[85] C. M. Milner, V. a Higman, and a J. Day, "TSG-6: a pluripotent inflammatory mediator?," *Biochem. Soc. Trans.*, vol. 34, no. Pt 3, pp. 446–50, Jun. 2006.

[86] S. Danchuk, J. H. Ylostalo, F. Hossain, R. Sorge, A. Ramsey, R. W. Bonvillain, J. A. Lasky, B. A. Bunnell, D. a Welsh, D. J. Prockop, and D. E. Sullivan, "Human multipotent stromal cells attenuate lipopolysaccharide-induced acute lung injury in mice via secretion of tumor necrosis factor-α-induced protein 6.," *Stem Cell Res. Ther.*, vol. 2, no. 3, p. 27, Jan. 2011.

[87] J. Y. Oh, G. W. Roddy, H. Choi, R. H. Lee, J. H. Ylöstalo, R. H. Rosa, and D. J. Prockop, "Anti-inflammatory protein TSG-6 reduces inflammatory damage to the

cornea following chemical and mechanical injury.," *Proc. Natl. Acad. Sci. U. S. A.*, vol. 107, no. 39, pp. 16875–16880, Sep. 2010.

[88] H. Choi, R. H. Lee, N. Bazhanov, J. Y. Oh, and D. J. Prockop, "Anti-inflammatory protein TSG-6 secreted by activated MSCs attenuates zymosan-induced mouse peritonitis by decreasing TLR2/NF-κB signaling in resident macrophages," *Blood*, vol. 118, no. 2, pp. 330–338, Jul. 2011.

[89] D. P. Dyer, J. M. Thomson, A. Hermant, T. a Jowitt, T. M. Handel, A. E. I. Proudfoot, A. J. Day, and C. M. Milner, "TSG-6 inhibits neutrophil migration via direct interaction with the chemokine CXCL8.," *J. Immunol.*, vol. 192, no. 5, pp. 2177–2185, 2014.

[90] S. Srouji, T. Kizhner, and E. Livne, "3D scaffolds for bone marrow stem cell support in bone repair.," *Regen. Med.*, vol. 1, no. 4, pp. 519–528, 2006.

[91] G. W. Roddy, J. Y. Oh, R. H. Lee, T. J. Bartosh, J. Ylostalo, K. Coble, R. H. Rosa, and D. J. Prockop, "Action at a distance: Systemically administered adult stem/progenitor cells (MSCs) reduce inflammatory damage to the cornea without engraftment and primarily by secretion of TNF-α stimulated gene/protein 6," *Stem Cells*, vol. 29, no. 10, pp. 1572–1579, Oct. 2011.

[92] X. Fang, A. P. Neyrinck, M. a Matthay, and J. W. Lee, "Allogeneic human mesenchymal stem cells restore epithelial protein permeability in cultured human alveolar type II cells by secretion of angiopoietin-1.," *J. Biol. Chem.*, vol. 285, no. 34, pp. 26211–22, Aug. 2010.

[93] J. E. Gotts, J. Abbott, and M. a Matthay, "Influenza causes prolonged disruption of the alveolar-capillary barrier in mice unresponsive to mesenchymal stem cell therapy.," *Am. J. Physiol. Lung Cell. Mol. Physiol.*, vol. 307, no. 5, pp. L395–406, Sep. 2014.

[94] L. A. Ortiz, M. Dutreil, C. Fattman, A. C. Pandey, G. Torres, K. Go, and D. G. Phinney, "Interleukin 1 receptor antagonist mediates the antiinflammatory and antifibrotic effect of mesenchymal stem cells during lung injury.," *Proc. Natl. Acad. Sci. U. S. A.*, vol. 104, no. 26, pp. 11002–11007, Jun. 2007.

[95] M. T. L. Castelo-Branco, I. D. P. Soares, D. V. Lopes, F. Buongusto, C. A. Martinusso, A. do Rosario, S. A. L. Souza, B. Gutfilen, L. M. B. Fonseca, C. Elia, K. Madi, A. Schanaider, M. I. D. Rossi, and H. S. P. Souza, "Intraperitoneal but not intravenous cryopreserved mesenchymal stromal cells home to the inflamed colon and ameliorate experimental colitis," *PLoS One*, vol. 7, no. 3, p. e33360, Jan. 2012.

[96] T. Wilson, C. Stark, J. Holmbom, A. Rosling, A. Kuusilehto, T. Tirri, R. Penttinen, and E. Ekholm, "Fate of bone marrow-derived stromal cells after intraperitoneal infusion or implantation into femoral bone defects in the host animal.," *J. Tissue*

Eng., vol. 2010, p. 345806, 2010.

[97] T. E. Meyerrose, D. A. De Ugarte, A. A. Hofling, P. E. Herrbrich, T. D. Cordonnier, L. D. Shultz, J. C. Eagon, L. Wirthlin, M. S. Sands, M. A. Hedrick, and J. A. Nolta, "In vivo distribution of human adipose-derived mesenchymal stem cells in novel xenotransplantation models.," *Stem Cells*, vol. 25, pp. 220–227, 2007.

[98] T. J. Bartosh, J. H. Ylöstalo, A. Mohammadipoor, N. Bazhanov, K. Coble, K. Claypool, R. H. Lee, H. Choi, and D. J. Prockop, "Aggregation of human mesenchymal stromal cells (MSCs) into 3D spheroids enhances their antiinflammatory properties.," *Proc. Natl. Acad. Sci. U. S. A.*, vol. 107, no. 31, pp. 13724–9, Aug. 2010.

[99] M. Rafei, P. M. Campeau, A. Aguilar-Mahecha, M. Buchanan, P. Williams, E. Birman, S. Yuan, Y. K. Young, M.-N. Boivin, K. Forner, M. Basik, and J. Galipeau, "Mesenchymal stromal cells ameliorate experimental autoimmune encephalomyelitis by inhibiting CD4 Th17 T cells in a CC chemokine ligand 2-dependent manner.," *J. Immunol.*, vol. 182, no. 10, pp. 5994–6002, May 2009.

[100] I. Sekiya, B. L. Larson, J. R. Smith, R. Pochampally, J.-G. Cui, and D. J. Prockop, "Expansion of human adult stem cells from bone marrow stroma: conditions that maximize the yields of early progenitors and evaluate their quality.," *Stem Cells*, vol. 20, no. 6, pp. 530–541, 2002.

[101] D. J. Prockop, "Marrow stromal cells as stem cells for nonhematopoietic tissues.," *Science*, vol. 276, no. 5309, pp. 71–74, Apr. 1997.

[102] F. Barry, R. Boynton, M. Murphy, S. Haynesworth, and J. Zaia, "The SH-3 and SH-4 antibodies recognize distinct epitopes on CD73 from human mesenchymal stem cells.," *Biochem. Biophys. Res. Commun.*, vol. 289, no. 2, pp. 519–524, Nov. 2001.

[103] F. P. Barry, R. E. Boynton, S. Haynesworth, J. M. Murphy, and J. Zaia, "The monoclonal antibody SH-2, raised against human mesenchymal stem cells, recognizes an epitope on endoglin (CD105).," *Biochem. Biophys. Res. Commun.*, vol. 265, no. 1, pp. 134–139, Nov. 1999.

[104] J. E. Dennis, J. P. Carbillet, A. I. Caplan, and P. Charbord, "The STRO-1+ marrow cell population is multipotential," *Cells Tissues Organs*, vol. 170, no. 2–3, pp. 73–82, 2001.

[105] J. M. García-Pacheco, C. Oliver, M. Kimatrai, F. J. Blanco, and E. G. Olivares, "Human decidual stromal cells express CD34 and STRO-1 and are related to bone marrow stromal precursors.," *Mol. Hum. Reprod.*, vol. 7, no. 12, pp. 1151–1157, 2001.

[106] S. Gronthos, A. C. Zannettino, S. E. Graves, S. Ohta, S. J. Hay, and P. J. Simmons,

"Differential cell surface expression of the STRO-1 and alkaline phosphatase antigens on discrete developmental stages in primary cultures of human bone cells.," *J. Bone Miner. Res.*, vol. 14, no. 1, pp. 47–56, Jan. 1999.

[107] S. E. Haynesworth, M. A. Baber, and A. I. Caplan, "Cell surface antigens on human marrow-derived mesenchymal cells are detected by monoclonal antibodies.," *Bone*, vol. 13, no. 1, pp. 69–80, 1992.

[108] E. A. Jones, S. E. Kinsey, A. English, R. A. Jones, L. Straszynski, D. M. Meredith, A. F. Markham, A. Jack, P. Emery, and D. McGonagle, "Isolation and characterization of bone marrow multipotential mesenchymal progenitor cells," *Arthritis Rheum.*, vol. 46, no. 12, pp. 3349–3360, Dec. 2002.

[109] P. J. Simmons and B. Torok-Storb, "Identification of stromal cell precursors in human bone marrow by a novel monoclonal antibody, STRO-1.," *Blood*, vol. 78, no. 1, pp. 55–62, 1991.

[110] K. Stewart, P. Monk, S. Walsh, C. M. Jefferiss, J. Letchford, and J. N. Beresford, "STRO-1, HOP-26 (CD63), CD49a and SB-10 (CD166) as markers of primitive human marrow stromal cells and their more differentiated progeny: A comparative investigation in vitro," *Cell Tissue Res.*, vol. 313, no. 3, pp. 281–290, Sep. 2003.

[111] H.-J. Yoo, S.-S. Yoon, S. Park, W.-S. Park, D.-J. Kim, E.-B. Lee, and Y.-W. Song, "Production and characterization of monoclonal antibodies to mesenchymal stem cells derived from human bone marrow.," *Hybridoma (Larchmt).*, vol. 24, no. 2, pp. 92–97, 2005.

[112] T. Mets and G. Verdonk, "Variations in the stromal cell population of human bone marrow during aging.," *Mech. Ageing Dev.*, vol. 15, no. 1, pp. 41–49, Jan. 1981.

[113] D. C. Colter, R. Class, C. M. DiGirolamo, and D. J. Prockop, "Rapid expansion of recycling stem cells in cultures of plastic-adherent cells from human bone marrow.," *Proc. Natl. Acad. Sci. U. S. A.*, vol. 97, no. 7, pp. 3213–3218, Mar. 2000.

[114] D. J. Prockop, C. A. Gregory, and J. L. Spees, "One strategy for cell and gene therapy: harnessing the power of adult stem cells to repair tissues.," *Proc. Natl. Acad. Sci. U. S. A.*, vol. 100 Suppl , no. SUPPL. 1, pp. 11917–11923, Sep. 2003.

[115] J. R. Smith, R. Pochampally, A. Perry, S.-C. Hsu, and D. J. Prockop, "Isolation of a highly clonogenic and multipotential subfraction of adult stem cells from bone marrow stroma.," *Stem Cells*, vol. 22, no. 5, pp. 823–31, Jan. 2004.

[116] C. Li and W. H. Wong, "Model-based analysis of oligonucleotide arrays: expression index computation and outlier detection.," *Proc. Natl. Acad. Sci. U. S. A.*, vol. 98, no. 1, pp. 31–36, Jan. 2001.

[117] C. Li and W. H. Wong, "DNA-Chip Analyzer (dChip)," in *The Analysis of Gene*

Expression Data: Methods and Software, New York: Springer New York, 2003, pp. 120–141.

[118] S. Zhong, C. Li, and W. H. Wong, "ChipInfo: Software for extracting gene annotation and gene ontology information for microarray analysis," *Nucleic Acids Res.*, vol. 31, no. 13, pp. 3483–3486, Jul. 2003.

[119] M. B. Eisen, P. T. Spellman, P. O. Brown, and D. Botstein, "Cluster analysis and display of genome-wide expression patterns.," *Proc. Natl. Acad. Sci. U. S. A.*, vol. 95, no. 25, pp. 14863–14868, Dec. 1998.

[120] T. R. Golub, D. K. Slonim, P. Tamayo, C. Huard, M. Gaasenbeek, J. P. Mesirov, H. Coller, M. L. Loh, J. R. Downing, M. A. Caligiuri, C. D. Bloomfield, and E. S. Lander, "Molecular classification of cancer: class discovery and class prediction by gene expression monitoring.," *Science*, vol. 286, no. 5439, pp. 531–537, Oct. 1999.

[121] M. Ashburner, C. A. Ball, J. A. Blake, D. Botstein, H. Butler, J. M. Cherry, A. P. Davis, K. Dolinski, S. S. Dwight, J. T. Eppig, M. A. Harris, D. P. Hill, L. Issel-Tarver, A. Kasarskis, S. Lewis, J. C. Matese, J. E. Richardson, M. Ringwald, G. M. Rubin, and G. Sherlock, "Gene ontology: tool for the unification of biology. The Gene Ontology Consortium.," *Nat. Genet.*, vol. 25, no. 1, pp. 25–29, May 2000.

[122] S. A. Kuznetsov, P. H. Krebsbach, K. Satomura, J. Kerr, M. Riminucci, D. Benayahu, and P. G. Robey, "Single-colony derived strains of human marrow stromal fibroblasts form bone after transplantation in vivo.," *J. Bone Miner. Res.*, vol. 12, no. 9, pp. 1335–47, Sep. 1997.

[123] N. Tremain, J. Korkko, D. Ibberson, G. C. Kopen, C. M. DiGirolamo, and D. G. Phinney, "MicroSAGE analysis of 2,353 expressed genes in a single cell-derived colony of undifferentiated human mesenchymal stem cells reveals mRNAs of multiple cell lineages.," *Stem Cells*, vol. 19, no. 5, pp. 408–18, Jan. 2001.

[124] S. G. B. Furness and K. McNagny, "Beyond mere markers: functions for CD34 family of sialomucins in hematopoiesis.," *Immunol. Res.*, vol. 34, no. 1, pp. 13–32, Jan. 2006.

[125] R. Doyonnas, J. S. Nielsen, S. Chelliah, E. Drew, T. Hara, A. Miyajima, and K. M. McNagny, "Podocalyxin is a CD34-related marker of murine hematopoietic stem cells and embryonic erythroid cells," *Blood*, vol. 105, no. 11, pp. 4170–4178, Jun. 2005.

[126] A. B. Choo, H. L. Tan, S. N. Ang, W. J. Fong, A. Chin, J. Lo, L. Zheng, H. Hentze, R. J. Philp, S. K. W. Oh, and M. Yap, "Selection against undifferentiated human embryonic stem cells by a cytotoxic antibody recognizing podocalyxin-like protein-1.," *Stem Cells*, vol. 26, pp. 1454–1463, 2008.

[127] T. Takeda, W. Y. Go, R. A. Orlando, and M. G. Farquhar, “Expression of podocalyxin inhibits cell-cell adhesion and modifies junctional properties in Madin-Darby canine kidney cells.,” *Mol. Biol. Cell*, vol. 11, no. 9, pp. 3219–3232, 2000.

[128] S. Sizemore, M. Cicek, N. Sizemore, P. N. Kwok, and G. Casey, “Podocalyxin increases the aggressive phenotype of breast and prostate cancer cells in vitro through its interaction with ezrin,” *Cancer Res.*, vol. 67, no. 13, pp. 6183–6191, Jul. 2007.

[129] The ARDS Definition Task Force, V. Ranieri, G. Rubenfeld, B. Thompson, N. Ferguson, E. Caldwell, E. Fan, L. Camporota, and A. Slutsky, “Acute Respiratory Distress Syndrome: The Berlin Definition,” *JAMA J. Am. Med. Assoc.*, vol. 307, no. 23, pp. 2526–33, 2012.

[130] G. R. Bernard, A. Artigas, K. L. Brigham, J. Carlet, K. Falke, L. Hudson, M. Lamy, J. R. LeGall, A. Morris, and R. Spragg, “Report of the American-European Consensus conference on acute respiratory distress syndrome: definitions, mechanisms, relevant outcomes, and clinical trial coordination. Consensus Committee.,” in *Journal of critical care*, 1994, vol. 9, pp. 72–81.

[131] M. O. Maybauer, D. M. Maybauer, and D. N. Herndon, “Incidence and outcomes of acute lung injury.,” *The New England journal of medicine*, vol. 354. pp. 416–417; author reply 416–417, 2006.

[132] R. G. Spragg, G. R. Bernard, W. Checkley, J. R. Curtis, O. Gajic, G. Guyatt, J. Hall, E. Israel, M. Jain, D. M. Needham, A. G. Randolph, G. D. Rubenfeld, D. Schoenfeld, B. T. Thompson, L. B. Ware, D. Young, and A. L. Harabin, “Beyond mortality: Future clinical research in acute lung injury,” in *American Journal of Respiratory and Critical Care Medicine*, 2010, vol. 181, pp. 1121–1127.

[133] M. A. Matthay, L. B. Ware, and G. A. Zimmerman, “The acute respiratory distress syndrome,” *J Clin Invest*, vol. 122, no. 8, pp. 2731–2740, 2012.

[134] B. Opitz, V. Van Laak, J. Eitel, and N. Suttorp, “Innate immune recognition in infectious and noninfectious diseases of the lung,” *American Journal of Respiratory and Critical Care Medicine*, vol. 181. pp. 1294–1309, 2010.

[135] A. Mantovani, M. A. Cassatella, C. Costantini, and S. Jaillon, “Neutrophils in the activation and regulation of innate and adaptive immunity.,” *Nat. Rev. Immunol.*, vol. 11, pp. 519–531, 2011.

[136] A. Caudrillier, K. Kessenbrock, B. M. Gilliss, J. X. Nguyen, M. B. Marques, M. Monestier, P. Toy, Z. Werb, and M. R. Looney, “Platelets induce neutrophil extracellular traps in transfusion-related acute lung injury,” *J. Clin. Invest.*, vol. 122, pp. 2661–2671, 2012.

[137] L. B. Ware and M. A. Matthay, “The acute respiratory distress syndrome.,” *N. Engl. J. Med.*, vol. 342, no. 18, pp. 1334–1349, May 2000.

[138] O. Peñuelas, J. A. Aramburu, F. Frutos-Vivar, and A. Esteban, “Pathology of Acute Lung Injury and Acute Respiratory Distress Syndrome: A Clinical-Pathological Correlation,” *Clinics in Chest Medicine*, vol. 27, no. 4. pp. 571–578, Dec-2006.

[139] N. Gupta, X. Su, B. Popov, J. W. Lee, V. Serikov, and M. A. Matthay, “Intrapulmonary delivery of bone marrow-derived mesenchymal stem cells improves survival and attenuates endotoxin-induced acute lung injury in mice.,” *J. Immunol.*, vol. 179, pp. 1855–1863, 2007.

[140] J. W. Lee, X. Fang, N. Gupta, V. Serikov, and M. A. Matthay, “Allogeneic human mesenchymal stem cells for treatment of E. coli endotoxin-induced acute lung injury in the ex vivo perfused human lung.,” *Proc. Natl. Acad. Sci. U. S. A.*, vol. 106, pp. 16357–16362, 2009.

[141] G. F. Curley, B. Ansari, M. Hayes, J. Devaney, C. Masterson, A. Ryan, F. Barry, T. O’Brien, D. O. Toole, and J. G. Laffey, “Effects of intratracheal mesenchymal stromal cell therapy during recovery and resolution after ventilator-induced lung injury.,” *Anesthesiology*, vol. 118, pp. 924–32, 2013.

[142] T. H. Lee, H. G. Wisniewski, and J. Vilcek, “A novel secretory tumor necrosis factor-inducible protein (TSG-6) is a member of the family of hyaluronate binding proteins, closely related to the adhesion receptor CD44,” *J. Cell Biol.*, vol. 116, no. 2, pp. 545–557, Jan. 1992.

[143] M. A. Matthay, G. Mednick, and Z. A. Matthay, “Aspiration-induced Lung Injury : Experimental and Human Studies,” in *Intensive care medicine Annual Update 2006*, F. Jean-Louis Vinvent MD, PhD, FCCM, Ed. Springer New York, 2006, pp. 359–365.

[144] J. Ylöstalo, N. Bazhanov, and D. J. Prockop, “Reversible commitment to differentiation by human multipotent stromal cells in single-cell-derived colonies,” *Exp. Hematol.*, vol. 36, no. 10, pp. 1390–1402, Oct. 2008.

[145] A. M. Foskett, N. Bazhanov, X. Ti, A. Tiblow, T. J. Bartosh, and D. J. Prockop, “Phase-directed therapy: TSG-6 targeted to early inflammation improves bleomycin-injured lungs.,” *Am. J. Physiol. Lung Cell. Mol. Physiol.*, vol. 306, no. 2, pp. L120–31, Jan. 2014.

[146] J. Walter, L. B. Ware, and M. A. Matthay, “Mesenchymal stem cells : mechanisms of potential therapeutic benefit in ARDS and sepsis,” *Lancet Respir. Med*, vol. 2, no. 12, pp. 1016–1026, 2014.

[147] J. Gao, J. E. Dennis, R. F. Muzic, M. Lundberg, and A. I. Caplan, “The dynamic in vivo distribution of bone marrow-derived mesenchymal stem cells after infusion,”

Cells Tissues Organs, vol. 169, pp. 12–20, 2001.

[148] D. Furlani, M. Ugurlucan, L. Ong, K. Bieback, E. Pittermann, I. Westien, W. Wang, C. Yerebakan, W. Li, R. Gaebel, R. K. Li, B. Vollmar, G. Steinhoff, and N. Ma, "Is the intravascular administration of mesenchymal stem cells safe?. Mesenchymal stem cells and intravital microscopy," *Microvasc. Res.*, vol. 77, no. 3, pp. 370–376, 2009.

[149] F. Yousefi, M. Ebtekar, M. Soleimani, S. Soudi, and S. M. Hashemi, "Comparison of in vivo immunomodulatory effects of intravenous and intraperitoneal administration of adipose-tissue mesenchymal stem cells in experimental autoimmune encephalomyelitis (EAE)," *Int. Immunopharmacol.*, vol. 17, pp. 608–616, 2013.

[150] U.S. National Institutes of Health., "Clinicaltrials.gov." [Online]. Available: https://clinicaltrials.gov. [Accessed: 30-Jun-2014].

[151] B. A. Syed and J. B. Evans, "Stem cell therapy market," pp. 1–2, 2013.

[152] R. S. Waterman, S. L. Henkle, and A. M. Betancourt, "Mesenchymal Stem Cell 1 (MSC1)-Based Therapy Attenuates Tumor Growth Whereas MSC2-Treatment Promotes Tumor Growth and Metastasis," *PLoS One*, vol. 7, 2012.

[153] J. L. Dembinski, S. M. Wilson, E. L. Spaeth, M. Studeny, C. Zompetta, I. Samudio, K. Roby, M. Andreeff, and F. C. Marini, "Tumor stroma engraftment of gene-modified mesenchymal stem cells as anti-tumor therapy against ovarian cancer," *Cytotherapy*, vol. 15, 2013.

[154] N. Eliopoulos, J. Zhao, M. Bouchentouf, K. Forner, E. Birman, S. Yuan, M. Boivin, and D. Martineau, "Human marrow-derived mesenchymal stromal cells decrease cisplatin renotoxicity in vitro and in vivo and enhance survival of mice post-intraperitoneal injection.," *Am. J. Physiol. Renal Physiol.*, vol. 299, no. 17, pp. F1288–F1298, 2010.

[155] B. A. Scruggs, X. Zhang, A. C. Bowles, P. A. Gold, J. A. Semon, J. M. Fisher-Perkins, S. Zhang, R. W. Bonvillain, L. Myers, S. C. Li, A. V. Kalueff, and B. A. Bunnell, "Multipotent stromal cells alleviate inflammation, neuropathology, and symptoms associated with globoid cell leukodystrophy in the twitcher mouse," *Stem Cells*, vol. 31, pp. 1523–1534, 2013.

[156] K. Cheng, P. Rai, A. Plagov, X. Lan, D. Kumar, D. Salhan, S. Rehman, A. Malhotra, K. Bhargava, C. J. Palestro, S. Gupta, and P. C. Singhal, "Transplantation of bone marrow-derived MSCs improves cisplatinum-induced renal injury through paracrine mechanisms," *Exp. Mol. Pathol.*, vol. 94, pp. 466–473, 2013.

[157] A. Keating, "Mesenchymal stromal cells: New directions," *Cell Stem Cell*, vol. 10.

pp. 709–716, 2012.

[158] K. M. Haas, J. C. Poe, D. A. Steeber, and T. F. Tedder, “B-1a and B-1b cells exhibit distinct developmental requirements and have unique functional roles in innate and adaptive immunity to S. pneumoniae,” *Immunity*, vol. 23, pp. 7–18, 2005.

[159] K. Moro, T. Yamada, M. Tanabe, T. Takeuchi, T. Ikawa, H. Kawamoto, J.-I. Furusawa, M. Ohtani, H. Fujii, and S. Koyasu, “Innate production of T(H)2 cytokines by adipose tissue-associated c-Kit(+)Sca-1(+) lymphoid cells.,” *Nature*, vol. 463, no. 7280, pp. 540–544, Jan. 2010.

[160] D. R. Neill, S. H. Wong, A. Bellosi, R. J. Flynn, M. Daly, T. K. a Langford, C. Bucks, C. M. Kane, P. G. Fallon, R. Pannell, H. E. Jolin, and A. N. J. McKenzie, “Nuocytes represent a new innate effector leukocyte that mediates type-2 immunity.,” *Nature*, vol. 464, no. 7293, pp. 1367–1370, Apr. 2010.

[161] S. a Saenz, M. C. Siracusa, J. G. Perrigoue, S. P. Spencer, J. F. Urban, J. E. Tocker, A. L. Budelsky, M. a Kleinschek, R. a Kastelein, T. Kambayashi, A. Bhandoola, and D. Artis, “IL25 elicits a multipotent progenitor cell population that promotes T(H)2 cytokine responses.,” *Nature*, vol. 464, no. 7293, pp. 1362–1366, Apr. 2010.

[162] A. E. Price, H.-E. Liang, B. M. Sullivan, R. L. Reinhardt, C. J. Eisley, D. J. Erle, and R. M. Locksley, “Systemically dispersed innate IL-13-expressing cells in type 2 immunity.,” *Proc. Natl. Acad. Sci. U. S. A.*, vol. 107, no. 25, pp. 11489–11494, Jun. 2010.

[163] J. E. Allen and R. M. Maizels, “Diversity and dialogue in immunity to helminths.,” *Nat. Rev. Immunol.*, vol. 11, no. 6, pp. 375–388, Jun. 2011.

[164] J. Rangel-Moreno, J. E. Moyron-Quiroz, D. M. Carragher, K. Kusser, L. Hartson, A. Moquin, and T. D. Randall, “Omental Milky Spots Develop in the Absence of Lymphoid Tissue-Inducer Cells and Support B and T Cell Responses to Peritoneal Antigens,” *Immunity*, vol. 30, no. 5, pp. 731–743, May 2009.

[165] D. a Carlow, M. R. Gold, and H. J. Ziltener, “Lymphocytes in the peritoneum home to the omentum and are activated by resident dendritic cells.,” *J. Immunol.*, vol. 183, no. 2, pp. 1155–1165, Jul. 2009.

[166] M. F. Abu-Hijleh, O. A. Habbal, and S. T. Moqattash, “The role of the diaphragm in lymphatic absorption from the peritoneal cavity.,” *J. Anat.*, vol. 186 (Pt 3, pp. 453–467, 1995.

[167] T. Nakatani, S. Tanaka, S. Mizukami, K. Okamoto, Y. Shiraishi, and T. Nakamura, “Peritoneal lymphatic stomata of the diaphragm in the mouse: Process of their formation,” *Anat. Rec.*, vol. 248, pp. 121–128, 1997.

[168] S. J. Turley, J.-W. Lee, N. Dutton-Swain, D. Mathis, and C. Benoist, “Endocrine self and gut non-self intersect in the pancreatic lymph nodes.,” *Proc. Natl. Acad. Sci. U. S. A.*, vol. 102, pp. 17729–17733, 2005.

[169] R. L. Reger and D. J. Prockop, “Should publications on mesenchymal stem/progenitor cells include in-process data on the preparation of the cells?,” *Stem Cells Transl. Med.*, vol. 3, pp. 632–5, 2014.

[170] J. L. Spees, C. A. Gregory, H. Singh, H. A. Tucker, A. Peister, P. J. Lynch, S. C. Hsu, J. Smith, and D. J. Prockop, “Internalized antigens must be removed to prepare hypoimmunogenic mesenchymal stem cells for cell and gene therapy,” *Mol. Ther.*, vol. 9, pp. 747–756, 2004.

[171] J. Tolar, A. J. Nauta, M. J. Osborn, A. Panoskaltsis Mortari, R. T. McElmurry, S. Bell, L. Xia, N. Zhou, M. Riddle, T. M. Schroeder, J. J. Westendorf, R. S. McIvor, P. C. W. Hogendoorn, K. Szuhai, L. Oseth, B. Hirsch, S. R. Yant, M. A. Kay, A. Peister, D. J. Prockop, W. E. Fibbe, and B. R. Blazar, “Sarcoma derived from cultured mesenchymal stem cells.,” *Stem Cells*, vol. 25, pp. 371–379, 2007.

[172] S. V. Boregowda, V. Krishnappa, J. W. Chambers, P. V. Lograsso, W. T. Lai, L. A. Ortiz, and D. G. Phinney, “Atmospheric oxygen inhibits growth and differentiation of marrow-derived mouse mesenchymal stem cells via a p53-dependent mechanism: Implications for long-term culture expansion,” *Stem Cells*, vol. 30, pp. 975–987, 2012.

[173] J. R. Munoz, B. R. Stoutenger, A. P. Robinson, J. L. Spees, and D. J. Prockop, “Human stem/progenitor cells from bone marrow promote neurogenesis of endogenous neural stem cells in the hippocampus of mice.,” *Proc. Natl. Acad. Sci. U. S. A.*, vol. 102, pp. 18171–18176, 2005.

[174] H. Ohtaki, J. H. Ylostalo, J. E. Foraker, A. P. Robinson, R. L. Reger, S. Shioda, and D. J. Prockop, “Stem/progenitor cells from bone marrow decrease neuronal death in global ischemia by modulation of inflammatory/immune responses.,” *Proc. Natl. Acad. Sci. U. S. A.*, vol. 105, no. 38, pp. 14638–14643, Sep. 2008.

[175] D. J. Kota, L. L. Wiggins, N. Yoon, and R. H. Lee, “TSG-6 produced by hMSCs delays the onset of autoimmune diabetes by suppressing Th1 development and enhancing tolerogenicity,” *Diabetes*, vol. 62, pp. 2048–2058, 2013.

[176] M. Horie, H. Choi, R. H. Lee, R. L. Reger, J. Ylostalo, T. Muneta, I. Sekiya, and D. J. Prockop, “Intra-articular injection of human mesenchymal stem cells (MSCs) promote rat meniscal regeneration by being activated to express Indian hedgehog that enhances expression of type II collagen,” *Osteoarthr. Cartil.*, vol. 20, pp. 1197–1207, 2012.

[177] J. Chen and J. Stubbe, “Bleomycins: towards better therapeutics.,” *Nat. Rev. Cancer*, vol. 5, no. 2, pp. 102–12, Feb. 2005.

[178] T. E. King, “Clinical advances in the diagnosis and therapy of the interstitial lung diseases,” *American Journal of Respiratory and Critical Care Medicine*, vol. 172, no. 3. pp. 268–279, 01-Aug-2005.

[179] S. E. Rossi, J. J. Erasmus, H. P. McAdams, T. A. Sporn, and P. C. Goodman, “Pulmonary drug toxicity: Radiologic and pathologic manifestations,” *Radiographics*, vol. 20, no. 5, pp. 1245–1259, 2000.

[180] S. Sleijfer, “Bleomycin-Induced Pneumonitis,” *Chest*, vol. 120, no. 2, pp. 617–624, Aug. 2001.

[181] T. T. Sakai, J. M. Riordan, N. G. Kumar, F. J. Haberle, G. A. Elgavish, J. D. Glickson, and A. Levy, “Studies on bleomycin-DNA and bleomycin-iron interactions,” *Journal of Biomolecular Structure and Dynamics*, vol. 1, no. 3. pp. 809–827, 1983.

[182] J. Hay, S. Shahzeidi, and G. Laurent, “Mechanisms of bleomycin-induced lung damage,” *Arch. Toxicol.*, vol. 65, no. 2, pp. 81–94, Feb. 1991.

[183] J. G. Hay, P. L. Haslam, A. Dewar, B. Addis, M. Turner-Warwick, and G. J. Laurent, “Development of acute lung injury after the combination of intravenous bleomycin and exposure to hyperoxia in rats,” *Thorax*, vol. 42, no. 5, pp. 374–382, 1987.

[184] R. S. Thrall, R. W. Barton, D. A. D’Amato, and S. B. Sulavik, “Differential cellular analysis of bronchoalveolar lavage fluid obtained at various stages during the development of bleomycin-induced pulmonary fibrosis in the rat,” *Am. Rev. Respir. Dis.*, vol. 126, no. 3, pp. 488–492, 1982.

[185] G. J. Laurent, R. J. McAnulty, B. Corrin, and P. Cockerill, “Biochemical and histological changes in pulmonary fibrosis induced in rabbits with intratracheal bleomycin,” *Eur. J. Clin. Invest.*, vol. 11, no. 6, pp. 441–448, 1981.

[186] J. B. Karlinsky, “Glycosaminoglycans in emphysematous and fibrotic hamster lungs,” *Am. Rev. Respir. Dis.*, vol. 125, no. 1, pp. 85–88, 1982.

[187] M. V Suresh, B. Yu, D. Machado-Aranda, M. D. Bender, L. Ochoa-Frongia, J. D. Helinski, B. A. Davidson, P. R. Knight, C. M. Hogaboam, B. B. Moore, and K. Raghavendran, “Role of macrophage chemoattractant protein-1 in acute inflammation after lung contusion,” *Am. J. Respir. Cell Mol. Biol.*, vol. 46, no. 6, pp. 797–806, Jun. 2012.

[188] J. W. Lee, X. Fang, A. Krasnodembskaya, J. P. Howard, and M. A. Matthay, “Concise review: Mesenchymal stem cells for acute lung injury: Role of paracrine soluble factors,” *Stem Cells*, vol. 29, no. 6, pp. 913–919, Jun. 2011.

[189] M. A. Matthay, B. T. Thompson, E. J. Read, D. H. McKenna, K. D. Liu, C. S. Calfee, and J.-W. W. Lee, “Therapeutic Potential of Mesenchymal Stem Cells for

Severe Acute Lung Injury," *Chest*, vol. 138, no. 4, pp. 965–972, Oct. 2010.

[190] S. H. J. Mei, J. J. Haitsma, C. C. Dos Santos, Y. Deng, P. F. H. Lai, A. S. Slutsky, W. C. Liles, and D. J. Stewart, "Mesenchymal stem cells reduce inflammation while enhancing bacterial clearance and improving survival in sepsis," *Am. J. Respir. Crit. Care Med.*, vol. 182, no. 8, pp. 1047–1057, 2010.

[191] N. Gupta, A. Krasnodembskaya, M. Kapetanaki, M. Mouded, X. Tan, V. Serikov, and M. A. Matthay, "Mesenchymal stem cells enhance survival and bacterial clearance in murine Escherichia coli pneumonia," *Thorax*, vol. 67, no. 6. pp. 533–539, 2012.

[192] D. J. Prockop, "Repair of tissues by adult stem/progenitor cells (MSCs): controversies, myths, and changing paradigms.," *Mol. Ther.*, vol. 17, no. 6, pp. 939–946, Jun. 2009.

[193] A. Leelahavanichkul, P. S. T. Yuen, A. Parmelee, K. Doi, P. G. Robey, K. Leelahavanichkul, B. H. Koller, J. M. Brown, X. Hu, I. Jelinek, R. A. Star, K. Nemeth, A. Leelahavanichkul, P. S. T. Yuen, B. Mayer, A. Parmelee, K. Doi, P. G. Robey, K. Leelahavanichkul, B. H. Koller, J. M. Brown, X. Hu, I. Jelinek, R. A. Star, and E. Mezey, "Bone marrow stromal cells attenuate sepsis via prostaglandin E(2)-dependent reprogramming of host macrophages to increase their interleukin-10 production.," *Nat. Med.*, vol. 15, no. 1, pp. 42–9, Jan. 2009.

[194] Y. Miyahara, N. Nagaya, M. Kataoka, B. Yanagawa, K. Tanaka, H. Hao, K. Ishino, H. Ishida, T. Shimizu, K. Kangawa, S. Sano, T. Okano, S. Kitamura, and H. Mori, "Monolayered mesenchymal stem cells repair scarred myocardium after myocardial infarction.," *Nat. Med.*, vol. 12, no. 4, pp. 459–65, Apr. 2006.

[195] F. Tögel, A. Cohen, P. Zhang, Y. Yang, Z. Hu, and C. Westenfelder, "Autologous and allogeneic marrow stromal cells are safe and effective for the treatment of acute kidney injury," *Stem Cells Dev.*, vol. 18, no. 3, pp. 475–485, Apr. 2009.

[196] F. Tögel, Z. Hu, K. Weiss, J. Isaac, C. Lange, and C. Westenfelder, "Administered mesenchymal stem cells protect against ischemic acute renal failure through differentiation-independent mechanisms.," *Am. J. Physiol. Renal Physiol.*, vol. 289, no. 1, pp. F31–42, Jul. 2005.

[197] H.-G. G. Wisniewski, J. Vilĉek, and J. Vilček, "TSG-6: An IL-1/TNF-inducible protein with anti-inflammatory activity," *Cytokine Growth Factor Rev.*, vol. 8, no. 2, pp. 143–156, Jun. 1997.

[198] N. S. Baranova, E. Nilebäck, F. M. Haller, D. C. Briggs, S. Svedhem, A. J. Day, and R. P. Richter, "The inflammation-associated protein TSG-6 cross-links hyaluronan via hyaluronan-induced TSG-6 oligomers," *J. Biol. Chem.*, vol. 286, no. 29, pp. 25675–25686, Jul. 2011.

[199] G. Nagyeri, M. Radacs, S. Ghassemi-Nejad, B. Tryniszewska, K. Olasz, G. Hutas, Z. Gyorfy, V. C. Hascall, T. T. Glant, and K. Mikecz, "TSG-6 protein, a negative regulator of inflammatory arthritis, forms a ternary complex with murine mast cell tryptases and heparin.," *J. Biol. Chem.*, vol. 286, no. 26, pp. 23559–69, Jul. 2011.

[200] T. V Cao, M. La, S. J. Getting, A. J. Day, and M. Perretti, "Inhibitory effects of TSG-6 Link module on leukocyte-endothelial cell interactions in vitro and in vivo.," *Microcirculation*, vol. 11, no. 7, pp. 615–24, Jan. 2004.

[201] A. I. Caplan and D. Correa, "The MSC: An injury drugstore," *Cell Stem Cell*, vol. 9, no. 1, pp. 11–15, Jul. 2011.

[202] R. J. Cersosimo, S. J. Matthews, and Waun Ki Hong, "Bleomycin pneumonitis potentiated by oxygen administration," *Drug Intell. Clin. Pharm.*, vol. 19, no. 12, pp. 921–923, 1985.

[203] T. S. Ingrassia, J. H. Ryu, V. F. Trastek, and E. C. Rosenow, "Oxygen-exacerbated bleomycin pulmonary toxicity," *Mayo Clin. Proc.*, vol. 66, no. 2, pp. 173–178, 1991.

[204] J. Rinaldo, R. H. Goldstein, and G. L. Snider, "Modification of oxygen toxicity after lung injury by bleomycin in hamsters," *Am. Rev. Respir. Dis.*, vol. 126, no. 6, pp. 1030–1033, 1982.

[205] J. Liang, Y. Jung, R. M. Tighe, T. Xie, N. Liu, M. Leonard, M. D. Gunn, D. Jiang, and P. W. Noble, "A macrophage subpopulation recruited by CC chemokine ligand-2 clears apoptotic cells in noninfectious lung injury.," *Am. J. Physiol. Lung Cell. Mol. Physiol.*, vol. 302, no. 9, pp. L933–40, May 2012.

[206] H. Roca, Z. S. Varsos, S. Sud, M. J. Craig, C. Ying, and K. J. Pienta, "CCL2 and interleukin-6 promote survival of human CD11b+ peripheral blood mononuclear cells and induce M2-type macrophage polarization.," *J. Biol. Chem.*, vol. 284, no. 49, pp. 34342–54, Dec. 2009.

[207] K. Raghavendran, B. A. Davidson, B. A. Mullan, A. D. Hutson, T. A. Russo, P. A. Manderscheid, J. A. Woytash, B. A. Holm, R. H. Notter, and P. R. Knight, "Acid and particulate-induced aspiration lung injury in mice: importance of MCP-1.," *Am. J. Physiol. Lung Cell. Mol. Physiol.*, vol. 289, no. 1, pp. L134–L143, Jul. 2005.

[208] H. Amano, K. Morimoto, M. Senba, H. Wang, Y. Ishida, A. Kumatori, H. Yoshimine, K. Oishi, N. Mukaida, and T. Nagatake, "Essential Contribution of Monocyte Chemoattractant Protein-1/C-C Chemokine Ligand-2 to Resolution and Repair Processes in Acute Bacterial Pneumonia," *J. Immunol.*, vol. 172, no. 1, pp. 398–409, 2004.

[209] R. Wang, G. Alam, A. Zagariya, C. Gidea, H. Pinillos, O. Lalude, G. Choudhary,

D. Oezatalay, and B. D. Uhal, “Apoptosis of lung epithelial cells in response to TNF-α requires angiotensin II generation de novo,” *J. Cell. Physiol.*, vol. 185, no. 2, pp. 253–259, 2000.

[210] D. Jiang, J. Liang, J. Fan, S. Yu, S. Chen, Y. Luo, G. D. Prestwich, M. M. Mascarenhas, H. G. Garg, D. A. Quinn, R. J. Homer, D. R. Goldstein, R. Bucala, P. J. Lee, R. Medzhitov, and P. W. Noble, “Regulation of lung injury and repair by Toll-like receptors and hyaluronan.,” *Nat. Med.*, vol. 11, no. 11, pp. 1173–9, Nov. 2005.

[211] P. Teder, R. W. Vandivier, D. Jiang, J. Liang, L. Cohn, E. Puré, P. M. Henson, and P. W. Noble, “Resolution of lung inflammation by CD44.,” *Science*, vol. 296, no. 5565, pp. 155–8, Apr. 2002.

[212] J. Y. Oh, H. Choi, R. H. Lee, G. W. Roddy, J. H. Ylöstalo, E. Wawrousek, and D. J. Prockop, “Identification of the HSPB4/TLR2/NF-κB axis in macrophage as a therapeutic target for sterile inflammation of the cornea.,” *EMBO Mol. Med.*, vol. 4, no. 5, pp. 435–48, May 2012.

[213] L. F. Krist, I. L. Eestermans, J. J. Steenbergen, E. C. Hoefsmit, M. a Cuesta, S. Meyer, and R. H. Beelen, “Cellular composition of milky spots in the human greater omentum: an immunochemical and ultrastructural study.,” *Anat. Rec.*, vol. 241, no. 2, pp. 163–74, Feb. 1995.

[214] K. S. Gray, C. M. Collins, and S. H. Speck, “Characterization of omental immune aggregates during establishment of a latent gammaherpesvirus infection.,” *PLoS One*, vol. 7, no. 8, p. e43196, Jan. 2012.

[215] S. Berberich, S. Dähne, A. Schippers, T. Peters, W. Müller, E. Kremmer, R. Förster, and O. Pabst, “Differential molecular and anatomical basis for B cell migration into the peritoneal cavity and omental milky spots.,” *J. Immunol.*, vol. 180, no. 4, pp. 2196–203, Feb. 2008.

[216] K. M. Ansel, R. B. S. Harris, and J. G. Cyster, “CXCL13 is required for B1 cell homing, natural antibody production, and body cavity immunity.,” *Immunity*, vol. 16, no. 1, pp. 67–76, Jan. 2002.

[217] S. Koyasu and K. Moro, “Type 2 innate immune responses and the natural helper cell.,” *Immunology*, vol. 132, no. 4, pp. 475–81, Apr. 2011.

APPENDIX A

SUPPLEMENTARY INFORMATION FOR CHAPTER II

Figure A-1. Quality of extracted RNA from laser-capture microdissection samples.

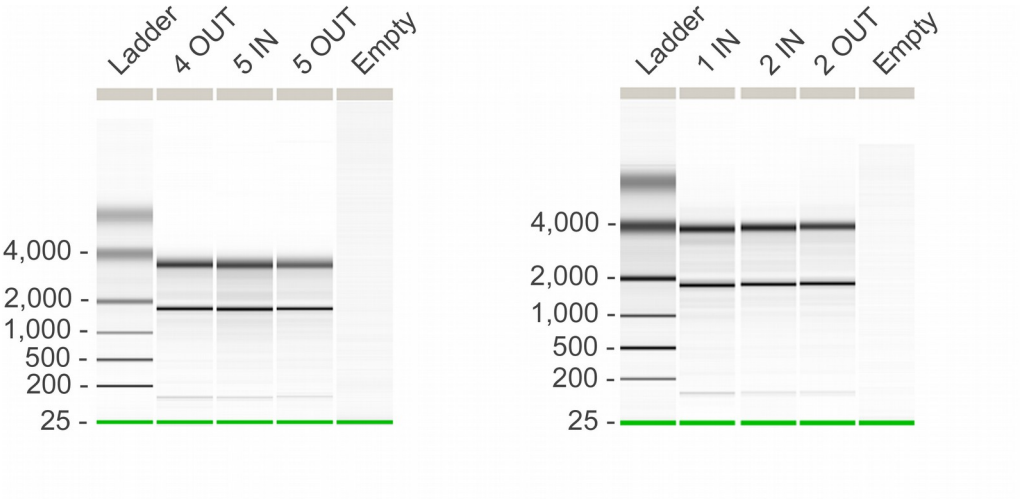

Figure A-2. Subcloning of IN and OUT cells. Representative colonies from the subcloning experiment at passage 2 and 6 for donor 5064. Both the IN and OUT regions generated similar colonies. Scale bar: 1 mm. Abbreviations: IN, inner region of a colony; OUT, outer region of a colony; P, passage.

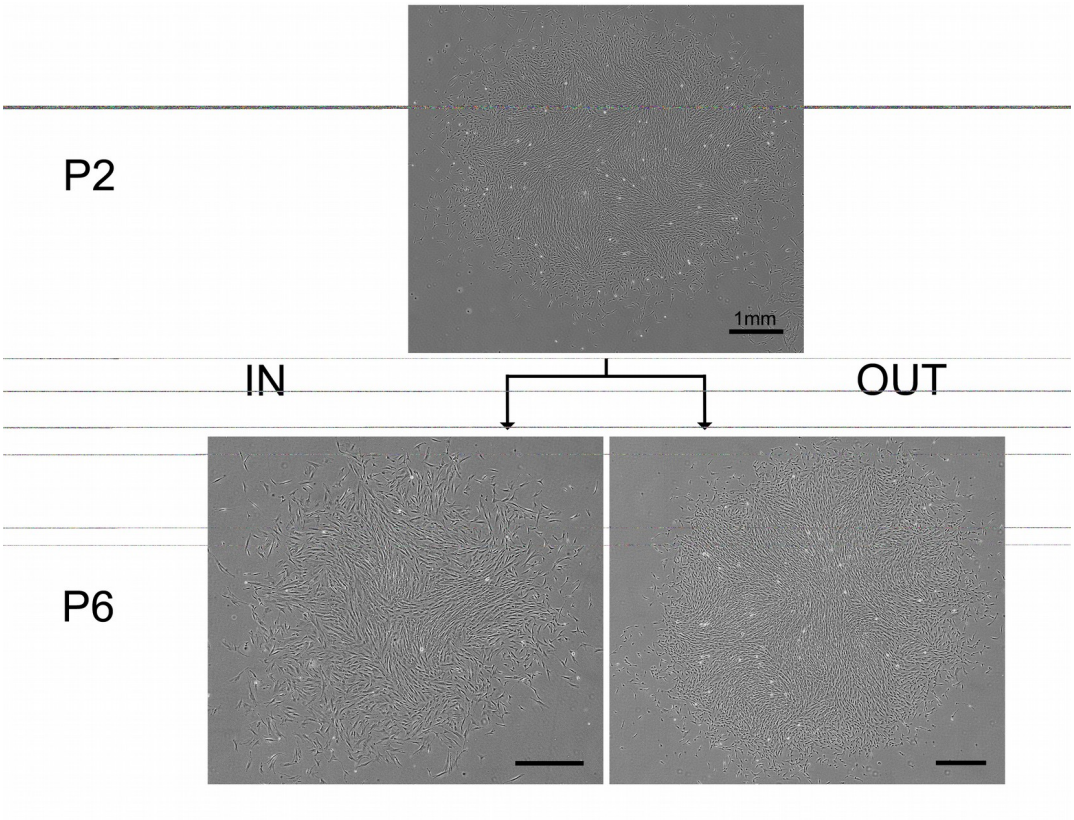

Figure A-3. Density analysis of type I and II colonies. Representative colonies from donor 7012 analyzed by staining with crystal violet and densitometry. Scale: 0-255 (black- white).

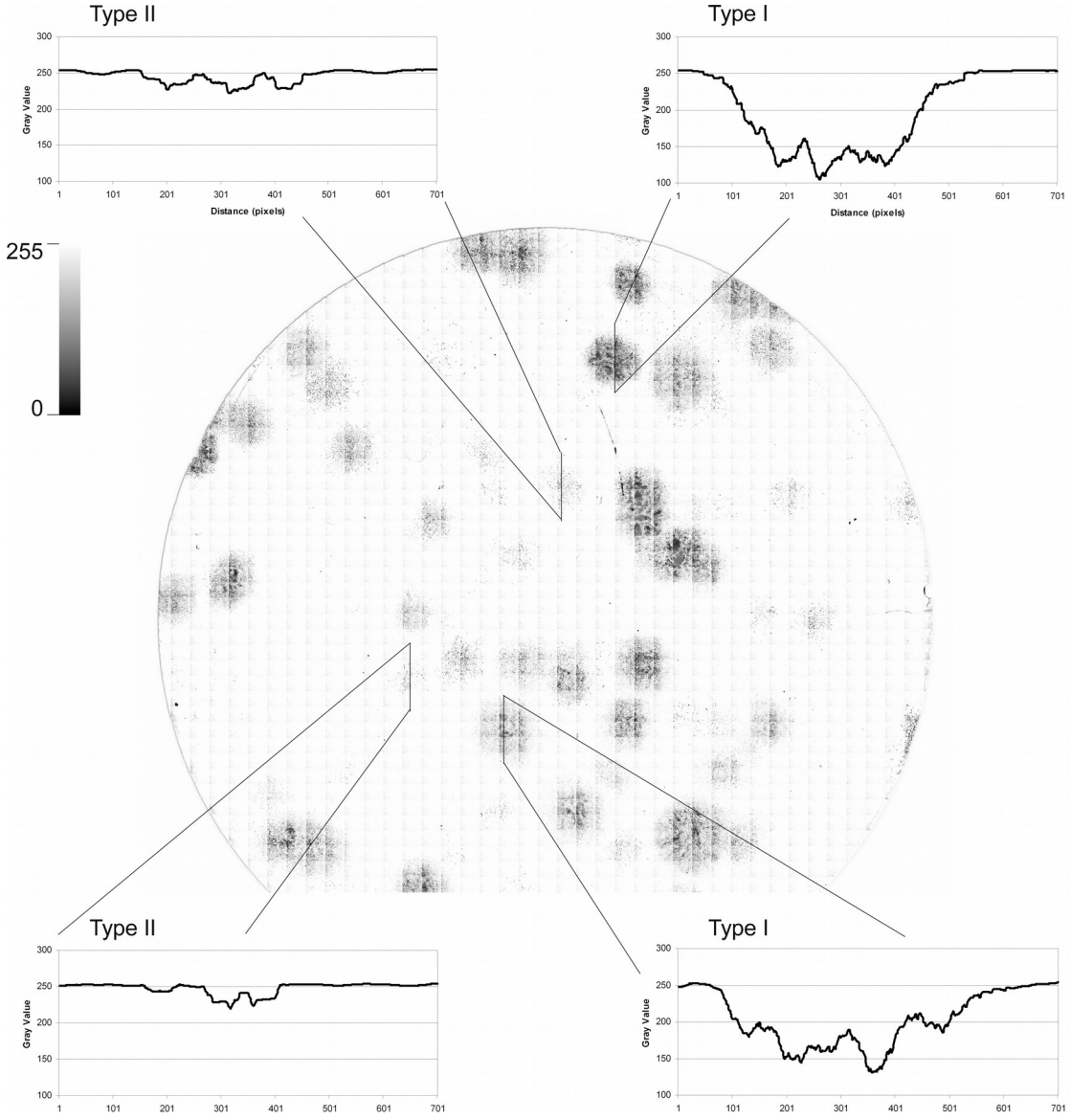

Table A-1. Genes significantly up-regulated in inside (IN) of the colony when compared to the outside (OUT) of the colony.

Gene	Accession	Gene ID	Fold change	P-value
IGF1: insulin-like growth factor 1	AU144912	3479	50.1	0.0494
Transcribed locus	BE671251	-	23.8	0.0434
DKFZP434P211: POM121-like protein	AL117484	29774	18.6	0.0263
DKFZP434P211: POM121-like protein	NM_014549	29774	14.8	0.0011
FAM13C1: family with sequence similarity 13 member C1	BC036453	220965	12.6	0.0120
SEMA6D: semaphorin 6D	AL036088	80031	12.4	0.0028
CDNA FLJ12087 fis clone HEMBB1002522	AU147125	-	11.6	0.0184
CDNA FLJ14388 fis clone HEMBA1002716	AI917494	-	9.9	0.0422
SULF2: sulfatase 2	AL133001	55959	8.7	0.0343
KIAA0367: KIAA0367	AB002365	23273	8.6	0.0194
CDNA clone IMAGE:4812643	AW236954	-	8.5	0.0496
KIAA1189: KIAA1189	AA736604	57471	8.3	0.0180
TMEM119: transmembrane protein 119	AL521682	338773	8.2	0.0138
GBP2: guanylate binding protein 2 interferon-inducible	NM_004120	2634	8.1	0.0189
KIF26B: kinesin family member 26B	NM_018012	55083	7.6	0.0442
JMJD2C: jumonji domain containing 2C	AI341811	23081	7.6	0.0019
CDNA clone IMAGE:4825733	BC032027	-	7.2	0.0318
TAT: tyrosine aminotransferase	NM_000353	6898	7.0	0.0427
MRVI1: Murine retrovirus integration site 1 homolog	N66571	10335	6.7	0.0422
C5orf4: chromosome 5 open reading frame 4	H93077	10826	6.7	0.0097
Hs.34851.1	BE550254	-	6.3	0.0479
CDNA clone IMAGE:5922621	AB011538	-	6.3	0.0233
LOC387758: similar to RIKEN cDNA 1110018M03	AI802391	387758	6.3	0.0061
SLIT3: slit homolog 3	NM_003062	6586	6.1	0.0344
LENG10: leukocyte receptor cluster member 10	AF211977	94057	6.0	0.0077
THBS2: thrombospondin 2	NM_003247	7058	5.8	0.0010
YPEL3: yippee-like 3	BC005009	83719	5.8	0.0384
C1RL: complement component 1 r subcomponent-like	NM_016546	51279	5.8	0.0258
LEPR: leptin receptor	U52914	3953	5.7	0.0199
NRP2: Neuropilin 2	AA127691	8828	5.6	0.0142
C10orf11: chromosome 10 open reading frame 11	AF267860	83938	5.5	0.0032
Hs.300070.0	R08129	-	5.5	0.0091
CDNA clone IMAGE:4827386	BG721449	-	5.5	0.0167
TGFB3: transforming growth factor beta 3	J03241	7043	5.5	0.0192
FASTKD2: FAST kinase domains 2	NM_014929	22868	5.2	0.0292
ALS2CR11: amyotrophic lateral sclerosis 2 chromosome 11	BC030659	151254	5.1	0.0130
SYTL2: synaptotagmin-like 2	N21426	54843	5.1	0.0413
PHF21A: PHD finger protein 21A	BC015714	51317	5.0	0.0123
FGFR2: fibroblast growth factor receptor 2	M87771	2263	5.0	0.0283
COL21A1: collagen type XXI alpha 1	NM_030820	81578	4.9	0.0402
HOXA5: homeobox A5	NM_019102	3202	4.9	0.0263
DDX3X: DEAD (Asp-Glu-Ala-Asp) box polypeptide 3 X-linked	BE379787	1654	4.8	0.0349
Transcribed locus	AL037805	-	4.7	0.0321

Table A-1 (continued)

Gene	Accession	Gene ID	Fold change	P-value
FNDC1: fibronectin type III domain containing 1	AI345957	84624	4.7	0.0067
Hs.107070.0	H93043	-	4.7	0.0470
ALS2CR11: amyotrophic lateral sclerosis 2 chromosome 11	NM_152525	151254	4.6	0.0260
Full length insert cDNA clone YI44E03	AF085839	-	4.6	0.0019
LMOD1: leiomodin 1	BC001755	25802	4.5	0.0498
Clone IMAGE:297403 mRNA sequence	AF339813	-	4.5	0.0128
TTC3: tetratricopeptide repeat domain 3	BC026260	7267	4.5	0.0163
TXNIP: thioredoxin interacting protein	NM_006472	10628	4.4	0.0268
SLC1A3: solute carrier family 1 member 3	NM_004172	6507	4.4	0.0263
Hs.159556.0	AA808178	-	4.4	0.0065
Transcribed locus	AI802768	-	4.4	0.0371
AKR1C3: aldo-keto reductase family 1 member C3	AB018580	8644	4.4	0.0182
SYTL2: synaptotagmin-like 2	AB046817	54843	4.3	0.0083
LAMA4: laminin alpha 4	U77706	3910	4.3	0.0256
MRNA; cDNA DKFZp564C203	AL049245	-	4.3	0.0004
VCAM1: vascular cell adhesion molecule 1	NM_001078	7412	4.2	0.0030
METTL7A: methyltransferase like 7A	NM_014033	25840	4.2	0.0235
CLEC3B: C-type lectin domain family 3 member B	NM_003278	7123	4.2	0.0176
Hs.189998.0	AA706922	-	4.2	0.0319
GOLGA1: Golgi autoantigen golgin subfamily a 1	AW675473	2800	4.0	0.0249
CDNA FLJ34664 fis clone LIVER2000592	BF930294	-	4.0	0.0357
FGFR2: fibroblast growth factor receptor 2	NM_022969	2263	4.0	0.0168
NEK1: NIMA never in mitosis gene a-related kinase 1	AK024912	4750	4.0	0.0034
PPFIA4: protein tyrosine phosphatase receptor type f alpha 4	AK023365	8497	4.0	0.0477
CLEC2D: C-type lectin domain family 2 member D	AF285089	29121	3.9	0.0323
TSFM: Ts translation elongation factor mitochondrial	AI796813	10102	3.9	0.0024
CDNA: FLJ23228 fis clone CAE06654	AK026881	-	3.9	0.0085
LUM: lumican	NM_002345	4060	3.9	0.0051
Transcribed locus	AW058580	-	3.8	0.0196
ZNF423: zinc finger protein 423	AW149417	23090	3.8	0.0063
PDE5A: phosphodiesterase 5A cGMP-specific	BF221547	8654	3.8	0.0163
GLT8D2: glycosyltransferase 8 domain containing 2	NM_031302	83468	3.7	0.0334
CDNA clone IMAGE:5259272	AA489100	-	3.7	0.0030
COL3A1: collagen type III alpha 1	AU144167	1281	3.7	0.0349
ACACB: acetyl-Coenzyme A carboxylase beta	AI057637	32	3.7	0.0269
BTN3A3: butyrophilin, subfamily 3, member A3	NM_006994	10384	3.7	0.0027
CDNA: FLJ21027 fis clone CAE07110	AK024680	-	3.7	0.0107
LAMA4: laminin alpha 4	NM_002290	3910	3.6	0.0081
COL28A1: collagen type XXVIII alpha 1	AA995791	340267	3.6	0.0381
C13orf31: chromosome 13 open reading frame 31	NM_153218	144811	3.6	0.0329
Hs.122116.0	AW469546	-	3.6	0.0280
TMEM67: transmembrane protein 67	BC031220	91147	3.6	0.0300
YPEL2: yippee-like 2	BE502982	388403	3.5	0.0071
PLSCR4: phospholipid scramblase 4	NM_020353	57088	3.5	0.0336
BCL3: B-cell CLL/lymphoma 3	NM_005178	602	3.4	0.0061
MLLT3: myeloid/lymphoid leukemia translocated to 3	NM_004529	4300	3.4	0.0443
Homo sapiens clone IMAGE:4250282 mRNA	BC017896	-	3.4	0.0216
Hs.122516.0	BF055144	-	3.4	0.0269

Table A-1 (continued)

Gene	Accession	Gene ID	Fold change	P-value
PFAAP5: phosphonoformate immuno-associated protein 5	NM_014887	10443	3.4	0.0225
RAB27B: RAB27B member RAS oncogene family	BF438386	5874	3.4	0.0193
PARP9: poly polymerase family member 9	AF307338	83666	3.3	0.0051
C16orf46: chromosome 16 open reading frame 46	AI921002	123775	3.3	0.0303
COL12A1: collagen type XII alpha 1	AA788946	1303	3.3	0.0121
GHR: growth hormone receptor	NM_000163	2690	3.2	0.0309
TP53INP1: tumor protein p53 inducible nuclear protein 1	AW341649	94241	3.2	0.0213
APOL6: apolipoprotein L 6	NM_030641	80830	3.2	0.0131
PRNP: prion protein	AK056897	5621	3.2	0.0468
ARHGEF3: Rho guanine nucleotide exchange factor 3	NM_019555	50650	3.1	0.0413
WDR27: WD repeat domain 27	AW194823	253769	3.1	0.0094
Transcribed locus	AI287817	-	3.1	0.0333
SDC3: syndecan 3	NM_014654	9672	3.0	0.0142
COL8A1: collagen type VIII alpha 1	BE877796	1295	3.0	0.0267
CDNA FLJ41303 fis clone BRAMY2042131	AI634543	-	3.0	0.0049
BTN3A3: butyrophilin subfamily 3 member A3	U90548	10384	3.0	0.0033
CAT: Catalase	AW015521	847	3.0	0.0071
PELO: Pelota homolog	X68742	53918	2.9	0.0025
BNC2: basonuclin 2	AW024890	54796	2.9	0.0166
AHSA2: AHA1 activator of heat shock 90kDa protein ATPase	AI986239	130872	2.9	0.0044
Transcribed locus	AI493276	-	2.9	0.0140
FLJ21963: FLJ21963 protein	AI123815	79611	2.8	0.0147
SLC22A5: solute carrier family 22 member 5	NM_003060	6584	2.8	0.0481
SLC35D1: solute carrier family 35 member D1	N80922	23169	2.8	0.0033
GPC4: glypican 4	NM_001448	2239	2.8	0.0030
SH3PXD2A: SH3 and PX domains 2A	NM_014631	9644	2.7	0.0380
CFH / CFHR1: complement factor H / complement factor H-related 1	X56210	3075 /// 3078	2.7	0.0059
FLJ23861: hypothetical protein FLJ23861	AL133053	151050	2.6	0.0007
Transcribed locus, moderately similar to XP_517655.1	AI004009	-	2.6	0.0011
CDNA FLJ26539 fis clone KDN09310	AW025579	-	2.5	0.0024
POLI: Polymerase iota	AW129145	11201	2.5	0.0058
CNN3: calponin 3 acidic	NM_001839	1266	2.5	0.0077

Table A-2. Genes significantly up-regulated in outside (OUT) of the colony when compared to the inside (IN) of the colony.

Gene	Accession	Gene ID	Fold change	P-value
MMP1: matrix metallopeptidase 1	NM_002421	4312	8.0	0.0015
Transcribed locus	AI608902	-	6.7	0.0415
HBEGF: heparin-binding EGF-like growth factor	M60278	1839	6.3	0.0167
ADRB2: adrenergic beta-2-receptor	NM_000024	154	5.9	0.0422
ESPL1: extra spindle pole bodies homolog 1	D79987	9700	5.4	0.0486
RGMB: RGM domain family, member B	AW004714	285704	5.4	0.0030
TACC3: transforming, acidic coiled-coil containing protein 3	NM_006342	10460	5.3	0.0155
HHIP: hedgehog interacting protein	AW444502	64399	5.2	0.0003
ESM1: endothelial cell-specific molecule 1	NM_007036	11082	4.9	0.0377
ANKRD30B: ankyrin repeat domain 30B	AF269088	374860	4.8	0.0069
CDNA FLJ42405 fis clone ASTRO3000474	AI822137	-	4.6	0.0069
Hs.112708.0	AI201116	-	4.6	0.0475
MKI67: antigen identified by monoclonal antibody Ki-67	BF001806	4288	4.5	0.0031
CDC45L: CDC45 cell division cycle 45-like	NM_003504	8318	4.5	0.0325
CDC20: cell division cycle 20 homolog	NM_001255	991	4.5	0.0190
MYB: v-myb myeloblastosis viral oncogene homolog	NM_005375	4602	4.4	0.0469
Transcribed locus	AI093492	-	4.3	0.0211
HMGA2: high mobility group AT-hook 2	U29113	8091	4.2	0.0479
HHIP: hedgehog interacting protein	AK098525	64399	4.2	0.0086
CDCA5: cell division cycle associated 5	BE614410	113130	4.1	0.0253
CDC25A: cell division cycle 25 homolog A	AI343459	993	4.1	0.0105
FAM64A: family with sequence similarity 64 member A	BC005004	54478	4.1	0.0423
MARCH4: membrane-associated ring finger 4	AB037820	57574	4.0	0.0001
Full length insert cDNA clone YZ11B11	BF003032	-	4.0	0.0112
AURKB: aurora kinase B	AB011446	9212	4.0	0.0399
STS-1: Cbl-interacting protein Sts-1	AA037664	84959	4.0	0.0087
CDCA3: cell division cycle associated 3	NM_031299	83461	3.9	0.0382
FGF5: fibroblast growth factor 5	NM_004464	2250	3.9	0.0301
Hs.30581.0	H05918	-	3.9	0.0025
PTGS2: prostaglandin-endoperoxide synthase 2	NM_000963	5743	3.8	0.0364
NGFB: nerve growth factor beta polypeptide	NM_002506	4803	3.8	0.0182
FANCI: Fanconi anemia complementation group I	BG403615	55215	3.7	0.0076
GTSE1: G-2 and S-phase expressed 1	BF973178	51512	3.7	0.0046
CCDC137: coiled-coil domain containing 137	BF115231	339230	3.7	0.0485
SGOL1: shugoshin-like 1	NM_138484	151648	3.7	0.0254
DTL: denticleless homolog	AK001261	51514	3.6	0.0372
SYTL3: synaptotagmin-like 3	AI674404	94120	3.5	0.0207
LIF: leukemia inhibitory factor	NM_002309	3976	3.5	0.0178
ETS2: v-ets erythroblastosis virus E26 oncogene homolog 2	AL575509	2114	3.4	0.0127
Clone 23641 mRNA sequence	U90917	-	3.4	0.0396
CENPI: centromere protein I	BF793446	2491	3.4	0.0104
PODXL: podocalyxin-like	NM_005397	5420	3.4	0.0029

Table A-2 (continued)

Gene	Accession	Gene ID	Fold change	P-value
FST: follistatin	NM_006350	10468	3.4	0.0040
SPAG5: sperm associated antigen 5	NM_006461	10615	3.4	0.0067
VEPH1: ventricular zone expressed PH domain homolog 1	AA988323	79674	3.4	0.0271
POLE: polymerase epsilon	AL080203	5426	3.3	0.0069
IL11: interleukin 11	NM_000641	3589	3.3	0.0388
Transcribed locus	AA969163	-	3.3	0.0240
LOC646576: hypothetical LOC646576	AA149654	646576	3.3	0.0326
Hs2.375188.1	BC033184	-	3.3	0.0094
HMGA2: high mobility group AT-hook 2	U29113	8091	3.3	0.0267
LYAR: hypothetical protein FLJ20425	AW958593	55646	3.3	0.0022
DCLRE1B: DNA cross-link repair 1B	NM_022836	64858	3.2	0.0082
FST: follistatin	NM_013409	10468	3.2	0.0045
CDNA FLJ33153 fis clone UTERU2000332	BU676221	-	3.2	0.0361
CENPJ: centromere protein J	AF141343	55835	3.2	0.0311
Hs.182426.4	L48784	-	3.2	0.0226
H2AFX: H2A histone family member X	NM_002105	3014	3.1	0.0012
VIL2: villin 2	AA670344	7430	3.1	0.0065
LRRC8C: leucine rich repeat containing 8 family member C	AL136919	84230	3.1	0.0044
RGMB: RGM domain family member B	AL117590	285704	3.1	0.0150
ARNTL2: aryl hydrocarbon receptor nuclear translocator-like 2	AF231339	56938	3.0	0.0059
NOL12 / TRIOBP: TRIO and F-actin binding protein / nucleolar protein 12	NM_024313	11078 / 79159	3.0	0.0050
IL11: interleukin 11	M57765	3589	3.0	0.0169
TM4SF1: transmembrane 4 L six family member 1	AI189753	4071	2.9	0.0039
TARS2: threonyl-tRNA synthetase 2 mitochondrial	NM_025150	80222	2.9	0.0048
WDR5: WD repeat domain 5	AL521101	11091	2.9	0.0014
GPATCH4: G patch domain containing 4	AI911518	54865	2.9	0.0012
ARNTL2: aryl hydrocarbon receptor nuclear translocator-like 2	NM_020183	56938	2.8	0.0033
TM4SF1: transmembrane 4 L six family member 1	M90657	4071	2.8	0.0086
GPATCH4: G patch domain containing 4	BE794289	54865	2.7	0.0031
STS-1: Cbl-interacting protein Sts-1	AA233308	84959	2.7	0.0028
CD44: CD44 molecule	AF098641	960	2.6	0.0227
SSR3: signal sequence receptor gamma	NM_007107	6747	2.5	0.0019
SPRY4: sprouty homolog 4	W48843	81848	2.5	0.0014
BXDC2: brix domain containing 2	NM_018321	55299	2.4	0.0001

APPENDIX B

SUPPLEMENTARY INFORMATION FOR CHAPTER IV

Figure B-1 Detection of MSCs in mouse tissues and peritoneal lavage by real-time PCR. (A) Standard curves of known amounts of human cells added to mouse tissues plotted versus corresponding delta Ct values (Ct human GAPDH - Ct values eukaryotic 18S) obtained by real-time PCR in the same tissues. Points represent average values for delta-Ct, lines represent logarithmic model fit. (B) Peritoneal lavage from human MSCs-injected BALB/c was collected and total number of recovered cells was enumerated with hemocytometer. Values are mean +/- SEM, n= 4-5. Abbreviations: OM – omentum, MT – mesentery, PLP – cell pellet from peritoneal lavage, JLN - jejunal lymph nodes, SP – spleen.

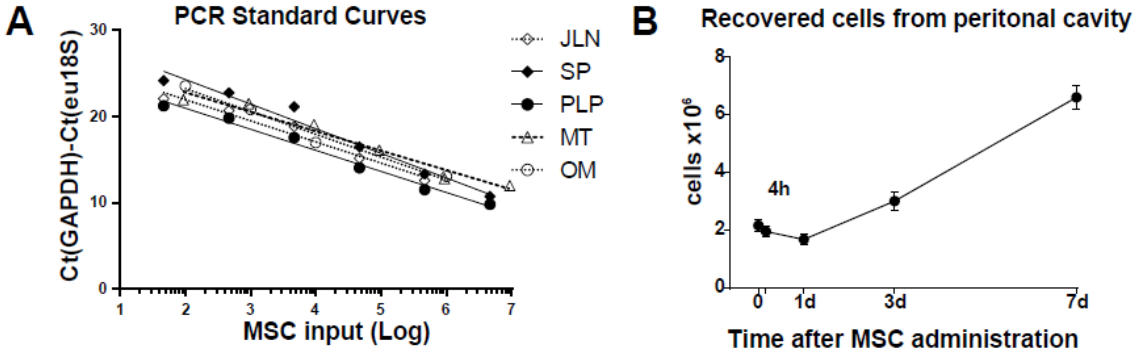

Figure B-2. Effects of IP injected MSCs to cytokine levels in the mouse serum. Mouse IL10 and IL13 levels in the serum were assayed 72 hours after IP injection of MSCs.

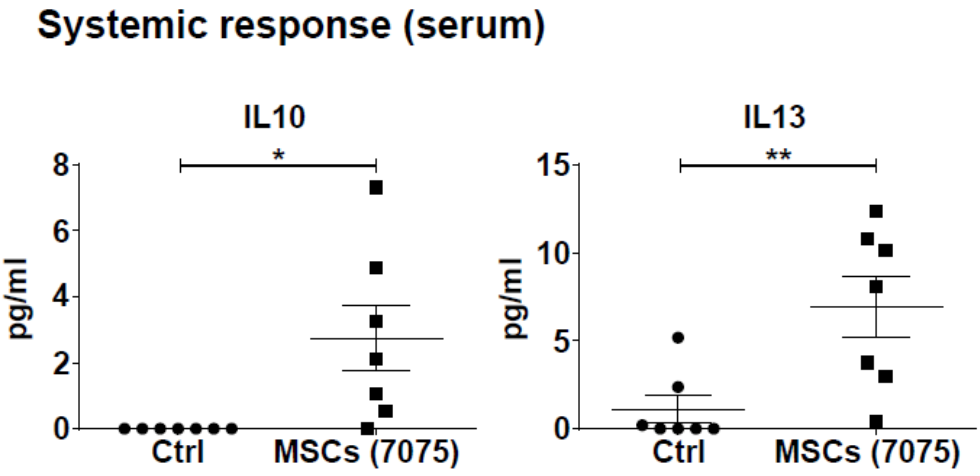

Figure B-3. Effect of MSCs dose and bone marrow donor to cytokine production in the peritoneum. Mouse IL10, IL13 and PGE_2 were assayed at 72 hours after IP MSCs or HBSS (Ctrl) administration into BALB/c mice. (A) Mouse cytokine production in the peritoneum in response to 3 donors. (B) Peritoneal levels of mouse cytokines after administration of various doses of MSCs. *, $p<0.05$; **, $p<0.01$; ***, $p<0.001$ compared to controls.

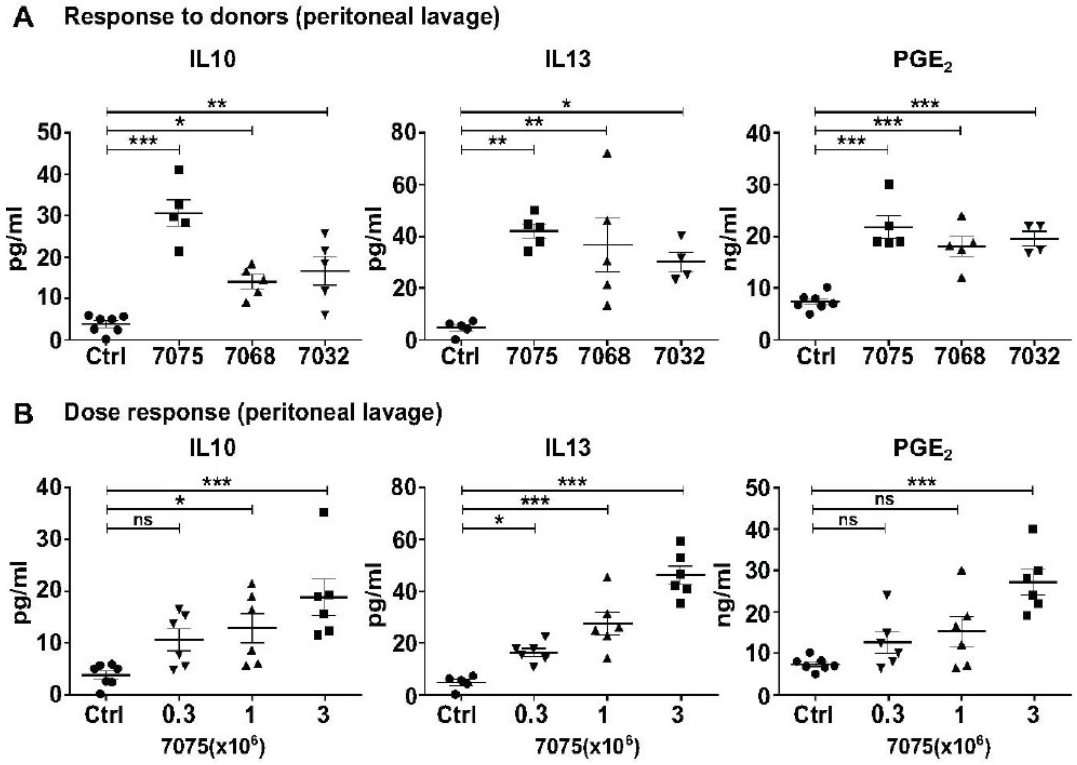

Table B-1. Characteristics of the MSCs donor samples used in the current study. Donors identified by anonymous number and sampling of marrow from left (L) or right (R) iliac crest/gender/age were assayed in vitro for growth, clonogenicity, osteogenic and adipogenic differentiation and epitope markers in vitro.

Donor[a] (ID#/gender /age)	**P0 Yield**[b] (x 10^6)/ days	**P0→P1 Yield (Master Bank)**[c] (plating cells per cm^2 / harvest cells per cm^2 /days)	**P1 Cumulative PDs**[d]	**P1→P2 Yield (Working Bank)** (plating cells per cm^2 /harvest cells per cm^2 /days)	**P2 Cumulative PDs**	**P2 Diff.**[e] (osteo/ adipo/ CFU)	**P2 Epitopes**[f] (+/-)
7032R/M/26	0.8/6	50/14557/8	j+8.3	50/6000/6	j+6.8	3/3/49	>95/<3
7068L/M/37	1.17/5	50/7595/8	j+7.2	100/7546/7	j+13.4	3/4/45	>95/<3
7075L/M/24	2.96/6	100/6329/7	j+6.0	100/9287/7	j+12.5	4/1/49	>95/<3

[a]Donors identified by anonymous number and sampling of marrow from left (L) or right (R) iliac crest/gender/age.
[b]P0 yield defined as number of cells obtained by plating mononuclear cells from ficoll gradient at high density (6,000 to 30,000 per cm^2)/ days cells were incubated.
[c]Master Bank (P1 cells) defined by number of cells plated per cm^2/number of cells harvested per cm^2/days of incubation.
[d]Cumulative population doublings (PD) defined as j + observed value because number of population doublings required to generate P0 cells cannot be estimated. PD calculated as 2^n = fold-increase or $n = \log_{10}$ [fold-increase]/0.301.
[e]P2 Diff. assayed by culture of aliquots in differentiation conditions and visually scoring on +1 to +4 scale after staining with Alizarin Red or Oil-Red-O. Coony forming units (CFUs) assayed by plating at very low density to obtain % cells that generate colonies in 2 weeks.
[f]Positive epitopes (CD-29, -44, -49c, -59, -90, -105, -147 and -166) and negative epitopes (CD-34, -36, -45, and -117)

Table B-2. Goodness of logarithmic fit of standard curves. Real-time PCR for human GAPDH and eukaryotic 18S was performed on RNA obtained from a mixture of mouse tissues and human MSCs. Standard curves were built and non-linear (logarithmic) regression model was fit into the data (Fig. III.1A). The table shows the goodness of fit (r^2) and formula used to derive MSCs number in the tissues.

Tissue	r^2	Formula
JLN	0.96	f(x)=-0.88ln(x)+25.20
SP	0.97	f(x)=-1.24ln(x)+29.97
PLP	0.96	f(x)=-0.93ln(x)+24.37
MT	0.96	f(x)=-0.98ln(x)+27.25
OM	0.99	f(x)=-1.21ln(x)+29.11

Abbreviations: OM – omentum, MT – mesentery, PLP – cell pellet from peritoneal lavage, JLN - jejunal lymph nodes, SP – spleen.

Table B-3. Biological replicates of Ct values for eukariotic 18S and human GAPDH assayed by real-time PCR in mouse tissues after MSCs administration. Individual Ct values for human GAPDH and eukaryotic 18S related to Figs. III.1C, B-1A and B-1B.

Tissue:		Jejunal lymph nodes		Spleen		Lavage pellet		Mesentery		Omentum	
Time[a]	Replicate[b]	Ct eu18S	Ct GAPDH	Ct eu18S	Ct GAPDH	Ct eu18S	Ct GAPDH	Ct eu18S	Ct GAPDH	Ct eu18S	Ct GAPDH
0 h	1	10.11	ND	10.57	ND	10.13	ND	9.85	ND	8.14	ND
	2	10.16	ND	11.2	ND	10.8	ND	9.8	ND	8.41	ND
	3	9.95	ND	11.34	ND	10.98	ND	9.71	ND	7.9	ND
	4	10.26	ND	10.52	ND	11.35	ND	9.91	ND	7.43	ND
4 h	1	10.53	34.25	10.68	29.05	11.05	21.13	9.93	34.94	6.89	21.04
	2	9.89	29.5	11.2	28.64	11.43	22.16	–	–	7.28	20.84
	3	10.24	30.68	10.82	30.71	10.92	22.25	10.18	26.45	7.61	22.33
	4	–	–	11.02	31.05	10.97	23.03	10.13	24.4	7.88	22.87
	5	10.66	32.22	9.99	30.68	10.57	22.28	10.14	28	6.91	25.74
24 h	1	9.81	ND	9.85	30.03	10.76	24.53	11.71	38.55	7.08	20.41
	2	10.22	29.92	10.57	29.58	11.26	30.12	11.73	25.43	6.8	22.34
	3	10.27	38.61	9.81	34.17	10.83	28.76	11.24	27.04	7.15	23.8
	4	10.69	39.82	10.77	31.24	11.13	26.17	10.5	25.62	6.66	21.1
	5	10.48	33.69	10.72	31.12	11.42	24.6	10.53	25.46	7.38	21.25
72 h	1	10.02	ND	10.85	39.63	10.64	38.69	10.58	31.53	8.8	31.46
	2	10.43	ND	10.88	36.84	10.61	31.89	9.86	30.07	10.09	25.78
	3	9.85	37.59	10.21	34.57	–	–	9.87	28.84	10.41	26.44
	4	9.87	ND	10.85	33.78	–	–	9.96	29.21	8.45	29.14
	5	9.39	ND	10.26	35.58	10.5	35.43	9.91	28.9	8.63	25.22
168 h	1	10.58	ND	10.16	ND	12.68	ND	9.8	ND	10.28	ND
	2	10.6	ND	10.85	ND	13.16	ND	11.15	ND	9.52	ND
	3	10.32	39.87	10.09	ND	13.97	ND	11.47	ND	9.53	ND
	4	9.76	ND	10.88	ND	13.22	ND	11.13	ND	8.97	ND